

Aus der Klinik für Neurologie
der Medizinischen Fakultät Charité – Universitätsmedizin Berlin

DISSERTATION

**Human perceptual decision making in the visual and tactile
domain**

zur Erlangung des akademischen Grades
Doctor of Philosophy (PhD) in Medical Neurosciences

vorgelegt der Medizinischen Fakultät
Charité - Universitätsmedizin Berlin

von

Hermine Wenzlaff
aus Berlin

Datum der Promotion: 14-Feb-2014

Table of Contents

1. General Introduction	1
1.1. Perceptual decision making	1
1.2. Perceptual decision making as a stochastic diffusion process	1
1.3. Neurophysiology of perceptual decision making	3
1.3.1. Perceptual decision making in the visual domain - temporal dynamics	3
1.3.2. Perceptual decision making in the somatosensory domain - temporal dynamics	5
1.4. The role of oscillatory activity in perception	6
1.4.1. Perceptual decision making in the visual domain - oscillatory dynamics.....	7
1.4.2. Perceptual decision making in the somatosensory domain - oscillatory dynamics	8
1.5. Research questions	9
2. Study 1 - Perceptual decision making in the visual domain using images of faces	11
2.1. Abstract	11
2.2. Introduction	12
2.3. Materials and Methods	13
2.3.1. Subjects	13
2.3.2. Stimuli.....	13
2.3.3. Task.....	14
2.3.4. Procedure	16
2.3.5. Behavioral data analysis.....	17
2.3.6. Diffusion model analysis.....	17
2.3.7. MEG time-domain analysis.....	18
2.3.8. Prediction of diffusion model parameters from MEG time-domain data	19
2.3.9. sLORETA source analysis	20
2.4. Results	22
2.4.1. Behavioral data.....	22
2.4.2. Diffusion model data.....	22
2.4.3. Effects of visual stimulation in the time domain.....	24
2.5. Discussion and interim conclusions	37

2.5.1.	Behavioral and diffusion model data.....	37
2.5.2.	Decision-related SAT component in the right SMA	38
2.5.3.	Decision-related SAT and COH components in the DLPFC	39
2.5.4.	Other components characterizing SAT processing	40
2.5.5.	Other components characterizing COH processing.....	40
3.	Studies 2 and 3 - Perceptual decision making in the tactile domain using Braille patterns with long (1000 ms) and short (100 ms) presentation time	42
3.1.	<i>Abstract</i>	42
3.2.	<i>Introduction</i>	43
3.3.	<i>Materials and Methods</i>	45
3.3.1.	Subjects	45
3.3.2.	Stimuli.....	45
3.3.3.	Task.....	46
3.3.4.	Procedure	48
3.3.5.	Behavioral data analysis.....	50
3.3.6.	Diffusion model analysis.....	51
3.3.7.	EEG time-domain data processing and analysis on the sensor level.....	51
3.3.8.	EEG time- frequency domain data analysis on the sensor level.....	52
3.3.9.	EEG time- and time-frequency domain data analysis on the beamformer source level.....	53
3.3.10.	Correlation of the time- and frequency-domain data with the drift rate, and RT	54
3.3.11.	Comparison of the studies using long and short presentation time.....	55
3.4.	<i>Results</i>	56
3.4.1.	Behavioral and diffusion model data.....	57
3.4.2.	Effects of tactile stimulation in the time domain.....	59
3.4.3.	Effects of tactile stimulation in the frequency domain.....	70
3.4.4.	Short versus long stimulus presentation	80
3.5.	<i>Discussion and interim conclusions</i>	82
3.5.1.	Behavioral and diffusion model data.....	82
3.5.2.	Effects of tactile stimulation on S1 area 3b.....	82
3.5.4.	Effects of tactile stimulation on parieto-occipital channels, possibly visual areas.....	85
3.5.5.	Effects of tactile stimulation on medio-frontal channels, possibly motor-related areas.....	86
3.5.6.	Differences between the short and long stimulus presentation	87
4.	Summary	90

5. References	93
6. List of Figures	105
7. List of Tables.....	108
8. List of Abbreviations.....	109
9. Acknowledgements.....	111
10. Eidesstattliche Versicherung.....	112
11. Curriculum Vitae.....	113

1. General Introduction

1.1. *Perceptual decision making*

Decision making is the process to commit to one option from a number of alternatives and to act accordingly (for review, see, e.g., Gold and Shadlen, 2007). It is an essential cognitive ability enabling humans to adapt to changing conditions in the environment. In *perceptual* decision making, the scope is somewhat narrower: information from the sensory systems is acquired, interpreted, and used to interact with the environment, usually via a motor response (Gold and Shadlen, 2007; Ho et al., 2009; Shadlen and Newsome, 2001). For example, when we perceive a red traffic light ahead (sensory stimulus) while driving a car, we apply the break (motor response) after some milliseconds taken to react (decision process). The advantage of such simple sensory-motor tasks as a model system to study decision making is that both sensory input and motor output can be quantified. To scale the sensory input, stimulus identity can be assessed, e.g., the amount of light emitted by the red light. The output of the decision on the behavioral level can be measured, e.g., the reaction time (RT) and whether the choice was correct or incorrect.

Decision processing profoundly depends on the difficulty of the task. If the task is easy, e.g., the red light is clearly visible, RT is short and the accuracy is high. In contrast, if the task is more difficult, e.g., it is a foggy night, RT increases and the accuracy decreases, i.e., we might overlook the red light. Apart from this difficulty, we also face a speed-accuracy tradeoff (SAT) when making decisions, i.e., fast decisions are more susceptible to errors while careful ones take longer (Bogacz et al., 2010).

But how can we approximate the process in between sensory input and motor output?

1.2. *Perceptual decision making as a stochastic diffusion process*

First tools to describe the decision process from behavioral data, so-called sequential sampling or bounded integrator models, have been developed in mathematical psychology (Laming, 1968; Ratcliff, 1978; Stone, 1960). A relatively simple class of these models is the diffusion or random walk model (e.g., Smith and Ratcliff, 2004, also see fig.1). It assumes that sensory information is continuously accumulated for or against alternative options (typically two) from a starting point until a specified threshold or boundary is reached. Reaching this boundary concludes the decision process and initiates the response. From the

RT distributions for correct and error responses over trials and from the frequency of correct responses, several parameters can be estimated: the starting point, the accumulation rate of the stimulus information (drift rate), the amount of information accumulated to reach the boundary, the portion of RT taken by nondecision components such as stimulus encoding and response execution, as well as the amount of variability within or across trials in some of these parameters (Ratcliff and McKoon, 2008) (fig.1). Variability in decision processing is due to noise either present in the stimulus itself, or introduced by the nervous system (Shadlen et al., 2008). Please note that in the Ratcliff diffusion model, shifts in the starting point are equivalent to shifts in the boundary (Ratcliff, 2006), resulting in changes in the *distance* between starting point and boundary.

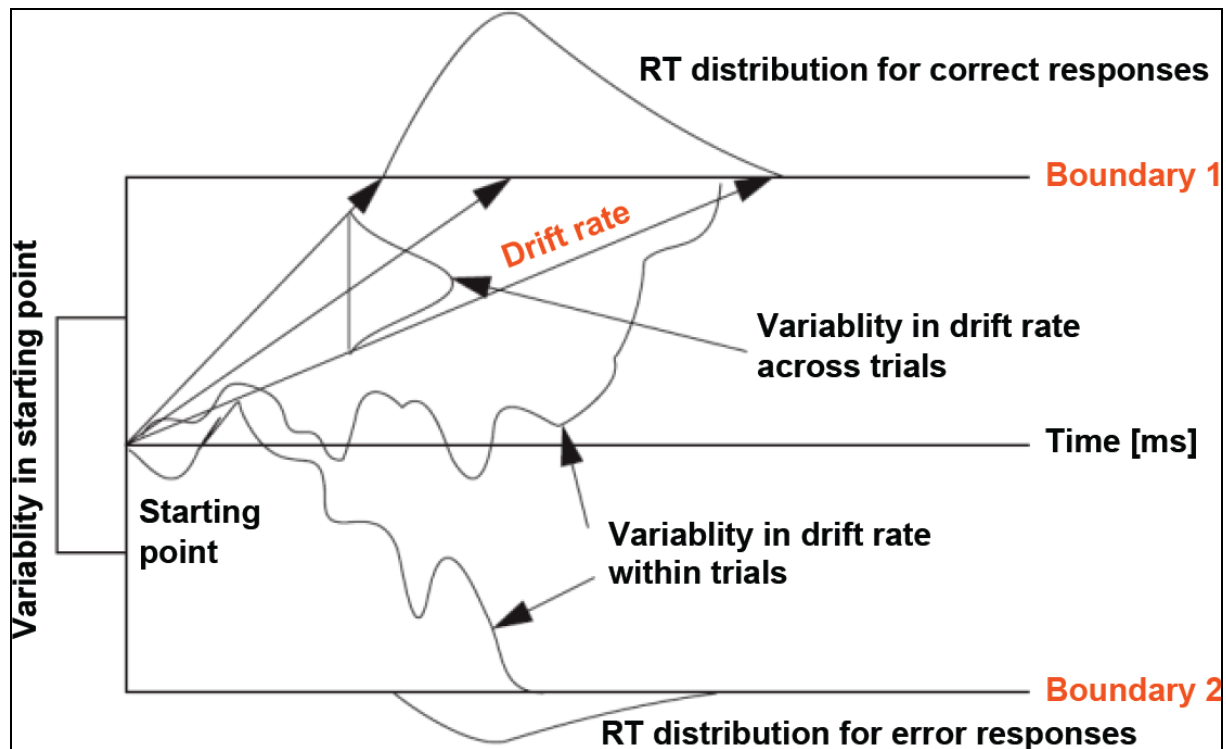


Fig.1: Diffusion model. Sensory information is continuously accumulated for or against one of two choices from a starting point until a specified boundary is reached which concludes the decision process and initiates the response. From the RT distributions for correct and error responses over trials and from the frequency of correct responses, several parameters can be estimated: the starting point, the accumulation rate of the stimulus information (drift rate), the amount of information accumulated to reach the boundary, the amount of variability within or across trials in some of these parameters. Variability in decision processing is due to noise either present in the stimulus itself, or introduced by the nervous system (modified from Ratcliff, 1978).

Interestingly, this model can not only explain behavioral outcomes quantitatively (Ratcliff et al., 1999) but parameter estimates also correspond to neurophysiological activity during decision processing as will be elaborated in the following sections.

1.3. Neurophysiology of perceptual decision making

When studying perceptual decision processing in neuroscience, four distinct but interacting systems can be differentiated: the ‘sensory system’ representing the sensory evidence; the ‘decision system’ integrating the sensory evidence and forming a decision variable; the ‘motor system’ representing the decision variable and executing a motor response, and the ‘performance monitoring system’ detecting errors and adjusting decision strategies to maximize performance (Heekeren et al., 2008). In the dissertation at hand I focus on investigating the first three systems. The concept of the decision variable accounts for priors, (sensory) evidence, and value from relevant information that is interpreted over time in order to commit the final choice (Gold and Shadlen, 2007).

1.3.1. Perceptual decision making in the visual domain - temporal dynamics

In a renowned experiment, Roitman and Shadlen (2002) found activity patterns in neurons of the lateral intraparietal area (area LIP) that suggested a temporal integration of sensory information as had been predicted from sequential sampling models. They used a motion-direction discrimination task where an array of moving dots was presented to a monkey. While some of the dots moved in one direction, others moved in random directions. The task difficulty was controlled by varying the percentage of dots moving coherently in one direction. The monkey was trained to look to the left target for leftward motion, and to the right target for rightward motion. While the monkey performed the task, the experimenters recorded activity from neurons in area LIP. Area LIP is anatomically positioned midway between the sensory-motor pathway, receiving input from areas representing the sensory evidence, e.g., the middle temporal area (area MT), and projecting to areas involved in preparing the motor output, e.g., the frontal eye field (FEF) and the superior colliculus (SC) (Andersen et al., 1992; Asanuma et al., 1985; Blatt et al., 1990; Lewis and Van Essen, 2000). About 200 ms after motion onset the firing rate began to increase until a plateau was reached. The steepness of this increase was proportional to the motion strength, i.e., the stronger the motion signal, the steeper the increase of the spike rate. This has been interpreted as neurophysiological evidence for the temporal integration of sensory information during the decision process, and matches predictions of sequential sampling models (modeled from behavioral data).

More generally, it suggests that area LIP is involved in decision processing though the computation of the decision variable might take place in other, e.g., frontal, areas. Like area LIP, the dorsolateral prefrontal cortex (DLPFC) was activated in eye-movement tasks, showed an increase in spike rate during decision processing, and a steepness of increase proportional to the motion strength (Kim and Shadlen, 1999). Furthermore, Kim and Shadlen (1999) found the activity in the left DLPFC to represent the differential output from neuronal populations in the middle temporal (MT) and medial superior temporal (MST) areas representing the different stimulus alternatives, i.e., leftward and rightward motion.

Heekeren et al. (2004), using functional magnetic resonance imaging (fMRI), tested if similar difference calculations are used in the human brain. Subjects discriminated between pictures of faces and houses with varying sensory evidence (coherence levels) whereby low sensory evidence or coherence implicated a more difficult task. Activity in category-specific regions of the ventral temporal cortex correlated with the sensory evidence for faces or houses, respectively. Furthermore, the activity in the left DLPFC (1) was more enhanced when pictures with higher coherence levels were presented compared to when pictures with lower coherence levels were shown, (2) covaried with the difference signal between face- and house-selective regions in the ventral temporal cortex, and (3) predicted behavioral performance. Their results provide indirect evidence for a comparator operation in the DLPFC and suggest comparable systems for perceptual decision processing in the monkey and human brain. Unfortunately, due to the poor time resolution of fMRI, little can be said about the relative timing of the cortical processes.

Philiastides et al. investigated the spatiotemporal characteristics of perceptual decision making using electroencephalography (EEG) and EEG-informed fMRI in humans (Philiastides and Sajda, 2006; Philiastides and Sajda, 2007; Philiastides et al., 2006). Applying a face-versus-car categorization task and single-trial analysis, they found three stimulus-locked components in the EEG data: an ‘early’ component (170 ms), a ‘late’ component (≥ 300 ms), and a ‘difficulty’ component in between the early and late component (around 220 ms). Whereas the early component showed little variability in time, the late component systematically shifted forward in time as the coherence level of the stimulus was reduced, i.e., the task became more difficult, and the strength of the difficulty component was highly correlated to the difficulty of the task. Also, the late component correlated significantly with the drift rate computed from diffusion model simulations. Using the same task in fMRI and the information from the EEG recordings to analyze the data (Philiastides and Sajda, 2007), they localized (1) the early component into regions that have been associated with

early visual processing of faces, such as the bilateral fusiform face area (FFA) with a bias to the right hemisphere (Haxby et al., 2000; Kanwisher et al., 1997). The FFA might be involved in the representation of sensory evidence rather than decision processing itself. (2) The difficulty component was localized into regions that have been associated with decision processing, such as the DLPFC (Heekeren et al., 2004), suggesting that this component represents processes of sensory evidence accumulation in order to commit a decision. (3) The late component was localized into regions that might either represent already computed decision variables or be directly involved in decision processing, such as the lateralized occipital complex (LOC) (Grill-Spector et al., 2001). To summarize, Philiastides and colleagues (Philiastides and Sajda, 2006; Philiastides and Sajda, 2007; Philiastides et al., 2006) not only spatiotemporally characterized the sensory, decision, and motor stages of perceptual decision making while human subjects processed face images but also linked it to behavior.

In the experiments described so far only changes in sensory evidence have been investigated. But, as already mentioned in section 1.1., the tradeoff between speed and accuracy (SAT) also strongly influences our decisions. Three recent fMRI studies (Forstmann et al., 2008; Ivanoff et al., 2008; van Veen et al., 2008) suggested that SAT affects the decision and motor rather than the sensory system because they found SAT-related changes in activity in decision-related brain regions including the DLPFC and parietal areas, and in pre-motor areas including the pre-supplementary motor area (SMA), SMA, and striatum. Several electroencephalography (EEG) studies addressed the temporal dynamics of neural processes underlying SAT (Osman et al., 2000; Rinkenauer et al., 2004; Sangals et al., 2002). However, they primarily focused on motor preparation and motor execution processes by analyzing the lateralized readiness potential.

Chapter 2 (study 1) of this dissertation reports at which temporal stages and in which neuroanatomical structures SAT affects human decision making in the visual domain, and whether this depends on the level of sensory evidence, i.e., task difficulty. Furthermore, it investigates whether neurophysiological activity is related to diffusion-model parameters, as theoretically the boundary can be set according to emphasis on speed or accuracy of the decision, whereas the accumulation or drift rate is determined by the quality of the sensory representation (Bogacz et al., 2010; Ratcliff and McKoon, 2008).

1.3.2. Perceptual decision making in the somatosensory domain - temporal dynamics

Recent studies suggest that decision-making mechanisms in the tactile domain are similar to those observed in the visual system. Romo and colleagues used a flutter-discrimination task where a monkey decided which of two, subsequently presented, vibratory stimuli had a higher frequency (for review, see Romo et al., 2003). Firing rates in the primary somatosensory cortex (S1) as well as the prefrontal cortex (PFC) increased with increasing stimulus frequency (Hernández et al., 2000; Romo et al., 1999), and the firing rate in S1 predicted the accuracy of the response (Salinas et al., 2000). Importantly, the activity of cells in the DLPFC was proportional to the differential activity of neural populations in the secondary somatosensory cortex (S2) that preferred high- and low-frequency vibratory stimuli, respectively. This suggests that neurons in ‘higher’ cortical areas (DLPFC) integrate sensory information processing of ‘lower’ cortical areas (S2) over time (Romo and Salinas, 2003).

Using the same task in humans, the areas activated were largely overlapping but additional areas were involved (Preuschhof et al., 2006). Activities in S1 and S2 were associated with the processing of the second stimulus. The authors concluded that the somatosensory regions represent sensory evidence to generate the decision but do not actively participate in the decision process, analogous to area MT in the visual domain (Ditterich et al., 2003). It is important to note that S1 predicted the behavioral outcome of the decision in monkeys (Salinas et al., 2000), and S1 has been shown to be connected to frontal regions, e.g., the middle frontal gyrus or Brodmann area 46/6 including the DLPFC (Hannula et al., 2010). Electrophysiological recordings combined with source estimations are necessary to examine the temporal dynamics underlying S1 activity, and define more precisely the contribution of S1 to decision processing.

Chapter 3 (study 2 and 3) of this dissertation reports at which temporal stages tactile stimulation affects human decision making by applying different levels of sensory evidence. S1 and S2 are a priori defined as regions of interest, and their contribution to decision processing is investigated. Furthermore, it is examined whether neurophysiological activity predicts the drift rate of the diffusion model, or RT.

1.4. The role of oscillatory activity in perception

In the studies mentioned above, spike rates (single-cell recordings), BOLD responses (fMRI), or event-related potentials (ERP) and therefore averages of neuronal activity in the *time domain* were used to measure neural activity. However, the spike rate of neurons might be

insensitive to some modulations while periodicity¹ and synchrony² change dramatically (Eckhorn et al., 1988; Gray et al., 1989).

Oscillatory neural activity has been investigated intensively in the context of the binding problem, i.e., the integration of various features of a complex scene or object into a coherent representation. In a revealing experiment, Tallon-Baudry and colleagues (1997) showed scrambled images to subjects and asked them to search for objects while recording EEG. For most of the subjects, the object was only visible when it was presented once, e.g., the shape of a Dalmatian dog isolated from the background. From then on, they grouped the previously unrelated elements of the physically identical stimuli into a coherent percept. Interestingly, this was accompanied by a large increase in induced³ gamma-band power over occipital sensors. While also later studies provided evidence that synchronized activity in the gamma-frequency range was instrumental for binding processes and perceptual fusion (Rose and Bichel, 2005), other studies could not find such activity patterns (Lamme and Spekreijse, 1998; Thiele and Stoner, 2003).

During recent years, additional functional roles have been suggested, e.g., that neural synchrony might modulate the efficacy of neural activation and thereby information transmission (Azouz and Gray, 2003; Salinas and Sejnowski, 2001). Correspondingly, efficient communication between different brain areas can best be achieved when they show coordinated fluctuations of excitability (Fries, 2005). Furthermore, sensory-induced oscillatory activity was predictive of behavioral measures such as RT (Gonzalez Andino et al., 2005; Womelsdorf et al., 2006). But up to date, only little is known about the role of neural oscillations in decision processing.

1.4.1. Perceptual decision making in the visual domain - oscillatory dynamics

Perceptual decision processing has also been investigated in the time-frequency domain using the motion-direction discrimination task already described in section 1.3.1. Siegel et al. (2007) found increased activity in the *gamma range* (here, 60-100 Hz) in extrastriate regions (primary visual area V1, visual area V2, visual area V3), and right area MT. Interestingly, at

¹ The frequency (measured in Hertz [Hz]) specifies how often a process is repeated in a time unit. Temporal periodicity (also measured in Hz) specifies that a process recurs at *regular* time intervals. In the dissertation at hand, I focus on alpha (~8-15 Hz), beta (~15-25 Hz), and gamma activity (~25-120 Hz) in the brain.

² Synchrony in the nervous system means that many nerve cells fire at the same time. It is accompanied by periodicity.

³ Evoked responses are characterized by a precise phase-locking to the stimulus onset. Induced responses, in contrast, have a loose relation to stimulus onset, and activity is not revealed by classical averaging techniques used for evoked responses but by time-frequency analysis (Tallon-Baudry C., Bertrand O. (1999) Oscillatory gamma activity in humans and its role in object representation. Trends in Cognitive Sciences 3:151-162.).

very low to low coherence, behavioral performance increased steeply whereas the gamma-band activity in area MT did not change significantly. In contrast, at 50 to 100 % coherence RT was identical but the gamma-band response increased strongly. Taken together, other than in the time domain, neural activity in the gamma-frequency range did not consistently predict the behavioral outcome. In another experiment, Donner et al. (2009; 2007), presented two different random dot patterns to human subjects, either at one level of motion coherence adjusted to the individual detection threshold (target), or at 0 % motion coherence (no target). After a delay of 0.5-1 s, subjects indicated their choice (yes for target, no for no target) by button press (left or right hand). Using Magnetoencephalography (MEG) and the beamformer technique for source reconstruction, they found higher *beta activity* (12-24 Hz) before correct than before erroneous decisions in the DLPFC, posterior intraparietal cortices, and to a lesser degree right area MT. Thus, beta activity levels predicted correct choices. Importantly, if no target was presented, beta activity in all three areas was larger before “no” than “yes” choices. Together this indicated that beta activity predicts the accuracy but not the content of visual decisions. Furthermore, they found choice-predictive *gamma-band activity* in the motor cortex that reflected the temporal integration of gamma-band activity in right area MT and suggested that motor plans both for “yes” and “no” choices resulted from continuously accumulating sensory evidence. This is in contrast to the findings from Siegel et al. (2007) but as Donner et al. (2009; 2007) applied one coherence level only, conclusions should be drawn with caution.

1.4.2. Perceptual decision making in the somatosensory domain - oscillatory dynamics

In the somatosensory cortex, ongoing rhythmic activity in the *alpha* (8-15 Hz, mu rhythm) and *beta* (15-25 Hz) range have been known for some time (Hari and Salmelin, 1997). Beta rhythms were identified in the motor cortex, at least partly due to an increase in GABAergic, inhibitory, post-synaptic currents onto inhibitory neurons (Jensen et al., 2005). Mechanical stimulation of the skin or movement initiation suppressed these rhythms, a process termed event-related desynchronization (ERD) (Cheyne et al., 2003; Pfurtscheller et al., 2002).

Spitzer and Blankenburg (2011) used EEG and a vibrotactile discrimination task comparable to the one already described in the time domain (cf. section 1.3.2.). After presentation of two distinct vibrotactile frequencies to different index fingers, a visual cue indicated which of the two previously presented stimuli had to be maintained in working memory for subsequent frequency discrimination against a probe stimulus. During

maintenance, alpha activity (8-13 Hz) over early somatosensory cortices was lateralized according to the cued tactile stimulus, even though the location was task-irrelevant. Importantly, the right prefrontal cortex systematically reflected the to-be-maintained frequency of the cued tactile vibration in the higher beta band (20-25 Hz) confirming a central role of dynamic β -band synchronization in human working memory.

Besides changes in the alpha and beta band due to tactile stimulation, electrical stimulation led to *gamma-frequency activity* in the somatosensory cortex (Hirata et al., 2002; Ihara et al., 2003). Recently, Bauer et al. (2006) used a Braille pattern discrimination task to study tactile spatial attention. Subjects reported the recurrence of an initially presented sample pattern in a series of up to eight test stimuli presented unpredictably to the right or left index finger. Attention was cued to one side at the beginning of each trial, and subjects performed the task at the attended side, ignoring the unattended side. They found sustained stimulus-induced *gamma-band oscillations* in S1 for attended stimuli. These stimulus-induced oscillations lasted approximately until a response was given suggesting a potentially important role of gamma-band oscillations in the decision process.

Chapter 3 (study 2 and 3) of this dissertation reports how oscillatory activity after tactile Braille stimulation at different levels of sensory evidence influences human decision making. S1 and S2 are, like in the time domain, a priori defined as regions of interest to investigate their contribution to decision processing in the time-frequency domain. Furthermore, I investigated whether neurophysiological activity predicts the behavioral outcome, i.e., whether it is correlated to the drift rate of the diffusion model, or RT.

1.5. Research questions

In three experiments, I investigated how the activity of neural populations in humans might be linked to perceptual choices.

In the first study, we presented the stimuli visually because sensory (mainly in occipital areas), associative (in frontal or parietal cortex) and (pre-)motor (in fronto-medial areas) activity can be optimally differentiated. We used an established face-house categorization task because the occurrence of some components, e.g., the N170 or M170 (Negative deflection when using EEG, or **m**agnetic field activation when using MEG), is well described, and modulations due to task difficulty are well investigated, e.g., by Philiastides et al (Philiastides and Sajda, 2006; Philiastides and Sajda, 2007; Philiastides et al., 2006). We aimed at investigating how emphasis on speed or accuracy influenced perceptual decision processing.

In particular, we asked whether the speed-accuracy tradeoff predominantly influenced phases of earlier stages of sensory processing, or motor preparation later in the decision process.

In the second and third experiment, we applied tactile stimuli to investigate the temporal dynamics of pattern discrimination and decision making within the somatosensory system. Task difficulty was varied by changing the spatial discriminability of Braille patterns. We investigated which components of neural activity were related to decision processing in sensory areas, indexed by their covariation with difficulty as well as their behavioral decision outcomes. Specifically, we asked whether (1) more difficult decisions with longer reaction times were associated with longer latencies of sensory ERP components, (2) accumulator signals similar to Roitman and Shadlen (2002) could be found, and (3) more difficult stimulus discriminations implied more sustained oscillatory activity potentially mediating neuronal interactions for recursive stimulus processing (cf. Friston, 2005; Hopfield, 1982; Romo et al., 2002).

2. Study 1 - Perceptual decision making in the visual domain using images of faces

2.1. Abstract

Decisions often necessitate a tradeoff between speed and accuracy (SAT), that is, fast decisions are more error prone while careful decisions take longer. Sequential sampling models assume that evidence for different response alternatives is accumulated over time and suggest that SAT modulates the decision system by setting a lower threshold (boundary) on required accumulated evidence to commit a response under time pressure. We investigated how such a speed accuracy tradeoff is implemented neurally under different levels of sensory evidence. Using MEG and a face-house categorization task, we show that the later decision- and motor-related systems rather than the early sensory system are modulated by SAT. Source analysis revealed that the bilateral supplementary motor areas (SMAs) and the medial precuneus were more activated under the speed instruction and correlated negatively (right SMA) with the boundary parameter, whereas the left dorsolateral prefrontal cortex (DLPFC) was more activated under the accuracy instruction and showed a positive correlation with the boundary. The findings are interpreted in the sense that SMA activity dynamically facilitates fast responses during stimulus processing, potentially by disinhibiting thalamo-striatal loops, whereas DLPFC reflects accumulated evidence before response execution.

This chapter is a modified version of: Wenzlaff H., Bauer M., Maess B., Heekeren H.R. (2011) Neural characterization of the Speed-Accuracy Tradeoff in a perceptual decision-making task. *Journal of Neuroscience*. 31(4):1254-1266.

2.2. *Introduction*

Every day when making decisions, e.g., when driving the car or playing ball, we trade off speed against accuracy (SAT), that is, fast decisions are more error prone while careful ones take longer (Bogacz et al., 2010). But how does SAT affect our decisions and how is it modulated under different levels of sensory evidence?

Three recent functional magnetic resonance imaging (fMRI) studies have identified brain regions involved in SAT (Forstmann et al., 2008; Ivanoff et al., 2008; van Veen et al., 2008). They suggest that SAT affects the decision and motor rather than the sensory system by modulating activity in association cortices including DLPFC, posterior lateral PFC and parietal areas, as well as in pre-motor areas including pre-SMA, SMA, and striatum.

Several electroencephalography (EEG) studies have addressed the temporal dynamics of neural processes underlying SAT (Osman et al., 2000; Rinkenauer et al., 2004; Sangals et al., 2002). However, they primarily focused on motor preparation and motor execution processes by analyzing the lateralized readiness potential. Hence, no inferences about the behavior of more distributed networks underlying decision processing, e.g., about the involvement of sensory systems, could be deduced from these studies.

In the present study, using MEG, we investigated at which temporal stages and in which neuroanatomical structures SAT affects decision making and whether that depends on sensory evidence. Subjects discriminated pictures of faces or houses presented under speed or accuracy instructions and at different levels of sensory evidence. We hypothesized that speed versus accuracy instructions might alter the level of activity in structures that have previously been associated with decision processing, such as the DLPFC (Heekeren et al., 2004; Kim and Shadlen, 1999). Further, we hypothesized that neurophysiological SAT effects should correlate with parameters from sequential sampling models.

2.3. *Materials and Methods*

2.3.1. Subjects

Twelve subjects (six females; age range 20 to 30 years) participated in the study, after having provided written informed consent in accordance with the guidelines and approval of the Max Planck Institute for Human Development, Berlin, Germany. All had normal or corrected to normal vision and no reported history of neurological problems. Handedness, i.e., the laterality quotient, was 96.7 ± 2.31 as assessed by the Edinburgh Handedness inventory (Oldfield, 1971).

2.3.2. Stimuli

We used the same set of 36 grayscale images of faces and houses as in Heekeren et al. (2004) (fig.2). Fast Fourier transformation was applied to separate amplitude and phase matrices of each image. Amplitudes of all images were averaged resulting in an identical frequency spectrum for all images. The phase matrix of each image was scrambled by adding a random offset of 0 to 100 % (in 1 % steps) to the original phase matrix. Inverse fast Fourier transformation of the average amplitude and individual phase matrices resulted in 36 face and 36 house images in different levels of sensory evidence (coherence, COH) that were used for the training and experiment.

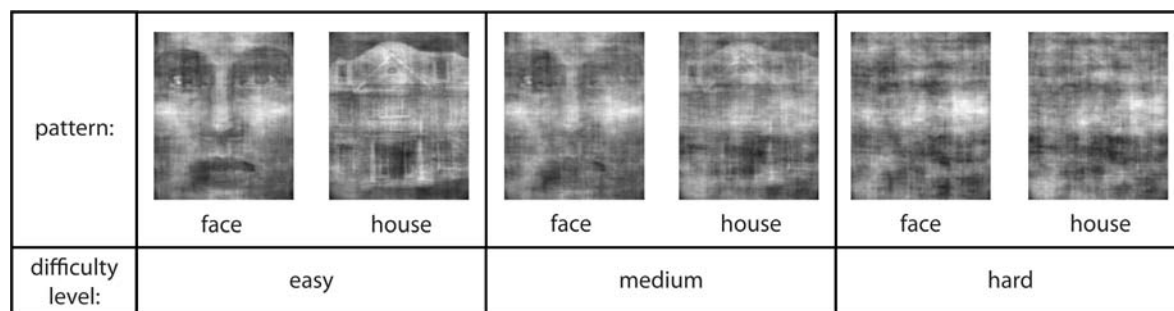


Fig.2: Images of faces and houses were presented on a screen. Difficulty was manipulated by adding a random offset to the original phase matrix of the image. Here, three examples are given for (left) high, i.e., easy, (middle) medium, and (right) low sensory evidence, i.e., hard difficulty level.

For feedback about their performance (cf. below), subjects heard high- or low-frequency tones via an MEG-compatible headphone system (Tip-300, Viasys Healthcare, Hoechberg, Germany) at 50dB.

Visual and auditory stimulation was controlled by an IBM-compatible computer and Presentation software (Neurobehavioral Systems Inc., Albany, CA, USA). To present the images (3.44x4.01 degrees visual angle), a projector with digital light processing (Panasonic Corporation, Osaka, Japan) was used with a 1024 x 768 resolution and a 60 Hz refresh rate. Pictures were shown in the center of a back projection screen (Elekta Neuromag, Helsinki, Finland) with a 0.6 grey filter and an illumination of 10.30.

2.3.3. Task

Subjects performed a two-alternative forced-choice task. Pictures of faces and houses were presented and subjects indicated their subjective report via an MEG-compatible response box by pressing the left button with their left thumb when they perceived a face and the right button with their right thumb when they perceived a house.

Subjects were tested on three successive days. In the *training* session (day 1), face and house stimuli were presented at six different COH levels (41, 44, 47, 50, 54, 58 %). They were instructed to respond as *fast and as accurately* as possible within 3000 ms. They received auditory feedback after each trial: a pleasant high-frequency tone following a correct, and an unpleasant low-frequency tone following an incorrect choice.

To define three COH levels for the experiment according to the individual performance levels, we computed a maximum-likelihood fit of a cumulative Weibull function

$$p = 1.0 - 0.5 * e^{-(x / \alpha_1)^{\beta_1}}$$

where p is the proportion of correct choices, x is the spatial phase coherence level of the stimuli, and α_1 and β_1 are free parameters of the function fitted to the data. We used the 'FitWeibTAFC.m' and 'FitWeibAlphTAFC.m' functions of the Psychophysics Toolbox (Brainard, 1997) to estimate α_1 and β_1 . With these values we computed the psychometric function (WeibAlphTAFCFitFun.m) to estimate the spatial phase coherence levels of the face and house stimuli corresponding to the individual performance levels of 95, 82 and 70 % correctness.

The RT was defined as the period between the onset of the visual stimulus and the button press. To estimate the three average RTs for the above chosen spatial phase coherence levels (matching individual performance levels), we fitted a logistic function to the RT data obtained from the training session:

$$y = 1 / (1 + 10^{-(\alpha_2 * x + \beta_2)})$$

where y is the RT for a given stimulus x (x is again the spatial phase coherence level), and α_2 and β_2 are free parameters of the function that are fitted to the RT data using the function 'FitLogistic.m'. With the fitted parameters we computed the chronometric function ('ComputeLogistic.m') to obtain the expected mean RTs for the above chosen individual spatial coherence levels .

Pictures at the three COH levels (matching individual performance levels) were shown in the following experimental sessions and the corresponding mean RT was used to determine the speed criterion in the speed condition of the experimental sessions.

In the *experimental* sessions (day 2 and 3), images of faces or houses at the three chosen COH levels were presented in random order. Subjects were further instructed on each individual trial to respond *either as fast or as accurately* as possible (SAT). Thus, stimuli were presented in a 2x3x2 factorial design (face and house stimuli; three COH levels; speed or accuracy instruction). Two identical experimental sessions were conducted on successive days to gain a sufficient number of trials for each of the conditions. Prior to the *training* session and *experimental* sessions, subjects completed 100 practice trials with a similar procedure to assure consistent performance during the *training* and *experimental* sessions.

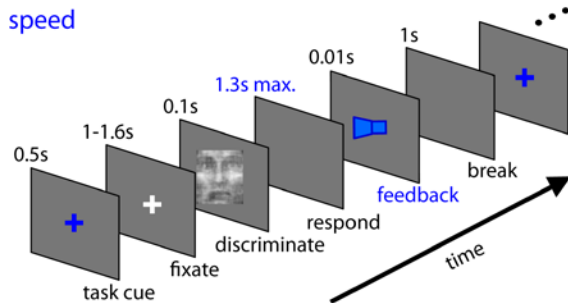
One block consisted of 36 trials, 18 face and 18 house trials with six (*training*) or three (*experiment*) COH levels in random order. Speed and accuracy instructions could change every two blocks in random order. At the end of each block, the subjects received feedback about their mean RT and accuracy (*training* and *experiment*). The *training* session consisted of 24 blocks resulting in 864 trials, 72 per condition. Each *experimental* session consisted of 24 blocks, twelve with accuracy and twelve with speed instructions. The two experimental sessions resulted in 144 trials per condition.

At the beginning of each trial, a colored cross was shown for 500 ms (red for speed, green for accuracy instruction) (fig.3). This task instruction cue was immediately followed by a white fixation cross (presentation time varying from 1000 to 1600 ms) which signaled subjects not to blink or move their eyes. Subsequently, a picture of a face or a house was presented for 100 ms in one out of three possible COH levels matching individual performance levels of 95, 82, and 70 % correctness, respectively. Under accuracy instructions, subjects had a maximum of 3000 ms to respond (otherwise the response was not counted) and heard an unpleasant low-frequency tone after an incorrect decision. Under speed instructions, they had a maximum of 1300 ms to respond and negative feedback was given if their RT was slower than their expected mean RT corresponding to the particular COH level presented, irrespective of the correctness of their decision. No positive feedback was given in

the experimental sessions. Button press and feedback, if given, were followed by a 1000 ms break before the next trial started.

task instruction:

speed



accuracy

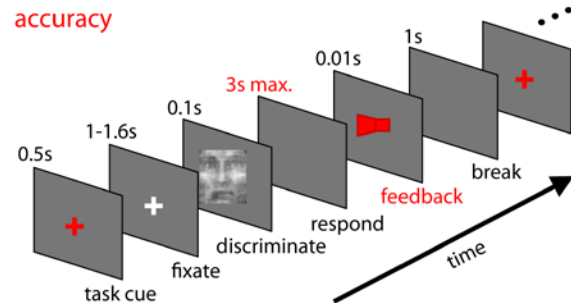


Fig.3: Experimental design. At each trial, initially one of two differently colored task cues (cross) indicated whether subjects should answer as fast or as accurately as possible (SAT). Subsequently, images of faces or houses at three different levels of sensory evidence (coherence, COH) were presented in random order. Subjects responded with a left button press with their left thumb when they perceived a face, and with a right button press with their right thumb when they perceived a house. Feedback, a low-frequency tone, was given when subjects responded slower than their expected mean RT corresponding to the particular COH level presented (speed instruction), or incorrectly (accuracy instruction). Please find further details in the text.

2.3.4. Procedure

Behavioral and electrophysiological data were recorded simultaneously in an electromagnetically shielded room (Vacuumschmelze, Hanau, Germany) using the Presentation software (Neurobiological Systems Inc., Albany, CA, USA) and Neuromag software (Elekta Neuromag, Helsinki, Finland). MEG data were acquired with a 306 channel Vectorview MEG (Elekta Neuromag, Helsinki, Finland), 204 planar gradiometers and 102 magnetometers, at 102 locations above the subject's head. Magnetic fields were sampled at 700 Hz with an online band-pass filter of 0.03 to 230 Hz. Two pairs of electrodes recorded vertical and horizontal bipolar electrooculograms (fig.4). Subjects' head positions were recorded by five continuous head position indicator (cHPI) coils (two placed on the auricles, three on the forehead). These coils emit small magnetic fields that are measured by the MEG sensors and can be used to locate each coil to correct for potential movements of the subject's head every 200 ms (fig.4).



Fig.4: (left) Two pairs of electrodes recorded vertical and horizontal bipolar electrooculograms (EOG). Five continuous head position indicator (cHPI) coils, two placed on the auricles (not visible here), three on the forehead (only two visible here), recorded the subjects' head positions. (right) Electromagnetically shielded room with the 306 channel Vectorview MEG, the back projection screen, and a subject holding the response button box.

2.3.5. Behavioral data analysis

There are four types of contaminants of behavioral data: (1) outliers (data points are out of the normal range of observation), (2) fast guesses (response occurs before the stimulus inspection), (3) random guesses (stimulus miss leads to a guess), and (4) delayed startups (response is inappropriately delayed). Outliers, defined as data above two standard deviations (sd) from the mean, were removed (a total of 4.23 %). This strict criterion was chosen because we applied no additional outlier treatment for the diffusion model analysis (next paragraph). After the outliers were removed, the shortest RT was > 250 ms, i.e., fast guesses were removed, too. We applied no additional contaminant treatment.

Mean RT and accuracy were analyzed, and separate two-way repeated-measures analyses of variance (ANOVAs) with the factors COH (high vs. medium vs. low coherence) and SAT (speed vs. accuracy instructions) were calculated to test for statistically significant differences between the experimental conditions.

2.3.6. Diffusion model analysis

The diffusion model assumes that decisions in two-alternative forced-choice tasks are made by a stochastic process that accumulates sensory information over time from a starting point toward one of two response thresholds (boundaries). Once either of the boundaries is reached, a response is initiated. For more detailed explanation, see chapter 1.2.

A classical interpretation in the context of the diffusion model is that changes in the emphasis of either speed or accuracy of a decision (here: SAT) are instantiated by changes in boundary whereas changes in the quality of the stimulus information (here: COH) are reflected by changes in drift rate (Ratcliff and McKoon, 2008). Furthermore, Rinkenauer et al. (2004) found that SAT also affects nondecision components of the decision process; more precisely, the speed instruction might lead to a decrease in encoding time. Therefore, calculations of the boundary, the drift rate, and the nondecision time were of special interest in this experiment.

We used the diffusion model analysis toolbox (DMAT, <http://ppw.kuleuven.be/okp/dmatoolbox/>) for parameter estimation. Here, a multinomial likelihood function expressing the probability of observing a certain proportion of responses in five RT bins was maximized for good parameter estimations (e.g., Vandekerckhove and Tuerlinckx, 2007). Four models were nested in the following order: (1) All parameters were restricted to be equal across the conditions, (2) the boundary was free to vary across conditions, (3) additionally, the drift rate was free to vary across conditions, (4) additionally, the nondecision time was free to vary across conditions. Nesting is advantageous as each set of parameter estimates is used as an initial guess for the next model, leading to an increase in efficiency, especially when choosing more restrictive models first and less restrictive later (Vandekerckhove and Tuerlinckx, 2008). To choose the best model for each subject, we used the Bayesian Information Criterion (BIC) and a likelihood ratio test under the assumption of an approximate chi-square distribution. Changes in the order of parameter release revealed identical results. Outliers were defined as RTs above two sd from the mean and removed before model calculations. After outliers were removed, the shortest RT was > 250 ms, i.e., fast guesses were removed, too. No additional outlier treatment was applied.

Separate two-way repeated-measures ANOVAs with the factors SAT and COH were calculated for the boundary, the drift rate, and the nondecision time, respectively, to test for statistical significance between the experimental conditions.

2.3.7. MEG time-domain analysis

Sensor-space data were preprocessed with the Neuromag software (Elekta Neuromag, Helsinki, Finland). Measured magnetic fields were corrected for head movements using the information from the cHPI coils. Thereby, Maxfilter® was applied to interpolate the measured data on a default-gradiometer position and to suppress external interferences (Taulu et al., 2004; Taulu et al., 2005). Bad channels were excluded after visual inspection and also interpolated by the Maxfilter® procedure. All further analysis was conducted using the MNE software provided by M. Hämäläinen, MGH, Boston, MA, USA (<http://www.nmr.mgh.harvard.edu/martinos/userInfo/data/sofMNE.php>).

Continuous MEG recordings were divided into epochs of 1200 ms, time-locked either to the stimulus (-200 to 1000 ms) or the response (-1000 to 200 ms). Epochs were artifact-corrected by excluding changes greater than 200 pT/m (gradiometers), 4 pT (magnetometers), or 100 μ V (electrooculogram, EOG). For the response-locked analysis, the same epochs were used as for the stimulus-locked analysis. Epochs were low-pass filtered with 25 Hz and averaged separately per condition. Baseline corrections were applied on the epoched stimulus- and response-locked data with respect to a 200 ms prestimulus baseline. Data were averaged across subjects. Two subjects had to be excluded from the MEG analysis due to technical problems. To detect components of interest, MEG amplitudes were averaged using a sliding time window of 50 ms from 0 to 400 ms for the stimulus-locked analysis, and from -400 to 0 ms for the response-locked analysis. 400 ms was chosen as this was the fastest mean RT (speed, high sensory evidence). The vector magnitude of each pair of orthogonal planar gradiometers was computed reflecting the magnetic field strength regardless of the orientation of the gradient. The resultant magnitude displays maximal activity in the sensors located directly above the source (Bastiaansen and Knösche, 2000).

Only correct trials, i.e., when subjects correctly identified the stimulus category irrespective of the given feedback, were included in the analysis. The analysis was restricted to face trials (for explanation, see methods section describing the task). To test for statistical significance between the experimental conditions, we calculated two-way repeated-measures ANOVAs with the factors SAT and COH. The significance threshold was set to the conservative value of 0.001. We did not apply a standard correction of the multiple comparison problem, e.g. Bonferroni correction, since this assumes independence of the data which is neither the case in the temporal nor in the spatial domain.

2.3.8. Prediction of diffusion model parameters from MEG time-domain data

To investigate whether the neural activity recorded with MEG could predict diffusion model parameters calculated from behavioral data, we correlated the amplitudes of the sensor space MEG components with the diffusion model parameters for each individual. As SAT showed a significant effect on the boundary (see results), we correlated the differential (accuracy-speed) MEG components showing an SAT effect with the differential (accuracy-speed) boundary. As COH had a significant effect on drift rate and boundary (see results), we correlated the differential (high-low COH) MEG components showing a COH effect with the differential (high-low COH) drift rate and the differential (high-low COH) boundary. For consistent description of the data, we also correlated the differential (accuracy-speed) MEG components showing an SAT effect with the differential (accuracy-speed) drift rate.

2.3.9. sLORETA source analysis

Cortical reconstruction

Individual T1-weighted MRI images were recorded with a 3T MRI scanner (Magnetom Trio, Siemens AG, Germany). Individual cortical surfaces were reconstructed with the Freesurfer software (<http://surfer.nmr.mgh.harvard.edu/>) by cutting off tissue which did not correspond to the brain (Ségonne et al., 2004), segmenting white matter (Fischl et al., 2002), estimating the boundary between gray and white matter, and tessellating the cortical surface for each hemisphere (Dale et al., 1999). The MRI coordinate system was transformed into the MEG coordinate system by aligning the individual white matter surface with the cHPI coil positions and approximately 40 additional points on the head surface recorded with the Polhemus FASTRAK 3D digitizer.

Source reconstruction

As a volume conductor, we used individual boundary element models with one compartment, namely the inner skull surface of the above mentioned reconstructed individual cortical surface. A single compartment volume conductor is widely considered to be sufficient to model MEG data (e.g., Hämäläinen and Sarvas, 1989). Individual white matter surfaces were estimated digitally by approximately 150,000 vertices for each hemisphere. Source spaces were derived by downsampling these vertices to about 5000 dipoles, resulting in about one dipole in ten square millimeters. For the inverse solution, the orientation of each dipole was restricted to be almost orthogonal to the cortical surface (loose factor of 0.2). The individual brain activity was computed with the sLORETA method (Pascual-Marqui, 2002; Pascual-

Marqui et al., 2002). To average across subjects, the individual cortical representations were interpolated to the inflated cortical surface of one subject and subsequently averaged (Fischl et al., 1999a; Fischl et al., 1999b).

For source analysis, we adjusted the time windows to the epochs where significant differences were found in sensor space. To provide statistical maps of the source results, we calculated whole-brain (20484 vertex locations) two-way repeated-measures ANOVAs for the stimulus- and response-locked analysis with the factors SAT and COH and a significance threshold of 0.001. We labeled regions of interest (ROIs) by calculating cytoarchitectonic probabilities at defined MNI coordinates using the SPM8 Anatomy Toolbox, version 1.7b (http://www.fz-juelich.de/inm/inm-1/spm_anatomy_toolbox). While some anatomical probability maps are very detailed, e.g., for motor cortices, maps for prefrontal regions are provided for Brodmann area (BA) 44 and BA45 only (Brodmann, 1909). For labeling of prefrontal regions we therefore used the Talairach Applet (<http://www.talairach.org/daemon.html>). It labels coordinates in the standardized Talairach space according to the atlas of Talairach and Tournoux (1988). The Talairach Applet also provides structural probability maps but currently integrates fewer structures than the SPM8 Anatomy Toolbox.

2.4. Results

Data are reported for ten subjects who indicated whether they saw a face or a house by pressing the left button with their left thumb when they perceived a face and the right button with their right thumb when they perceived a house (fig.2, 3). In different blocks they were cued to respond either as fast or as accurately as possible (SAT). Sensory evidence of the stimuli (COH) was manipulated by changing the phase coherence of the pictures according to individual performance of 95, 82 and 70 % (fig.2). In the present report, we restricted the analysis to the face stimuli for two reasons. Firstly, face and house stimuli entail different sensory processes (e.g., Haxby et al., 2000; Kanwisher et al., 1997). We used the face stimuli to assure the occurrence of the M170, a component involved in sensory processing that is extensively described in the literature (e.g., Liu et al., 2000; Swithenby et al., 1998). Secondly, motor processing for the two types of stimuli differed because subjects were asked to press a left button with their left thumb when they perceived a face, and a right button with their right thumb when they perceived a house.

2.4.1. Behavioral data

In the speed compared to the accuracy condition, subjects showed significantly faster RTs ($F_{(1,9)} = 21.42$, $p = 0.0012$) (fig.5A) and committed more errors ($F_{(1,9)} = 9.89$, $p = 0.012$) (fig.5B). With decreasing COH, subjects had slower RTs ($F_{(2,9)} = 30.52$, $p < 0.001$) (fig.5A) and lower % correct ($F_{(2,9)} = 104.43$, $p < 0.001$) (fig.5B). Interactions between SAT and COH were significant for RT ($F_{(1,9)} = 9.01$, $p = 0.0019$) indicating that RT differences between speed and accuracy conditions were larger with decreasing COH. As the interaction was ordinal, main effects could also be interpreted. The interaction was not significant for % correct ($F_{(1,9)} = 2.28$, $p = 0.13$). Average values per condition (speed versus accuracy and high versus medium versus low coherence) and statistics are presented in table 1.

2.4.2. Diffusion model data

According to the classical interpretation of the diffusion model, changes in the speed-accuracy tradeoff primarily affect the boundary (BO) while changes in the quality of sensory information (COH) primarily affect the drift rate (DR) (e.g., Ratcliff and McKoon, 2008). Additionally, Rinkenauer et al. (2004) found the nondecision time to be shorter under speed

than accuracy instructions. Therefore, these three parameters were of special interest here. To calculate the diffusion model, four models were nested in the following order: (1) all parameters were restricted to be equal across the conditions, (2) the boundary was free to vary across conditions, (3) additionally, the drift rate was free to vary across conditions, (4) additionally, the nondecision time was free to vary across conditions (see materials and methods). For all subjects, the model fit improved significantly when leaving boundary and drift rate free (model 3) compared to when only leaving the boundary free (model 2). For five out of ten subjects, BIC values revealed a significantly better fit when leaving additionally the nondecision time free (model 4). Accordingly, we chose the 'best fit' model for each subject: for five subjects, only boundary and drift rate were allowed to vary freely across conditions whereas the nondecision time was restricted to be equal across conditions. For the other five subjects, all three parameters were allowed to vary freely across conditions.

As expected, under speed compared to accuracy conditions the boundary was significantly lower ($F_{(1,9)} = 10.35$, $p = 0.011$) (fig.5D) but the drift rate did not differ significantly ($F_{(1,9)} = 1.66$, $p = 0.23$) (fig.5C). Speed versus accuracy conditions also had no effect on the nondecision time ($F_{(1,9)} = 2.57$, $p = 0.14$). With decreasing COH, the drift rate decreased ($F_{(2,18)} = 11.27$, $p < 0.001$) (fig.5C), and the nondecision time did not differ significantly ($F_{(2,18)} = 2.20$, $p = 0.14$) (not shown here), also meeting the expectations. Surprisingly, the boundary also showed a significant COH effect ($F_{(2,18)} = 4.89$, $p < 0.020$) (fig.5D). Interactions between SAT and COH were not significant for any of the parameters (boundary: $F_{(2,18)} = 1.80$, $p = 0.19$; drift rate: $F_{(2,18)} = 0.28$, $p = 0.76$; nondecision time: $F_{(2,18)} = 3.08$, $p = 0.071$). For the average values as well as statistics of the diffusion model parameters we refer the reader to table 1.

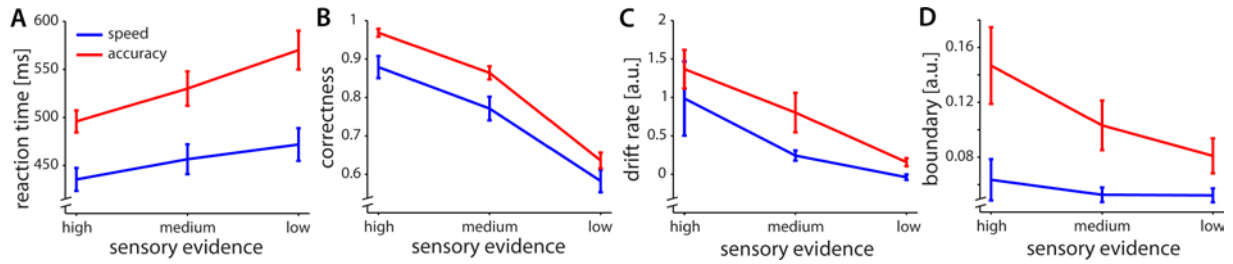


Fig.5: Behavioral and modeling results. Under the speed compared to the accuracy instruction, subjects showed significantly (A) faster RTs ($F_{(1,9)} = 21.42$, $p = 0.0012$) and (B) lower correctness ($F_{(1,9)} = 9.89$, $p = 0.012$). Furthermore, (D) the boundary of the diffusion model was significantly lower under speed than accuracy conditions ($F_{(1,9)} = 10.35$, $p = 0.011$) but was neither significantly different for (C) the drift rate ($F_{(1,9)} = 1.55$, $p = 0.23$) nor the nondecision time ($F_{(1,9)} = 2.57$, $p = 0.14$). With decreasing COH, subjects showed (A) slower RTs ($F_{(2,18)} = 30.52$, $p < 0.001$), (B) higher error rates ($F_{(2,18)} = 104.43$, $p < 0.001$), (D) lower boundaries ($F_{(2,18)} = 4.89$, $p = 0.020$) (for explanation see text), and, as expected, (C) lower drift rates ($F_{(2,18)} = 11.27$, $p < 0.001$) as well as no significant differences in nondecision time ($F_{(2,18)} = 2.20$, $p = 0.14$). Interactions between SAT and COH were significant only for RTs ($F_{(2,18)} = 9.01$, $p = 0.0019$) indicating that with decreasing COH, RT differences between speed and accuracy conditions were larger. As the interaction is ordinal, main effects could also be interpreted. Error bars present ± 1 standard error of the mean (SEM).

	Experimental conditions						Main effect SAT		Main effect COH		Interaction SAT x COH	
	Speed, High COH	Speed, medium COH	Speed, low COH	Accuracy, high COH	Accuracy, medium COH	Accuracy, low COH	$F_{(1,9)}$	p	$F_{(2,18)}$	p	$F_{(2,18)}$	P
Reaction time [ms]	435	456	472	496	530	570	21.42	0.0012	30.52	<0.001	9.01	0.0019
% correct	0.88	0.77	0.58	0.97	0.86	0.64	9.89	0.012	104.43	<0.001	2.28	0.13
Bondary	0.064	0.053	0.052	0.15	0.10	0.081	10.35	0.011	4.89	0.020	1.80	0.19
Drift rate	0.99	0.24	0.04	1.37	0.80	0.16	1.66	0.23	11.27	<0.001	0.28	0.76
Nondecision time	418	413	415	409	440	447	2.57	0.14	2.20	0.14	3.08	0.071

Table 1: Average values and statistics (two-way repeated-measures analysis of variance) for behavioral data (reaction times and percentage of correct responses), and diffusion model parameters (boundary, drift rate and nondecision time).

2.4.3. Effects of visual stimulation in the time domain

All MEG sensor data were baseline-corrected to the period before stimulus onset (-200 to 0 ms) and MEG amplitudes were averaged using a sliding time window of 50 ms. The sensor data show the combined measurements of orthogonal planar gradiometers, reflecting the absolute strength of stimulus-evoked neural activity with a spatial peak in sensors closely overlying its cortical source (Bastiaansen and Knösche, 2000). To test for statistical significance, we calculated two-way repeated-measures ANOVAs for the stimulus- and

response-locked analysis with the factors SAT and COH and a significance threshold of 0.001.

To localize these components, we conducted a distributed source analysis (standardized Low Resolution Electromagnetic Tomography, sLORETA) for the time windows showing significant effects in the sensor space, and evaluated significance again using repeated-measures ANOVAs for the stimulus- and response-locked analysis with the factors SAT and COH and a significance threshold of 0.001.

We correlated the amplitudes of the sensor space MEG components with the diffusion model parameters for each individual to investigate whether the neural activity recorded with MEG could predict diffusion model parameters calculated from behavioral data. As SAT showed a significant effect on the boundary, we correlated the differential (accuracy-speed) MEG components showing an SAT effect with the differential (accuracy-speed) boundary. As COH had a significant effect on drift rate and boundary, we correlated the differential (high-low COH) MEG components showing a COH effect with the differential (high-low COH) drift rate and the differential (high-low COH) boundary. For consistent description of the data, we also correlated the differential (accuracy-speed) MEG components showing an SAT effect with the differential (accuracy-speed) drift rate.

We identified four MEG components that differed significantly between the speed and the accuracy condition, two in the stimulus-locked and two in the response-locked analysis. Furthermore, five components differed significantly with respect to COH, four in the stimulus-locked and one in the response-locked analysis. No significant interactions between SAT and COH manipulations were found. In the following sections we describe each of the components, the corresponding source localization results, and their correlation with the appropriate diffusion model parameter(s) in temporal order, starting with significant SAT effects.

2.4.3.1. SAT component between 275 and 325 ms after stimulus onset in the right SMA negatively correlated with the boundary

A right medio-frontal sensor showed a greater MEG amplitude under the speed instruction than the accuracy instruction between 275 and 325 ms after stimulus onset ($F_{(1,9)} = 23.21$, $p < 0.001$) (fig.6A). The sensor with the significant effect was also the one with the greatest activity in the difference topography (accuracy-speed) (fig.6B). The time course of activity of

this sensor showed higher activity under speed than accuracy instructions between 275 and 325 ms (fig.6C). Source localization during the epoch of interest localized the component in the right SMA, BA6, with a probability of 90 % [70-100 %], central MNI coordinates x: 6, y: -13, z: 71 (fig.6D). Similar to the results in the sensor space, the activity in the source space showed greater activity under the speed than the accuracy instruction ($F_{(1,9)} = 25.64$, $p < 0.001$). Difference (accuracy-speed) in the sensor space MEG amplitude and the boundary were highly negatively correlated ($r = -0.85$, $p = 0.0016$) (fig.6E). On the contrary, differential MEG activity and drift rate were not significantly correlated ($r = -0.52$, $p = 0.11$).

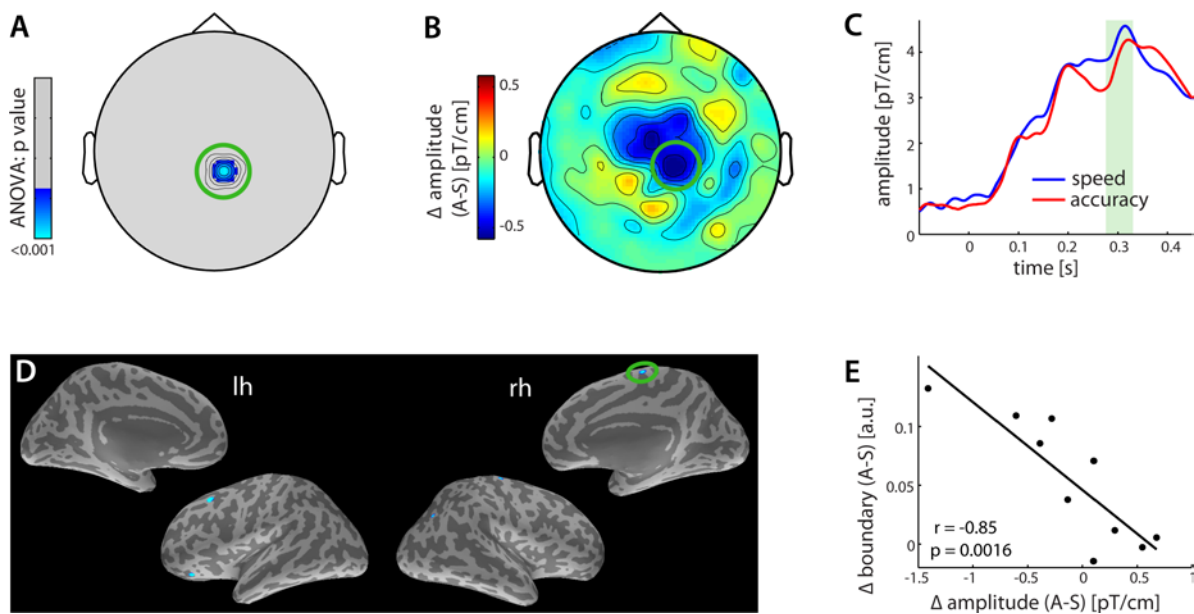


Fig.6: SAT effect between 275 and 325 ms after stimulus onset in the right SMA negatively correlated with the boundary. (A) Significant SAT effect on the MEG amplitude during the epoch of interest in a sensor located medio-frontally above the right hemisphere ($F_{(1,9)} = 23.21$, $p < 0.001$). (B) Group average of difference topography (accuracy-speed) of the MEG activity during the epoch of interest. (C) Time course of this sensor of interest in speed and accuracy instructions. Stimulus onset at 0 ms. The epoch of interest is highlighted by a green box showing higher activity under speed than accuracy conditions. (D) Significant SAT effect on the MEG amplitude during the epoch of interest was localized in the right SMA, BA6, central MNI coordinates x: 6, y: -13, z: 71 ($F_{(1,9)} = 25.64$, $p < 0.001$). (E) Highly significant negative correlation during the epoch of interest between the differential (accuracy-speed) sensor space MEG amplitude and the differential (accuracy-speed) boundary ($r = -0.85$, $p = 0.0016$), one correlation point per subject.

2.4.3.2. *SAT component between 300 and 350 ms after stimulus onset in the left SMA not significantly correlated with the boundary*

A left medio-frontal sensor showed a greater MEG amplitude under the speed than the accuracy instruction between 300 and 350 ms after stimulus onset ($F_{(1,9)} = 24.04$, $p < 0.001$)

(fig.7A). The sensor showing the significant effect also showed the greatest activity in the difference topography (accuracy-speed) (fig.7B), together with the aforementioned sensor localized in the right SMA (fig.7B). The time course of the activity under speed and accuracy instructions of this sensor showed that higher activity levels under speed than accuracy instructions started around 220 ms and thereafter stayed on these activity levels (fig.7C). Source localization during the epoch of interest localized the component in the left paracentral lobule, BA6, with a probability of 70 % [50-80 %] whereas the probability for the anterior part of the primary motor cortex (BA4a) was 10 % only, central MNI coordinates x: -2, y: -15, z: 71 (fig.7D). The medial BA6 includes SMA, pre-SMA and the supplementary eye field (Nachev et al., 2008) but the anatomical coordinates argue against pre-SMA along the anterior-posterior axis (Johansen-Berg et al., 2004) and against SEF along the dorsal-ventral axis (Grosbras et al., 1999). Therefore we label this area left SMA. As for the sensor-space analysis, the activity in the source space showed greater activity under the speed instruction than the accuracy instruction ($F_{(1,9)} = 23.72$, $p < 0.001$). The differential sensor space MEG activity was neither significantly correlated with the boundary ($r = 0.26$, $p = 0.47$) nor the drift rate ($r = 0.55$, $p = 0.10$).

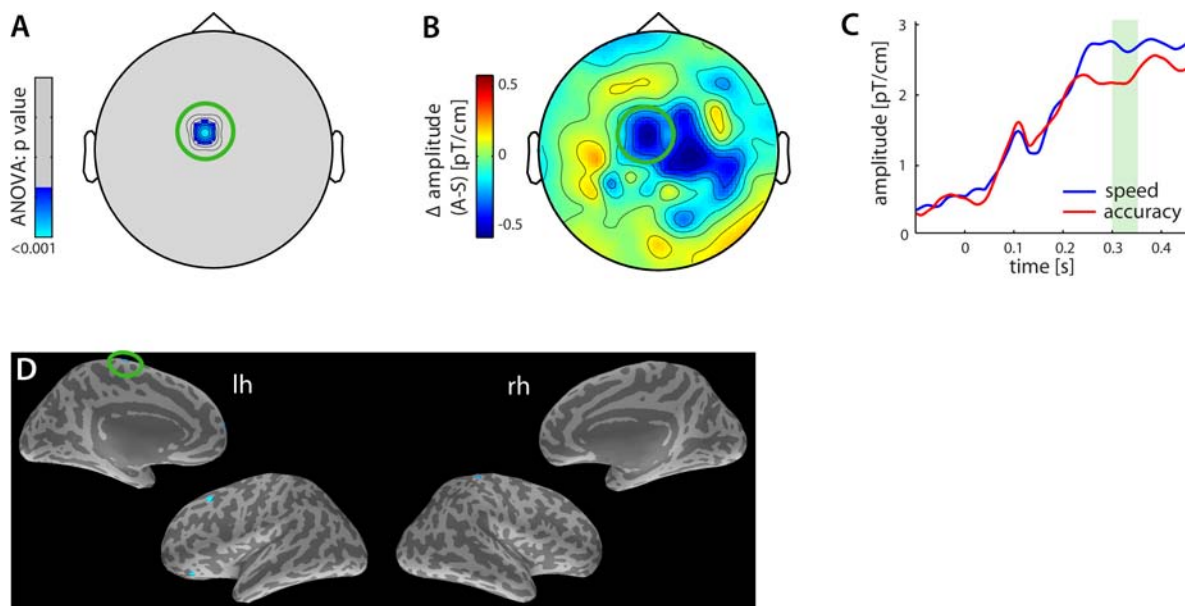


Fig.7: SAT effect between 300 and 350 ms after stimulus onset in the left SMA not correlated with the boundary. (A) Significant SAT effect on the MEG amplitude during the epoch of interest in a sensor located medio-frontally above the left hemisphere ($F_{(1,9)} = 24.04$, $p < 0.001$). (B) Group average of difference topography (accuracy-speed) during the epoch of interest. (C) Time course of this sensor of interest under speed and accuracy instructions. Stimulus onset at 0 ms. The epoch of interest is highlighted by a green box showing higher activity under speed than accuracy instructions. (D) The SAT effect on the MEG amplitude during the epoch of interest was localized in the left SMA, BA6, central MNI coordinates $x: -2$, $y: -15$, $z: 71$ ($F_{(1,9)} = 23.72$, $p < 0.001$).

2.4.3.3. SAT component between 200 and 150 ms before the response in the right precuneus not significantly correlated with the boundary

A medio-parietal sensor showed a greater MEG amplitude under the speed than the accuracy instruction between 200 and 150 ms before the response ($F_{(1,9)} = 23.59$, $p < 0.001$) (fig.8A). The sensor showing the significant effect also showed the greatest activity in the difference topography (accuracy-speed) (fig.8B). The time course of the activity under speed and accuracy instructions measured on this sensor showed that greater activity under the speed than the accuracy instruction was most pronounced between 220 ms and 150 ms before the response (fig.8C). Seemingly greater activity under accuracy than speed instructions from around 500 to 300 ms before the response is likely due to the different mean RTs under speed and accuracy instructions and hence different stimulus-onset times in this response-locked time reference, i.e., reaction time effects. Source localization during the epoch of interest localized this component in the right precuneus (no probability given), BA31, central MNI coordinates $x: 14$, $y: -59$, $z: 22$ (fig.8D). As for the sensor space data, in the source space the precuneus showed greater activity under the speed than the accuracy instruction

($F_{(1,9)} = 29.14$, $p < 0.001$). The differential sensor space MEG activity was neither significantly correlated with the differential boundary ($r = -0.33$, $p = 0.35$) nor with the differential drift rate ($r = -0.14$, $p = 0.70$).

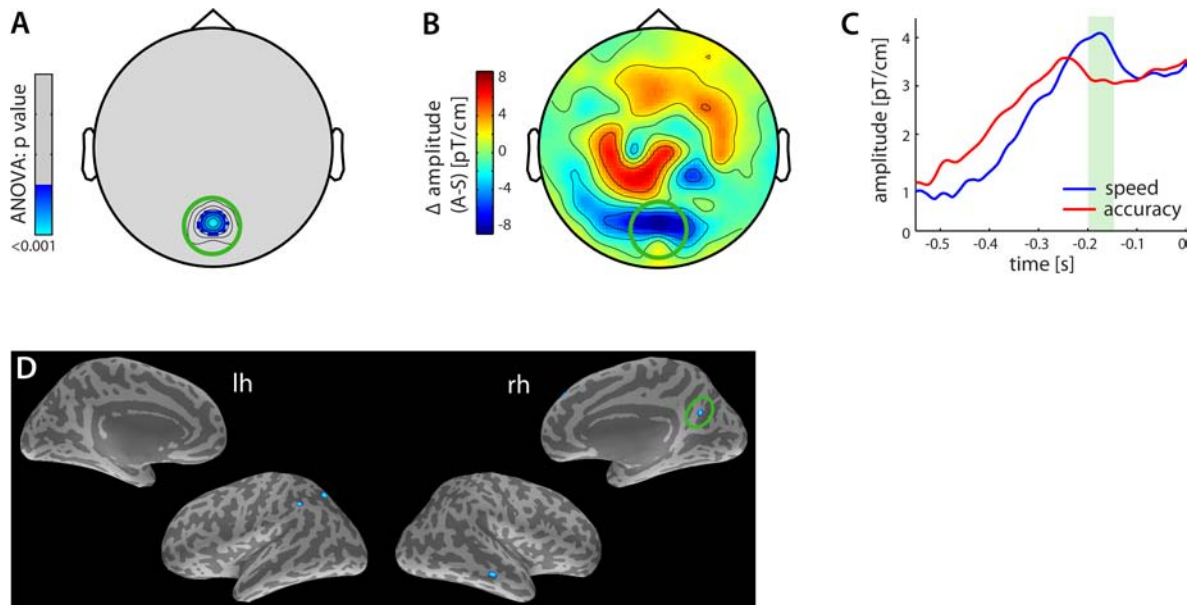


Fig.8: SAT effect between 200 and 150 ms before the response in the medial precuneus not correlated with the boundary. (A) Significant SAT effect on the MEG amplitude during the epoch of interest in a right parietal sensor ($F_{(1,9)} = 23.59$, $p < 0.001$). (B) Group average of difference topography (accuracy-speed) during the epoch of interest. (C) Time course of this sensor of interest under speed and accuracy instructions. Response at 0 ms. The epoch of interest is highlighted by a green box where activity was greater under speed than accuracy conditions. (D) Significant SAT effect on the MEG amplitude during the epoch of interest was localized in the right medial precuneus, BA31, central MNI coordinates $x: 14$, $y: -59$, $z: 22$ ($F_{(1,9)} = 29.17$, $p < 0.001$).

2.4.3.4. *SAT component between 300 and 250 ms in the left dorsolateral prefrontal cortex (DLPFC) positively correlated with the boundary*

A left lateral prefrontal sensor showed a greater MEG amplitude under the accuracy than the speed instruction between 300 and 250 ms before the response ($F_{(1,9)} = 22.89$, $p < 0.001$) (fig.9A). The sensor showing this effect also showed a high magnitude in the difference topography (accuracy-speed) (fig.9B). Source localization during the epoch of interest localized the component in the DLPFC in the left middle frontal gyrus, BA9, central Talairach coordinates $x: -41$, $y: 15$, $z: 26$ (for labeling of prefrontal regions we used the Talairach Applet as the SPM8 Anatomy Toolbox provides maps in prefrontal regions for BA44 and 45 only, cf. materials and methods for further details) (fig.9D). Similar to the sensor level results, the activity in the source space showed greater activity under the

accuracy than the speed instruction ($F_{(1,9)} = 28.83$, $p < 0.001$). Differential sensor space MEG activity was highly positively correlated with the boundary ($r = 0.80$, $p = 0.0052$) (fig.9E), whereas it was not significantly correlated with the drift rate ($r = 0.59$, $p = 0.07$).

When looking at the time course of this sensor (fig.9C), the question might arise if the SAT effect is due to reaction time effects. However, the amplitudes under both instructions reached their maximum between 150 and 100 ms before response onset and the amplitude under the accuracy instruction was again significantly higher than under the speed instruction (sensor level: $F_{(1,9)} = 6.41$, $p = 0.032$; source space: $F_{(1,9)} = 25.49$, $p < 0.001$). This suggests that the effect derived from reaction time effects as well as true amplitude differences.

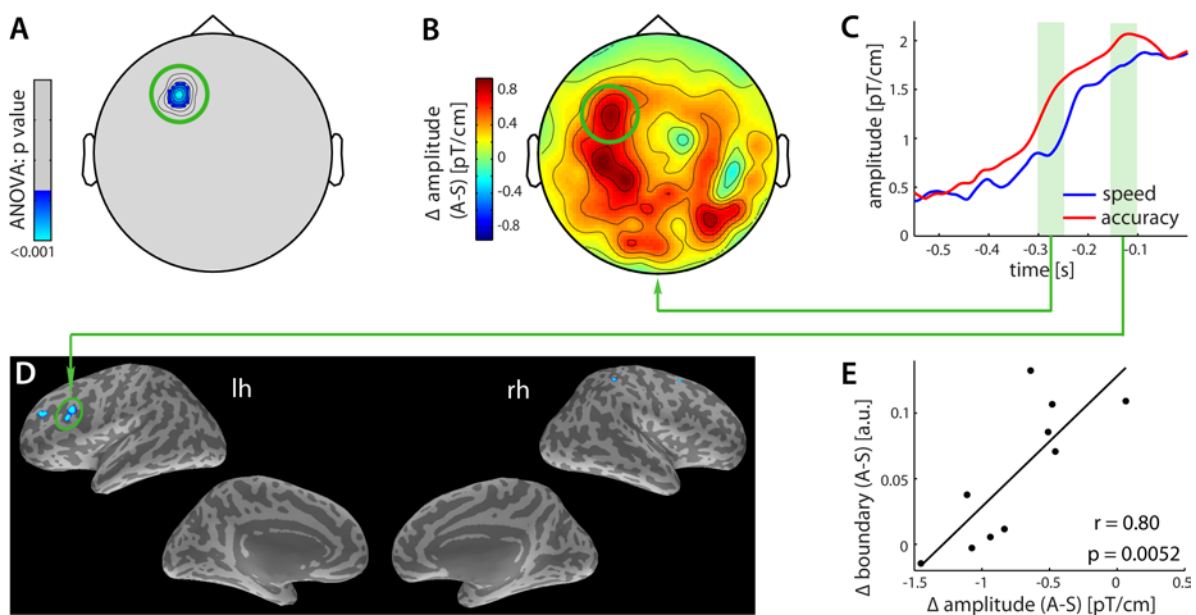


Fig.9: SAT effects between 300 and 250 ms (early epoch of interest) and between 150 and 100 ms (late epoch of interest) before the response in the left dorsolateral prefrontal cortex (DLPFC), middle frontal gyrus, BA9. Early differential (accuracy-speed) activity positively correlated with the boundary. (A) Significant SAT effect on the MEG amplitude during the early epoch of interest in a left latero-frontal sensor ($F_{(1,9)} = 22.89$, $p < 0.001$). (B) Group average of difference topography (accuracy-speed) during the early epoch of interest. (C) Time course of this sensor of interest under speed and accuracy instructions showing that activity was always higher under accuracy than speed conditions (but see text for details). Response at 0 ms. Early and late epochs of interest are highlighted by green boxes. (D) Significant SAT effect on the MEG amplitude in the late epoch of interest in the source space ($F_{(1,9)} = 25.49$, $p < 0.001$). Early and late left frontal SAT effects were located in the left DLPFC in the middle frontal gyrus, BA9, central Talairach coordinates $x: -41$, $y: 15$, $z: 26$. (E) Positive correlation between differential (accuracy-speed) sensor space MEG activity and boundary ($r = 0.80$, $p = 0.0052$).

2.4.3.5. *COH component 150 to 200 ms after stimulus onset in the right fusiform gyrus not significantly correlated with either drift rate or boundary*

Multiple right medio-temporal sensors showed *no SAT effect* on the MEG amplitude between 150 and 200 ms after stimulus onset but they showed a significant *COH effect* on the amplitude ($F_{(1,9)} = 15.36$, $p < 0.001$) (fig.10A). These sensors also showed the greatest activity in the difference topography (high-low COH) (fig.10B). The time courses for the different COH levels in this time interval reveal that with decreasing COH the amplitude decreased (fig.10C). Source localization during the epoch of interest localized the COH component in the right fusiform gyrus (no probability given), the probability for area hOC4v (V4) was 20 % [10-30 %], central MNI coordinates x: 31, y: -61, z: -15 (fig.10D). The right fusiform gyrus showed a significant COH effect on the amplitude ($F_{(1,9)} = 17.07$, $p < 0.001$). The differential (high-low COH) sensor space MEG activity was neither correlated with the differential drift rate ($r = -0.18$, $p = 0.62$) nor with the differential boundary ($r = 0.42$, $p = 0.23$).

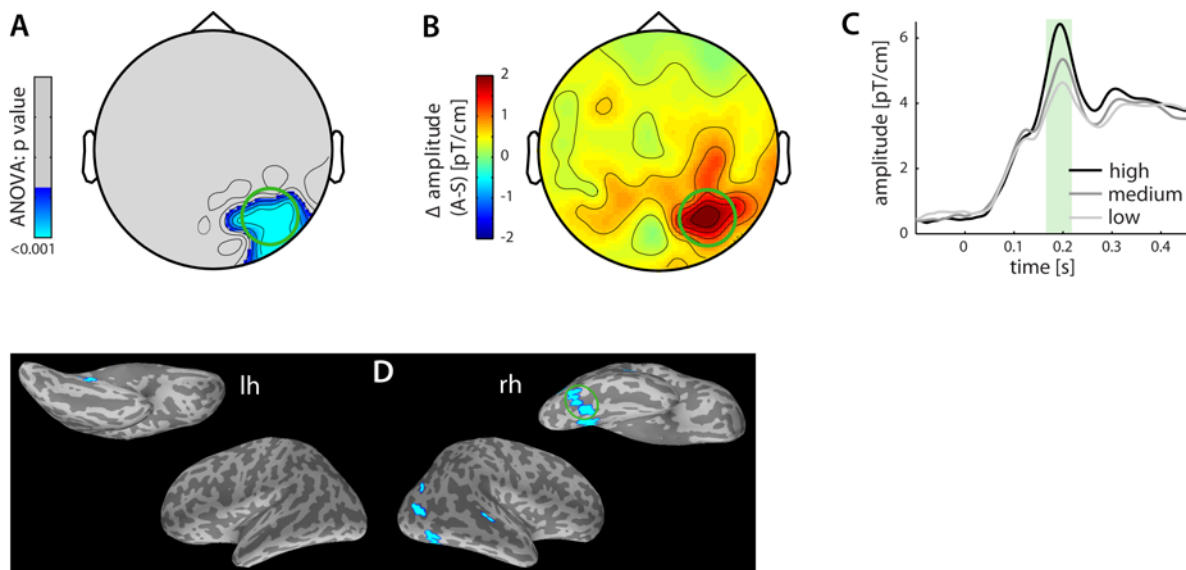


Fig.10: COH effect between 150 and 200 ms (M170) after stimulus onset in the right fusiform gyrus not correlated with the drift rate. (A) Significant COH effect on the MEG amplitude during the epoch of interest in right medio-temporal sensors ($F_{(1,9)} = 15.36$, $p < 0.001$). (B) Group average of difference topography (high-low coherence) during the epoch of interest. (C) Time course of these sensors of interest in response to high, medium, and low COH stimuli. Stimulus onset at 0 ms. The epoch of interest is highlighted by a green box showing decreasing amplitudes with decreasing COH. (D) Significant COH effect on the MEG amplitude during the epoch of interest in the source space ($F_{(1,9)} = 17.07$, $p < 0.001$). It was located in the right fusiform gyrus, central MNI coordinates x: 35, y: -64, z: -16.

2.4.3.6. *COH component 185 to 235 ms after stimulus onset in the left fusiform gyrus neither significantly correlated with drift rate nor boundary*

A left medio-temporal sensor showed a significant COH effect on the MEG amplitude between 185 and 235 ms after stimulus onset ($F_{(1,9)} = 13.03$, $p < 0.001$) (fig.11A). This sensor also showed a high magnitude in the difference topography (high-low COH), together with the aforementioned sensors localized in the right fusiform gyrus (fig.11B). Like in the right fusiform gyrus, the time courses in this time interval show decreasing amplitudes with decreasing COH (fig.11C). Compared to the right fusiform gyrus, activity was distributed over a smaller area and reached lower peak amplitudes, at least when COH was high. Source localization during the epoch of interest localized the COH component in the left fusiform gyrus (no probability given), central MNI coordinates x: -41, y: -56, z: -14 (fig.11D). As for the sensor space, for the source space data, the left fusiform gyrus showed a significant COH effect on the amplitude ($F_{(1,9)} = 12.87$, $p < 0.001$). The differential (high-low COH) sensor space MEG activity was neither correlated with the differential drift rate ($r = 0.17$, $p = 0.64$) nor with the differential boundary ($r = 0.26$, $p = 0.46$).

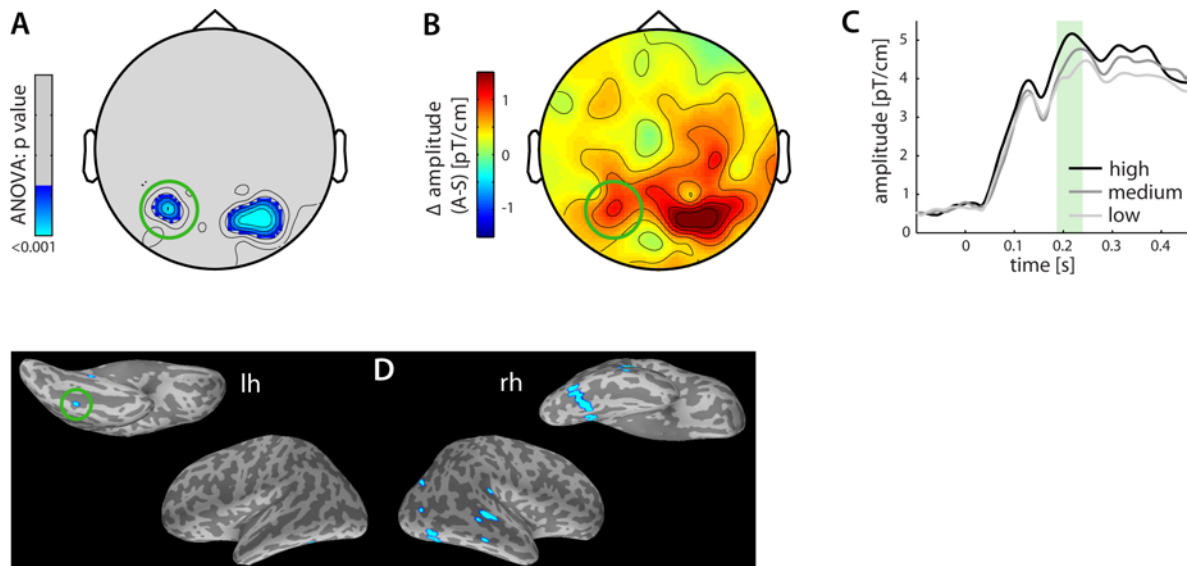


Fig.11: Significant COH effect between 185 and 235 ms (M170) after the stimulus onset in the left fusiform gyrus not correlated with the drift rate. (A) Significant COH effect on the MEG amplitude during the epoch of interest in left medio-temporal sensors ($F_{(1,9)} = 13.03$, $p < 0.001$), together with the aforementioned COH effect in right medio-temporal sensors. (B) Group average of difference topography (high-low coherence) during the epoch of interest. (C) Time course of these sensors of interest in response to high, medium, and low COH stimuli. Stimulus onset at 0 ms. The epoch of interest is highlighted by a green box showing, similar to right fusiform gyrus, decreasing amplitudes with decreasing COH. (D) Significant COH effect on the MEG amplitude during the epoch of interest in the source space ($F_{(1,9)} = 12.87$, $p < 0.001$). It was located in the left fusiform gyrus, central MNI coordinates x: -41, y: -56, z: -14.

2.4.3.7. *COH component 285 to 335 ms after stimulus onset in the right DLPFC positively correlated with the drift rate but not significantly correlated with the boundary*

A right lateral prefrontal sensor showed a significant COH effect on the MEG amplitude between 285 and 335 ms after stimulus onset ($F_{(1,9)} = 10.86$, $p < 0.001$) (fig.12A). This sensor also showed high activity in the difference topography (high-low COH) (fig.12B). The time courses for the different COH levels in this time interval show higher amplitudes with increasing COH (fig.12C). Source localization during the epoch of interest localized the COH component in the right middle frontal gyrus, BA9, central Talairach coordinates x: 38, y: 15, z: 28 (for labeling of prefrontal regions we used the Talairach Applet as the SPM8 Anatomy Toolbox provides maps in prefrontal regions for BA44 and 45 only, cf. materials and methods for further details) (fig.12D). As for the sensor space, for the source space data the right DLPFC showed a significant COH effect on the amplitude ($F_{(1,9)} = 12.22$, $p < 0.001$). The differential (high-low COH) sensor space MEG activity was highly correlated with the

differential drift rate ($r = 0.83$, $p = 0.0032$) (fig.11E). It was not significantly correlated with the differential boundary ($r = -0.17$, $p = 0.64$).

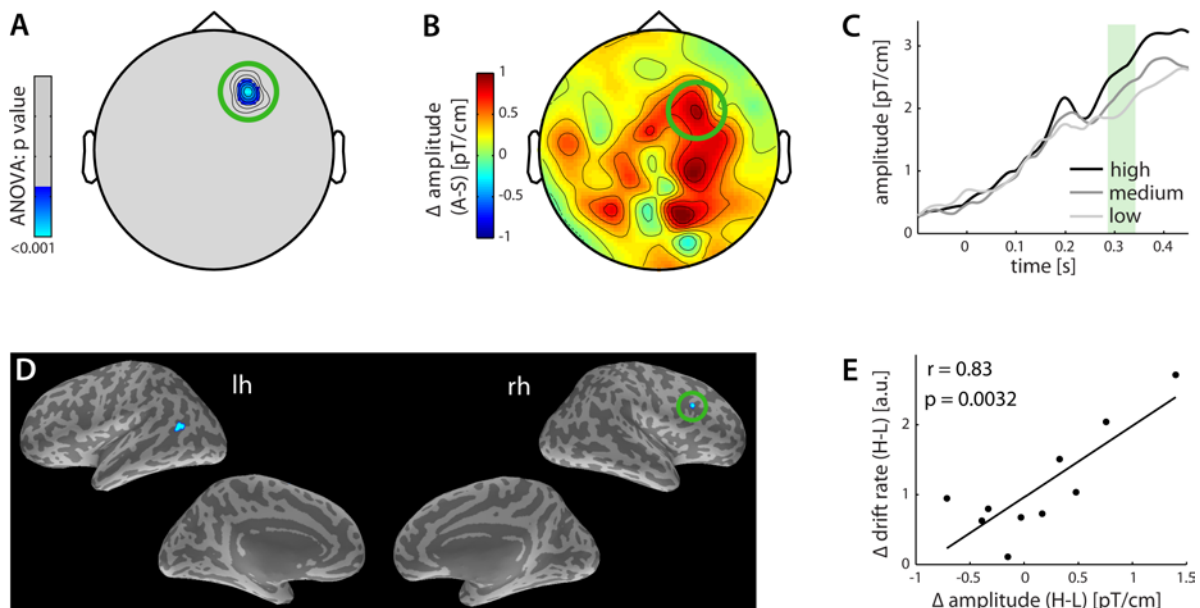


Fig.12: Significant COH effect between 285 and 335 ms after the stimulus onset in the right DLPFC positively correlated with the drift rate. (A) Significant COH effect on the MEG amplitude during the epoch of interest in a right lateral frontal sensor ($F_{(1,9)} = 10.86$, $p < 0.001$). (B) Group average of difference topography (high-low COH) during the epoch of interest. (C) Time course of this sensor of interest in response to high, medium, and low COH stimuli showing that with decreasing COH the amplitude decreased. Stimulus onset at 0 ms. The epoch of interest is highlighted by a green box. (D) Significant COH effect on the MEG amplitude in the source space ($F_{(1,9)} = 12.22$, $p < 0.001$). The COH effect was located in the right DLPFC in the middle frontal gyrus, BA9, central Talairach coordinates $x: 38$, $y: 15$, $z: 28$. (E) Positive correlation between differential (high-low COH) sensor space MEG activity and drift rate ($r = 0.83$, $p = 0.0032$).

2.4.3.8. *COH component 350 to 400 ms after stimulus onset in the right calcarine gyrus not significantly correlated with either drift rate or boundary*

A right medial parietal sensor showed a significant COH effect on the MEG amplitude between 350 and 400 ms after stimulus onset ($F_{(1,9)} = 12.14$, $p < 0.001$) (fig.13A). This sensor also showed high amplitude in the difference topography (high-low COH) (fig.13B). The time courses for the different COH levels in this time interval show higher amplitudes with increasing COH (fig.13C). Source localization during the epoch of interest localized the COH component in the right calcarine gyrus, assigned to BA17 with a probability of 90 % [70-100 %], probability for BA18 was 30 % [20-50 %], central MNI coordinates $x: 8$, $y: -75$, $z: 7$ (fig.13D). As for the sensor space, for the source space data, the right calcarine gyrus showed

a significant COH effect on the amplitude ($F_{(1,9)} = 11.70$, $p < 0.001$). The differential (high-low COH) sensor space MEG activity was neither correlated with the differential drift rate ($r = -0.045$, $p = 0.90$) nor with the differential boundary ($r = -0.54$, $p = 0.11$).

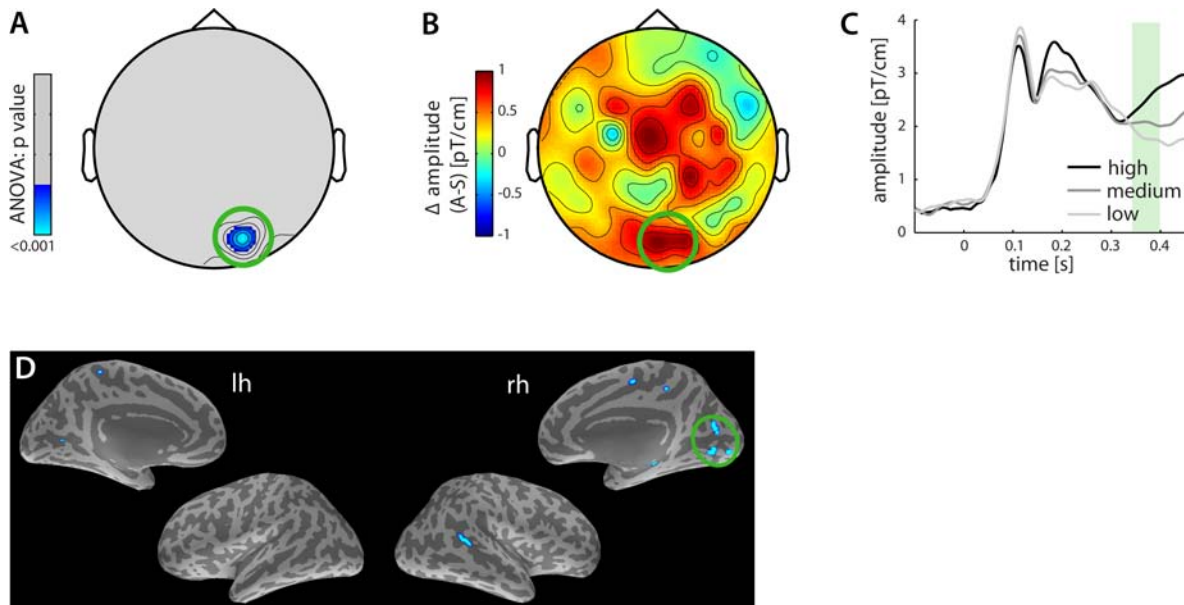


Fig.13: Significant COH effect between 350 and 400 ms after the stimulus onset in the right calcarine gyrus not significantly correlated with the drift rate. (A) Significant COH effect on the MEG amplitude during the epoch of interest in a right medial parietal sensor ($F_{(1,9)} = 12.14$, $p < 0.001$). (B) Group average of difference topography (high-low COH) during the epoch of interest. (C) Time course of this sensor of interest in response to high, medium, and low COH stimuli showing that with decreasing COH the amplitude decreased. Stimulus onset at 0 ms. The epoch of interest is highlighted by a green box. (D) Significant COH effect on the MEG amplitude in the source space ($F_{(1,9)} = 11.70$, $p < 0.001$). The COH effect was located in the right calcarine gyrus, assigned to BA17 with a probability of 90 % [70-100 %], probability for BA18 was 30 % [20-50 %], central MNI coordinates $x: 8$, $y: -75$, $z: 7$.

2.4.3.9. *COH component 315 to 265 ms before the response in the left precentral gyrus not significantly correlated with either drift rate or boundary*

A left lateral frontal sensor showed a significant COH effect on the MEG amplitude between 315 and 265 ms before the response ($F_{(1,9)} = 10.64$, $p < 0.001$) (fig.14A). This sensor also showed high activity in the difference topography (high-low COH) (fig.14B). The time courses for the different COH levels in this time interval show higher amplitudes under low COH than under medium or high COH (fig.14C). Source localization during the epoch of interest localized the COH component in the left precentral gyrus, BA6, central Talairach coordinates $x: -62$, $y: 2$, $z: 21$ (for labeling of prefrontal regions we used the Talairach Applet

as the SPM8 Anatomy Toolbox provides maps in prefrontal regions for BA44 and 45 only, cf. materials and methods for further details) (fig.14D). As for the sensor space, for the source space data, the left precentral gyrus showed a significant COH effect on the amplitude ($F_{(1,9)} = 12.08$, $p < 0.001$). The differential (high-low COH) sensor space MEG activity was neither highly correlated with the differential drift rate ($r = -0.38$, $p = 0.28$) nor with the differential boundary ($r = 0.37$, $p = 0.29$).

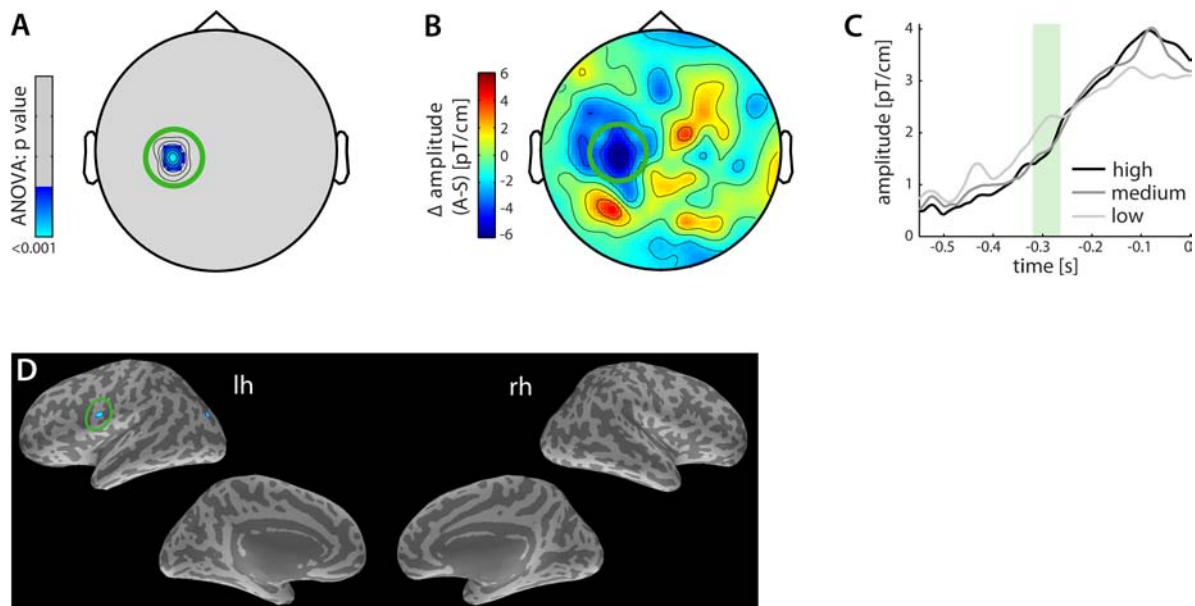


Fig.14: Significant COH effect between 315 and 265 ms before the response in left BA6 not correlated with the drift rate. (A) Significant COH effect on the MEG amplitude during the epoch of interest in a left latero-frontal sensor ($F_{(1,9)} = 10.64$, $p < 0.001$). (B) Group average of difference topography (high-low COH) during the epoch of interest. (C) Time course of this sensor of interest in response to high, medium, and low COH. Response at 0 ms. The epoch of interest is highlighted by a green box where amplitude was high for low COH and lower for medium and high COH. (D) Significant COH effect on the MEG amplitude in the source space ($F_{(1,9)} = 12.08$, $p < 0.001$). The COH effect was located in the left precentral gyrus, BA6, central Talairach coordinates x: -62, y: 2, z: 21.

2.5. *Discussion and interim conclusions*

In the present study, we used MEG and a face-house categorization task to investigate how perceptual decision processes unfold in the human brain when emphasizing speed or accuracy of a decision (SAT) under different levels of sensory evidence (coherence, COH). Emphasis on speed resulted in higher activation of SMA and precuneus whereas the left DLPFC showed the inverse pattern. When correlating these physiological effects with the boundary parameter, this dissociation was confirmed: changes in activity in right SMA were negatively correlated with the changes in response threshold (boundary), whereas changes in activity in left DLPFC were positively correlated with changes in boundary. Furthermore, we did not find SAT effects in sensory areas, i.e., bilateral fusiform gyrus and BA17 but these areas showed together with the right DLPFC enhanced activation for higher levels of sensory evidence. Activity in these areas was not correlated with the boundary.

2.5.1. Behavioral and diffusion model data

Behavioral data showed that subjects indeed traded speed for accuracy as they reacted faster at the cost of more errors when speed was emphasized. With decreasing sensory evidence, the task became more difficult as RTs were slower and error rates higher. In context of the diffusion model, congruent with a priori expectations, emphasis on accuracy compared to speed led to a significantly higher boundary while the drift rate was not significantly affected. The COH manipulation had a significant effect on the drift rate and also on the boundary. The latter might seem surprising since, according to a classical interpretation of the diffusion model, the amount of sensory information primarily affects the drift rate while changes in the speed-accuracy tradeoff primarily affect the boundary (e.g., Ratcliff and McKoon, 2008). However, several authors (Churchland et al., 2008; Cisek et al., 2009; Ditterich, 2006) have suggested variants of the sequential sampling model where the accumulator process does not only rely on sensory evidence but is complemented by an urgency signal that increases as a function of elapsed time and effectively reduces the boundary for decisions that take longer. Accordingly, subjects may have lowered their response threshold when sensory evidence was low resulting in a lower boundary estimate. In our data, this effect seemed particularly pronounced in the accuracy condition but the interaction (between SAT and COH) was far from significant ($F_{(2,18)} = 1.80$, $p = 0.19$). This pattern, however, is congruent with results from Cisek et al (Cisek et al., 2009). They showed that while initially the criterion of subjects

to make a decision was higher when accuracy was emphasized compared to speed, the threshold was lowered at a steeper rate in the accuracy compared to the speed condition as time elapsed. This is convergent with the trend in our data. Future research should investigate the precise mechanisms behind such a dynamic threshold adaptation.

2.5.2. Decision-related SAT component in the right SMA

We measured higher activity levels under speed than accuracy between 275 and 325 ms after stimulus onset in the right SMA (fig.6A,D). The SMA seems to be involved in motor preparation as well as direct motor output (for review, see Nachev et al., 2008). Via connections with the basal ganglia, more precisely the striatum (Takada et al., 1998) or subthalamic nucleus (Nambu et al., 1996), it forms a circuit that is optimally suited to modulate action readiness, i.e., movement preparation or inhibition (Brinkman and Porter, 1979; Tanji and Kurata, 1982). Differential activations in pre- SMA and SMA were also found in SAT tasks using fMRI in humans. Forstmann et al. (2008) found greater activity under speed instructions in the right pre-SMA during the pre-stimulus period. Van Veen et al. (2008) found greater activation before and less activation after stimulus onset in bilateral SMA but overall activity was higher when emphasizing speed. Ivanoff et al. (2008) found higher stimulus-locked activation under speed instructions in right pre-SMA. In summary, greater activity under speed than accuracy instructions was found *before* or *after* stimulus onset.

Differential (accuracy-speed) activity in the right SMA was negatively correlated with the differential boundary, i.e., subjects with a low boundary difference showed higher difference in SMA activity (fig.6E). At a first glance, this may seem at odds with an interpretation that the SMA is engaged in a process that sets the boundary. However, two hypotheses could explain this finding: (1) Enhanced SMA activity under speed conditions might be involved in overcoming the tonic inhibition provided by the output nuclei of the basal ganglia, thereby effectively lowering the boundary (e.g., Lo and Wang, 2006). (2) Enhanced SMA activity may be instrumental for a more efficient, i.e., faster, transformation of sensory signals into a motor response. In this context it would be of interest to study whether the connectivity of sensorimotor networks is enhanced under speed conditions.

2.5.3. Decision-related SAT and COH components in the DLPFC

Higher activity levels under accuracy than speed instructions were measured between 300 and 100 ms before the response in the left DLPFC, middle frontal gyrus (fig.9A,D). One may wonder whether the amplitude differences between speed and accuracy 300 to 250 ms before the response are attributable to different reaction times (fig.9C). Between 150 and 100 ms before the response, however, the amplitudes under both instructions reached their maximum and the amplitude under accuracy was again significantly higher. This suggests that the observed differences reflect a combination of true differences in amplitude and relative onset latencies given the different mean RTs. Higher activation under accuracy than speed instructions in the middle frontal gyrus was also found by Forstmann and colleagues (2008). Van Veen et al. (2008) reported greater activity under speed before stimulus onset in left DLPFC. Notably, their figure 5 shows no higher peak activation after stimulus onset under the speed instruction.

The DLPFC receives input from secondary visual, auditory, or somatosensory cortices and is connected with pre-motor structures including the SMA and the basal ganglia which makes it a candidate structure for the translation of higher-level sensory signals into motor commands (for review, see Miller and Cohen, 2001). Correspondingly, Kim and Shadlen (1999) in monkeys and Heekeren et al. (2004) in humans found the activity in left DLPFC to represent the differential output from neuronal populations representing the different stimulus alternatives. Hence, the DLPFC seems to be involved in computing the outcome of a decision or the subjective evidence for one alternative over the other. In that sense, the enhanced DLPFC activity for accuracy compared to speed conditions and its positive correlation with the boundary (fig.9E) might reflect a higher level of accumulated evidence.

While we did not find a significant effect of the COH manipulation on activity in the left DLPFC at a very conservative threshold, we found a significant one in the right DLPFC between 285 and 335 ms after stimulus onset (fig.12A,D). Differential activity in the right DLPFC in a task modulating sensory evidence was also found by Philiastides and Sajda (2007) using EEG-informed fMRI. Furthermore, differential (high-low COH) activity in the right DLPFC correlated positively with the differential drift rate providing further evidence that the DLPFC integrates sensory information to compute a decision variable (fig.12E).

Summarizing, our results are consistent with the literature and add to the evidence that while activity in the left DLPFC was correlated with the boundary, activity in the right DLPFC was correlated with the drift rate.

2.5.4. Other components characterizing SAT processing

Higher activity levels under speed than accuracy were also measured in the left SMA, slightly later than in the right hemisphere and smaller in amplitude (fig.7A,C,D). A predominant right lateralization was expected as we included only correct answers after seeing pictures of faces in the analysis where subjects always responded with their left thumb. Likewise, intracranial EEG recordings (from epilepsy patients) preceding finger movements showed activity in bilateral SMA with higher amplitudes in the contralateral hemisphere (Ikeda et al., 1992). Activity in the left SMA might be attributed to a general dominance of the left hemisphere in (pre-) motor processing (Kim et al., 1993). Differential activity in the left SMA did not correlate significantly with the differential boundary indicating that it was less directly involved in the decision process.

Furthermore, significantly higher activity levels under speed than accuracy were measured in the mesial extent of the precuneus, BA 31 (fig.8A,D). This region is, amongst others, functionally connected with the SMA via adjacent dorsal precuneus regions (Margulies et al., 2009), suggesting a role in (pre-) motor processing. In line with this, studies from Rushworth et al. (1998) and Bauer et al. (2009) suggest that the precuneus is involved in sensorimotor transformation processes. Like in the left SMA, differential activity in the precuneus did not correlate significantly with the differential boundary.

2.5.5. Other components characterizing COH processing

We measured activity that was parametrically modulated by COH in the following sensory regions: in the right and left fusiform gyrus around 170 ms, and in the right calcarine gyrus, BA17, around 375 ms after stimulus onset (fig.10A,D, 11A,D, 13A,D). The M170 in the fusiform gyrus has repeatedly been shown to be related to processing of face stimuli (e.g., Liu et al., 2000; Swithenby et al., 1998). Late differential activity in BA17 might be due to activation of sensory feedback loops (e.g., Desmurget, 2000; Lamme and Roelfsema, 2000). Importantly, none of the sensory areas showed either SAT effects or a correlation with diffusion model parameters. This does, however, not preclude modulations in neural activity due to SAT that the ERF is not sensitive to, e.g., changes in induced rhythms or connectivity to pre-motor regions.

In conclusion, we show differential behavior of SMA and DLPFC activity under emphasis of speed against accuracy that can be interpreted such that the SMA under speed emphasis seems to facilitate fast responses by disinhibiting basal-ganglia-thalamic loops whereas the DLPFC may represent higher levels of accumulated evidence under emphasis of accuracy. Our results also show that the SMA seems dynamically active during stimulus processing, potentially reflecting an adaptive threshold regulation.

3. Studies 2 and 3 - Perceptual decision making in the tactile domain using Braille patterns with long (1000 ms) and short (100 ms) presentation time

3.1. Abstract

Recent evidence has shown that perceptual decision making may be implemented by evidence accumulation as formalized in diffusion-to-boundary models. Supporting evidence derives from mathematical modeling of behavioral data as well as neural recordings in humans and monkeys. However, the majority of these studies employed dynamic visual stimuli where factual sensory evidence is increased over time.

In the two studies presented here, we used tactile Braille patterns that differed in pattern discriminability, thereby modulating task difficulty, but not in physical energy. Stimuli were presented transiently for 100 ms in the one study, in the other study for 1000 ms. Presentation time did not alter neurophysiological processing significantly which could suggest that ‘perceptual persistence’ after stimulus removal might be implemented via feedback pathways. In both studies, late neurophysiological activity in the primary somatosensory cortex (S1) underwent ramp-like changes modulated by task difficulty in the same direction as in monkey studies. Contrary to the late ERP components, early components were unaffected by task difficulty. Investigating the oscillatory activity, we found no task difficulty effects in S1, in particular for the gamma range. However, in parieto-occipital cortex, alpha-beta band activity showed a marked covariation with task difficulty suggesting a graded recruitment of visual cortex for more complex tactile patterns.

The results show that drift-diffusion processes are a more general principle that also applies in situations where stimulus information is constant or presented briefly, involving areas as early as S1. Furthermore, stimulus-induced somatosensory gamma-band oscillations do not seem to reflect decision processes in this task suggesting that they are rather a consequence of the afferent input caused by tactile stimulation.

3.2. *Introduction*

Several reports claim that the earliest neural responses to sensory stimuli contain substantial information about the underlying stimuli. Van Rullen and Koch (2003) showed that very fast human responses to visual presentations are clearly above chance in certain discrimination tasks. In contrast, Lamme and Roelfsema (2000) using a figure-ground segregation task showed that in neurons in the primary visual cortex (V1) only later spiking activity, attributed to feedback-related signals, distinguished between figure and ground. This suggests that in some situations sufficient information is encoded in the first spikes, whereas in other, possibly more complex, situations crucial information is encoded not until the late phases of sensory processing.

When looking at human and animal behavior in perceptual decision tasks, subjects usually take longer to commit a decision under conditions of high difficulty and uncertainty (for review, see Heekeren et al., 2008). For decades it has been known that such behavior can be captured by so-called sequential sampling models (e.g., Ratcliff, 1978). Invasive recordings in monkeys have provided direct evidence for such an accumulator process (Kim and Shadlen, 1999; Mazurek et al., 2003). Non-invasive human studies have found similar phenomena in different brain areas and for various signals (Heekeren et al., 2006; Siegel et al., 2007). Crucially, these studies used dynamic stimuli where factual evidence increases over time. However, in many sensory experiments stimuli are presented transiently, and yet the diffusion model can explain the behavioral data by an accumulation process (e.g., Philiastides et al., 2006). Several theoretical models of perception (e.g., Friston, 2005; Hopfield, 1982; Romo et al., 2002) assume that sensory inference relies on recursive processing of stimulus information spanning across different levels of the cortical hierarchy, and the temporal dynamics underlying these reverberations might explain such evidence accumulation, also in absence of the actual stimulus. We presented the tactile stimuli for either a short (100 ms), or a long (1000 ms) presentation time, and proposed to find no significant differences between the two studies.

Bauer et al. (2006) observed sustained somatosensory gamma oscillations to Braille stimuli when subjects took a decision by matching patterns to a working-memory template. In contrast, they found weaker and shorter-lasting gamma activity when subjects did not decide upon stimulus identity. Interestingly, gamma activity terminated shortly before the average response time. Oscillatory activity in the sensory cortex has been suggested to support

interactions between different levels of the hierarchy (Salinas and Sejnowski, 2001) as well as synchronize spiking activity that facilitates sensory encoding (Kayser et al., 2009).

Using EEG, we investigated the temporal dynamics of decision processing in the human somatosensory system when task difficulty was varied. We aimed at finding neural correlates (evoked and oscillatory activity) of temporal integration based on activation patterns within the somatosensory system, and at predicting the behavioral outcome modeled with the diffusion model, e.g., faster reactions under high certainty due to a high accumulation rate.

3.3. *Materials and Methods*

The study design and analyses were largely congruent in the two studies presenting Braille patterns for a long (1000 ms study) or a short (100 ms study) time period. The description given here generally applies to both studies; differences are highlighted.

3.3.1. Subjects

Sixteen subjects (8 females; age 26.19 ± 0.73 years (mean ± 1 SEM)) participated in the 1000 ms study, and twelve subjects (5 females; age 26.08 ± 1.01 years) in the 100 ms study; all after having provided written informed consent in accordance with the guidelines and approval of the Max Planck Institute for Human Development, Berlin, Germany. All had normal or corrected to normal vision and no reported history of neurological problems. The laterality quotient, assessed by the Edinburgh Handedness inventory (Oldfield, 1971), was 91.07 ± 4.08 in the 1000 ms study, and 91.67 ± 3.22 in the 100 ms study. In the 100 ms study, one subject had to be excluded from the analysis because she or he intentionally gave incorrect answers in multiple blocks.

3.3.2. Stimuli

We used a Braille stimulator (Metec, Stuttgart, Germany) with a matrix of four rows by two columns of individually controllable pins to present tactile stimuli to the right index finger. For each pattern, four of the eight pins were elevated. One pin covered approximately an area of 1 mm², and two pins were separated by 0.45 cm.

Three pattern pairs varied in spatial separability and therefore difficulty across pairs (fig.15). The precise Braille patterns were not shown to the subjects.

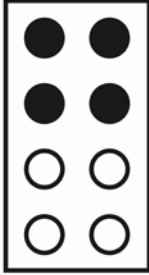
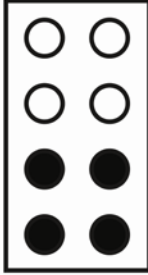
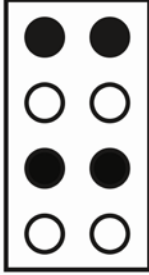
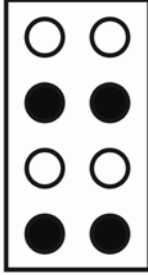
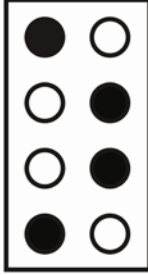
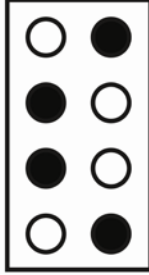
pattern:						
	A1	A2	B1	B2	C1	C2
difficulty level:	easy		medium		hard	

Fig.15: Braille-pattern pairs (black circles) were presented to the right index finger at three difficulty levels: A = easy, B = medium, C = difficult. The difficulty was realized by changes in spatial separability. Subjects responded correctly by left button press with the middle finger of the left hand when pattern 1 (A1, B1, or C1) was presented, or by right button press with the index finger of the left hand when pattern 2 (A2, B2, or C2) was presented.

The low currents to actuate the piezoelectrical membranes of the Braille stimulator created small, short-lived artifacts (duration 1 ms). Those artifacts occurred at three occasions: while specifying the stimulus pattern in the electronic circuit driving the Braille cells 100 ms before stimulus presentation, when the pins were raised, or when the pins were lowered. No artifacts were measured when the stimulus remained stationary (either elevated or lowered).

Additionally, elevation and lowering of the pins caused a sound. To mask this sound, we presented auditory white noise to the subjects via pneumatic earphones (Aearo, Indianapolis, Indiana, USA) (fig.16).

A flat screen, type DELL 2001 FP (DELL Inc., Round Rock, TX, US), was used to present the fixation cross and to give visual feedback (cf. 2.2.3 Task).

3.3.3. Task

In a two-alternative forced-choice task, subjects discriminated three Braille pattern pairs that varied in difficulty across pairs (fig.15).

Before the experiment, subjects were extensively trained to recognize the Braille patterns and map them to the correct response to assure consistent performance during the experiment. The *training session* consisted of six blocks by 18 trials (two blocks per difficulty level) and lasted about 15 minutes. Per block, only one pattern pair was presented. To inform the subjects which pattern pair was chosen for this block, the two patterns were presented two

times each at the beginning of each block, immediately followed by the arrowhead pointing in the direction of the button that should be pressed. At the beginning of each trial, a white fixation cross was shown with presentation time varying between 1 and 2 s which signaled the subjects not to blink or move their eyes (fig.16). Subsequently, one Braille stimulus was presented to the right index finger for either 1000 ms (1000 ms study) or 100 ms (100 ms study). Exploratory finger movements were not allowed. Subjects responded correctly by left button press with the middle finger of the left hand when pattern 1 (A1, B1, or C1) was presented, and by right button press with the index finger of the left hand when pattern 2 (A2, B2, or C2) was presented (cf. fig.15). They then received the visual feedback “Richtige Antwort!” (German for “correct response”) for 500 ms (fig.16 A1). Correspondingly, they received the visual feedback “Falsche Antwort!” (German for “erroneous response”) if they responded incorrectly. If they did not respond within 2 s, an arrowhead was presented pointing in the direction of the button that should have been pressed (fig.16 A2). However, subjects were instructed to answer whenever possible and not to wait for the arrowhead because in the experimental session such assistance was not available. The trials within one block as well as the blocks within one session were presented in randomized order.

The subsequent *test session* lasted about five minutes and differed from the training session insofar as the arrowhead was shown 4 s after stimulus presentation to further encourage subject’s answers (otherwise the test session lasted very long).

Subsequently, one *experimental session* consisted of 24 blocks by 30 trials (8 blocks per difficulty level) and lasted about 1.5 hours. In the 1000 ms study, two sessions were recorded whereas in the 100 ms study, only one session was recorded because the number of trials was sufficient to yield robust ERP signals. The experimental session differed from the training and test sessions in two aspects: subjects could respond within 3 s, and no trialwise feedback was given. Instead, subjects were informed about their error rate and mean reaction time (RT) visually at the end of each block. The RT was defined as the period between the onset of the Braille stimulus and the button press. Similar to the training and test session, at the beginning of each block the two patterns were presented two times each, immediately followed by the arrowhead to inform the subjects which pattern pair was chosen for this block. The two patterns per difficulty level were analyzed as one resulting in 240 trials per condition (24 blocks * 30 trials / 3 conditions).

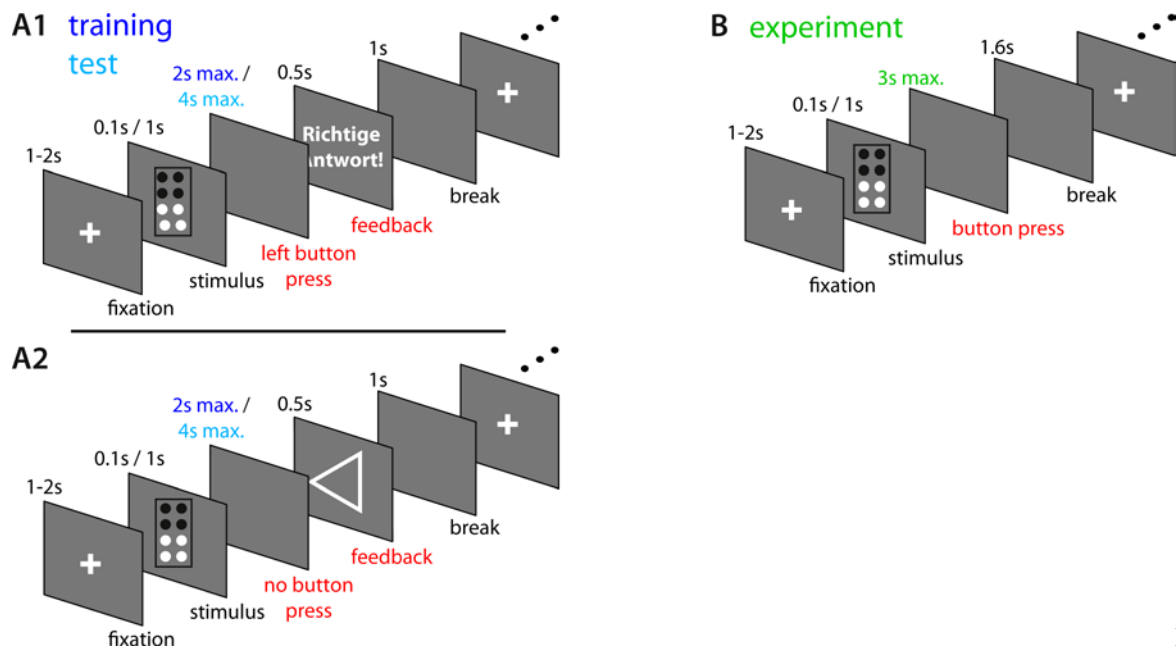


Fig:

Fig.16: Trial course for the (A) training, test and (B) experimental sessions. Initially, a fixation cross was presented between one and two seconds. Then, the Braille stimulus was applied for 1000 ms (1000 ms study) or 100 ms (100 ms study) to the index finger of the right hand. Subjects were asked to press a left button with the middle finger of the left hand or a right button with the index finger of the left hand, according to their decision upon the stimulus identity. (A1) In the training and test sessions, subjects received the visual feedback “Richtige Antwort” (German for “correct response”) if the answer was correct. Correspondingly, they received the visual feedback “Falsche Antwort” (German for “erroneous response”) if the answer was incorrect (not shown). (A2) If subjects did not press a button within 2 s (training) or 4 s (test), an arrowhead was presented pointing in the direction of the button that should have been pressed. The trial finished after a 1 s break. (B) In the experiment, subjects received no feedback after each response. One trial finished after a 1.6 s break.

3.3.4. Procedure

For all sessions, subjects were seated in an electrically and acoustically shielded room in front of a flat screen with the index finger of their right hand on the Braille stimulator and the left hand on the response buttons (fig.17).



Fig.17: Experimental setup. The subject was seated in an electrically and acoustically shielded room in front of a flat screen. The index finger of the right hand was placed on the Braille stimulator, and the index and the middle fingers of the left hand were placed on the response buttons. The 123-channel electrode cap and the additional five electrodes to record electrooculogram (EOG) and electromyogram (EMG) were joined in a control box which in turn was connected to four 32-channel high-impedance amplifiers (for detailed description, see text). The signal was then relayed to a laptop for data acquisition (not visible here).

We used the Presentation software (Neurobehavioral Systems Inc., Albany, CA, USA) for stimulus presentation (braille patterns and visual cues) and behavioral data acquisition, and we used the BrainVision Recorder (Brain Products GmbH, Gilching, Germany) for EEG data acquisition.

EEG data were acquired continuously from 123 dense equidistant active Ag/AgCl electrodes mounted in an elastic cap (ActiCAP 128Ch, Falk Minow, Herrsching, Germany). This cap covers more inferior parts of the skull than the traditional 10-20 system. The reference electrode during recording was ‘Cz’, and the ground electrode was located on the forehead. Electrode localization was conducted for each subject after each session using the ELPOS system (Zebris Medical systems[®], Isny).

ActiCAP has an amplification circuitry built into the electrodes that increases the signal and decreases the noise. Therefore, electrode-skin impedances below 20 k Ω were sufficient to achieve a good signal-to-noise ratio. This was adjusted after a short preparation time of about 20 minutes.

Data were sampled at a rate of 1.000 Hz, using a high-pass filter with a time constant of 10 s and an anti-aliasing filter set to 250 Hz (BrainAmp DC amplifiers, Brain Products GmbH, Gilching, Germany).

Vertical eye movements (electrooculogram, EOG) were recorded from one of five additional electrodes placed below the left eye. An electromyogram (EMG) was recorded from two additional electrodes placed on the right forearm above the flexor digitorum superficialis to control for flexion of the index finger while the Braille stimulus was applied. Because tensed neck muscles might cause severe artifacts in the lower occipital electrodes, a second EMG was recorded from one additional electrode placed above the left trapezius to monitor if the subjects elevated or depressed the shoulder or flexed the neck during the recording session. Subjects were asked to recapture a comfortable position if applicable. The fifth additional electrode was placed above the left common carotid artery to measure arterial pulsation.

3.3.5. Behavioral data analysis

Outliers, defined as data above three standard deviations (sd) from the mean, were removed before the analysis (a total of 2.92 % in the 1000 ms study, and 2.86 % in the 100 ms study). Furthermore, fast guesses were defined as trials with RT < 180 ms and removed from the analysis (a total of 0.53 % in the 1000 ms study, and 0.19 % in the 100 ms study). Other contaminants (see section 2.1.5. for more details) were treated in the diffusion model analysis (see next section).

Since bimodal RT distributions contradict diffusion model assumptions (Vandekerckhove and Tuerlinckx, 2007), we excluded subjects with bimodal distributions from the analysis. As reaction time distributions are typically non-Gaussian (Townsend and Ashby, 1983), we first used the Linear-Approach-to-Threshold-with-Ergodic-Rate (LATER) model (Carpenter and Williams, 1995) to calculate the inverse of the RT distributions, so-called recinormal RT distributions, which are normally distributed. Secondly, we used the recinormal distributions and a Gaussian Mixture Model (MATLAB function 'gmdistribution.fit' (McLachlan and Peel, 2000)) in order to decide whether the RT distribution of the subject was better fitted by either one or two different Gaussian processes (two different models). For each model, we obtained the Bayesian Information Criterion (BIC) as a measure for the goodness of the fit (the smaller the value the higher the evidence). We calculated the mean difference of the BICs of the two and the one Gaussian process models, and subjects with a difference greater than two standard errors (SE) from the mean difference were defined as bimodal and excluded, all others unimodal.

Mean RT and accuracy were analyzed and separate one-way repeated-measures ANOVAs with difficulty (easy vs. medium vs. hard) as the independent variable were calculated to test for statistically significant differences between the experimental conditions.

3.3.6. Diffusion model analysis

For a general introduction to the diffusion model and its parameter estimations, see section 2.3.6. As the quality of the stimulus information (here: DIFF) was an independent variable in this experiment, calculations of the drift rate were of special interest.

We used the diffusion model analysis toolbox (DMAT, <http://ppw.kuleuven.be/okp/dmatoolbox/>) for parameter estimation. Two models were nested in the following order: (1) All parameters were restricted to be equal across the conditions, (2) the drift rate was free to vary across conditions. To choose the best model for each subject, we used the Bayesian Information Criterion (BIC) and a likelihood ratio test under the assumption of an approximate chi-square distribution. Outliers and fast guesses were removed before model calculations (cf. section 2.3.5). Random guesses or delayed startups were treated in each of the nested models by using built-in DMAT functions.

A one-way repeated-measures ANOVA with the factor DIFF was calculated for the drift rate to test for statistical significance between the experimental conditions.

3.3.7. EEG time-domain data processing and analysis on the sensor level

Data were analyzed using FieldTrip (<http://fieldtrip.fcdonders.nl/>), a Matlab[®]-based toolbox for the analysis of electrophysiological data.

Continuous EEG recordings were divided into epochs of 2000 ms, time-locked to the stimulus (-700 to 1300 ms). Artifact removal was conducted as follows. Firstly, eye blinks were detected using semiautomatic procedures (cf. Bauer et al., 2006), and stored as separate epochs. Secondly, data were checked for bad channels using the FieldTrip routine 'rejectartifact.m'. Thirdly, linear components associated with eye blinks from the separate blink epochs, movements, or general noise from the main epoched data around stimulus onset were determined using principle component analysis (Hotelling, 1933; Pearson, 1901), and subtracted from the EEG data.

Artifact-corrected EEG recordings were divided into stimulus-locked epochs from -300 to 900 ms. The epochs were band pass-filtered between 0.5 and 40 Hz and averaged over

trials per condition. Baseline corrections were applied on the epoched stimulus-locked data using a 100 ms pre-stimulus baseline. Data were firstly averaged across trials, and secondly across subjects. This greatly suppresses the influence of background activity that is randomly distributed around zero and enhances the influence of potentials that are phase-locked to defined events and can therefore be related to stimulus processing (Luck, 2005; Rugg and Coles, 1996). Results were averaged over the two Braille patterns with identical DIFF as well as over correct and incorrect trials.

For statistical assessment, EEG amplitudes were averaged using a sliding time window of 50 ms from 0 to 650 ms, as the mean RT was 641 ms in the 1000 ms study, and 605 ms in the 100 ms study. To assess statistical significance between the experimental conditions, we calculated one-way repeated-measures ANOVAs with the factor DIFF. The significance threshold was set to the conservative value of 0.001. We did not apply a standard correction of the multiple comparison problem, e.g., Bonferroni correction, because this assumes independence of the data which is neither the case in the temporal nor in the spatial domain.

We correlated the differential (easy-hard) slope of the ERP with the differential drift rate (cf. section 3.4.2.4.). To calculate the slope, we firstly approximated the cumulative integral of the ERP per subject, per condition, for selected channels, and a selected time window, using the MATLAB[®] function ‘cumtrapz.m’. Subsequently, we calculated a linear regression of the cumulative integral to receive the slope of the integral.

3.3.8. EEG time- frequency domain data analysis on the sensor level

Induced brain responses can reflect processes that are not reflected in the time-domain average of electrical activity (Gray and Singer, 1989; Tallon-Baudry et al., 1997). To assess these components, we generated time-frequency representations for each trial (-450 to 900 ms). For low-frequencies (2.5 Hz to 40 Hz), we used Hanning windows of 400 ms length (step size 25 ms), and frequencies were transformed in steps of 2.5 Hz. For higher frequencies (40 to 150 Hz), we used the multi-taper technique (Mitra and Pesaran, 1999) to account for the broader spectral peaks (Siegel and Konig, 2003) but also to provide sufficient smoothing in the time domain. We calculated three ‘discrete prolate slepian tapers’ with a window length of 200 ms in steps of 25 ms, and frequencies from 40 to 150 Hz in steps of 5 Hz.

We calculated measures of event-related synchronization and desynchronization (Pfurtscheller and Lopes da Silva, 1999) to obtain consistent stimulus-induced changes of the

spectral composition of EEG activity. To this end, power spectra were z-transformed (the average pre-stimulus baseline in the interval from -100 to 0 ms was subtracted from average time- and frequency-resolved power estimates divided by the standard error as estimated from the combined standard deviation of baseline and time-frequency bin of interest). These z-scores were then pooled across subjects using the following formula:

$$z = \frac{1}{N} \sum_{i=1}^N z_i,$$

with z_i being the z score of the i th subject. The z scores are normalized for intrasubject variance and therefore can be better compared across subjects than differences in absolute power. Those grand-average time-frequency z images showed clear spectral components and allowed the definition of time-frequency windows of interest.

In order to assess statistical significance between the experimental conditions, we calculated one-way repeated-measures ANOVAs with the factor DIFF. The significance threshold was set to the conservative value of 0.001.

3.3.9. EEG time- and time-frequency domain data analysis on the beamformer source level

We used linear ‘beamforming’ for source analysis (Gross et al., 2001; Van Veen et al., 1997). This adaptive spatial filtering technique applies location- and frequency- specific filters to the EEG data to estimate the local power spectral density in source space. Regions of interest (ROIs) were: left S1 area 3b (contralateral to the stimulated finger), left S1 area 1, left and right S2. ERP were low-pass filtered with a cutoff at 30 Hz, low-frequency data with a cutoff at 40 Hz. High-frequency data were band-pass filtered from 40 to 150 Hz.

Firstly, we projected the measured head position relative to the EEG channels onto the surface of the standard Montreal Neurological Institute (MNI) brain using the Fieldtrip function ‘electroderealign.m’. The resulting boundary element model volume conductor was used as a head model, or leadfield matrix.

Secondly, we calculated the forward model, or leadfield, from the grand average ERPs and the leadfield matrix using the Fieldtrip function ‘dipolefit.m’. We fitted the individual dipoles serially to 50 ms (it is well established that the P50 originates from Brodmann area 3b, cf. Elbert et al., 1995; Simões et al., 2001), 80 ms (S1 area 1 is likely to show peak activity around this time, cf. Bauer et al., 2006), and a symmetrical dipole pair to the ERP component at 140 ms (S2 is likely to show peak activity around this time). The obtained electrode positions were used to individually fit the orientation of the dipoles (position kept constant) according to individual ERP topographies to receive the leadfields of the oriented

dipoles. The topographies of individual ERPs and leadfields were visually inspected and verified.

Thirdly, we calculated time-domain beamformers (linearly constrained minimum variance spatial filtering, Van Veen et al., 1997), based on the individual leadfields for S1 and S2, and the covariance matrix of the average-referenced, artifact-cleaned data. For the ERP and the low-frequency analysis, the raw data were filtered with a low-pass filter (cutoff at 30 Hz), whereas the high-frequency data were filtered with a bandpass filter from 40-150 Hz. Each set of beamformer filters were then calculated using the following formula:

$$\mathbf{w}(\mathbf{r}) = (\mathbf{h}(\mathbf{r})'(\mathbf{C} + \lambda\mathbf{I})^{-1}(\mathbf{h}(\mathbf{r}))^{-1} \mathbf{h}(\mathbf{r})'(\mathbf{C} + \lambda\mathbf{I})^{-1}$$

where \mathbf{r} denotes the position vector of the respective grid point, \mathbf{h} is the leadfield matrix for a given point, \mathbf{C} is the covariance matrix of the sensor (electrode) data, \mathbf{I} is the identity matrix, λ is the regularization parameter and \mathbf{w} is the resulting spatial filter, or beamformer, coefficient vector. λ was set to half the mean of the diagonal of the cross-correlation matrix, a heuristic that yielded smooth sensor topographies of the filter coefficients without ‘overfitting’ signs. Instead of the inverse of the regularized covariance matrix, the Moore-Penrose pseudoinverse was taken, as standard in Fieldtrip.

The corresponding average-referenced, artifact-cleaned EEG data were projected through the filters, and the respective analyses were calculated (ERP, low-frequency, high-frequency analysis on respective filter coefficients). This procedure allowed the spatially most specific extraction of neural activity (time courses) from the a priori defined sources of interest.

In order to assess statistical significance between the experimental conditions, we calculated one-way repeated-measures ANOVAs with the factor DIFF. The significance threshold was set to the conservative value of 0.005.

3.3.10. Correlation of the time- and frequency-domain data with the drift rate, and RT

To investigate if the neural activity recorded with EEG could predict diffusion model parameters calculated from behavioral data, we correlated the amplitudes of the sensor space EEG components with the diffusion model parameter for each individual. As DIFF showed a significant effect on the drift rate (see results), we correlated the differential (high-low difficulty level) EEG components showing a DIFF effect with the differential (high-low difficulty level) drift rate.

3.3.11. Comparison of the studies using long and short presentation time

Behavioral as well as neurophysiological data were tested for significant differences between the two studies presenting the Braille patterns for 1000 ms or 100 ms, respectively. Firstly, we tested if the variances in the two studies were equal (sphericity assumption) using Mauchly's test of sphericity. Secondly, we calculated ANOVAs to test for within- and between-subjects effects. When sphericity was violated, we adjusted the degrees of freedom by using the Greenhouse-Geisser correction to produce a more accurate significance value.

3.4. Results

Per block, two different Braille patterns were presented to the right index finger and subjects indicated whether they perceived pattern 1 or 2 by left button press with the middle finger of their left hand, or a right button press with the index finger of their left hand, respectively (fig.15, 16). In different blocks, subjects were presented with three Braille pattern pairs varying in spatial separability and therefore difficulty (DIFF) (fig.15). Results were averaged over the two Braille patterns with identical DIFF as well as over correct and incorrect trials.

1000 ms study

Data were measured from 16 subjects. As bimodal RT distributions cannot be explained by the diffusion model, we established a procedure to separate unimodal and bimodal RT distributions (cf. section 3.3.5). We calculated recinormal RT distributions, fitted one and two Gaussian processes, and subtracted the two BIC values per subject to determine the relative superiority of the two over the one Gaussian process model. The differential BIC was for the 'bimodal subjects' ≥ 280 , and ≤ 43 for the 'unimodal subjects'. Four subjects (fig.18: subject 2, 3, 6, 16) with a difference greater than two standard errors (SE) from the mean difference were defined bimodal, and excluded from all analyses; all others were defined unimodal.

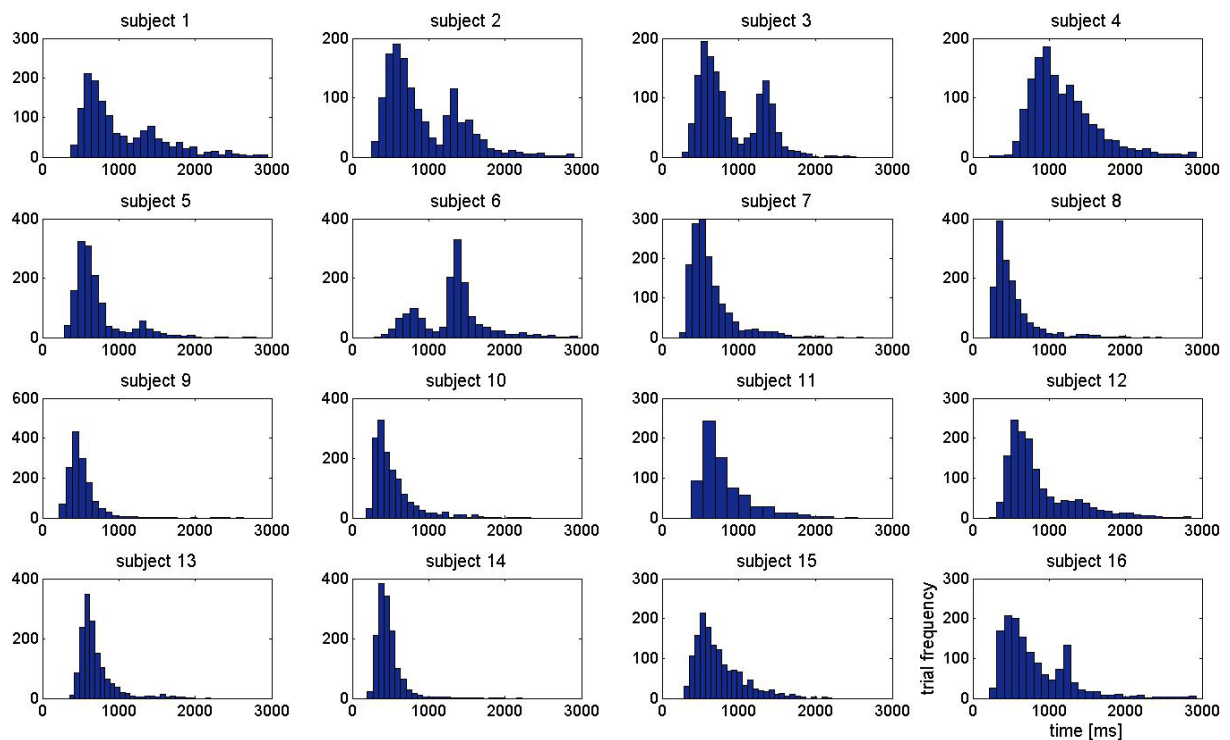


Fig.18 (1000 ms study): RT distribution per subject, per time bin at least 50 trials.

100 ms study

Data are reported for eleven subjects. In this study, none of the subjects showed a bimodal RT distribution (fig.19).

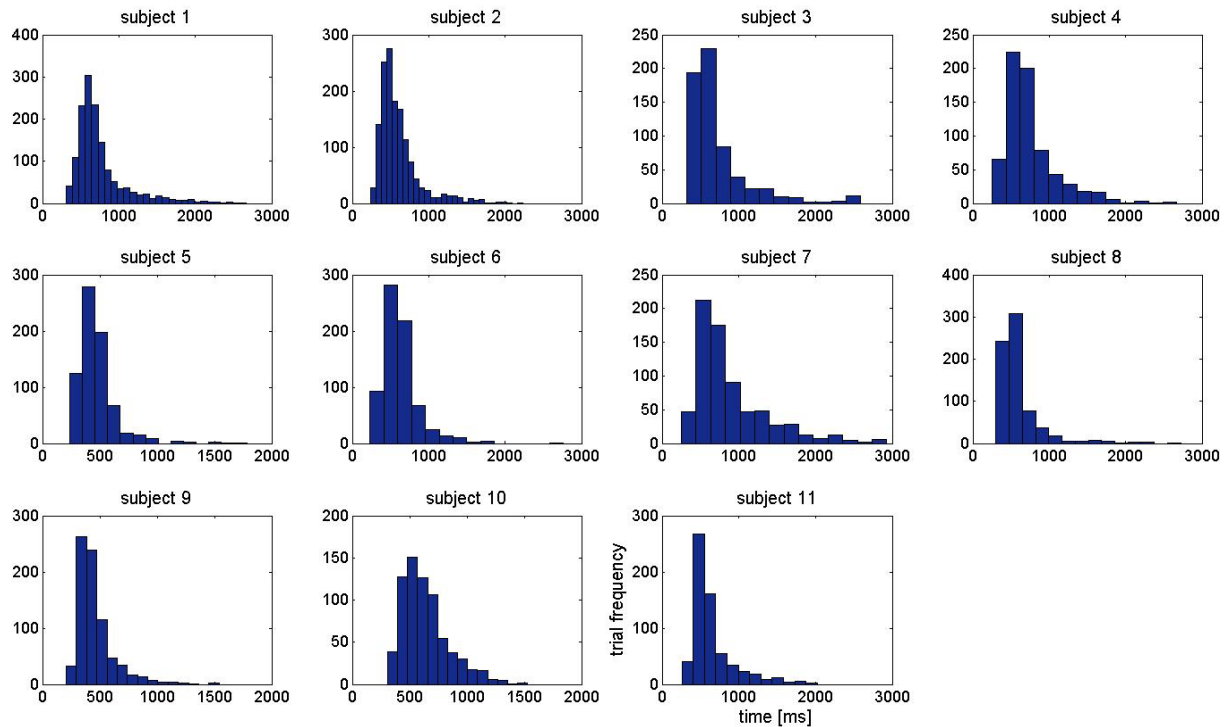


Fig.19 (100 ms study): RT distribution per subject, per time bin at least 50 trials.

3.4.1. Behavioral and diffusion model data

1000 ms study

With increasing DIFF, subjects responded more slowly ($F_{(2,11)} = 26.85$, $p < 0.001$) (fig.20A) and committed more errors ($F_{(2,11)} = 12.62$, $p < 0.001$) (fig.20B). Average values per condition (easy versus medium versus hard) as well as statistics of RT and % correct are presented in table 2.

As in the diffusion model the quality of sensory information (DIFF) is seen to primarily affect the drift rate, we nested two models as follows: (1) all parameters were restricted to be equal across conditions; (2) the drift rate was free to vary across conditions (for further details, see sections 2.3.6. and 3.3.6). For all subjects, BIC values revealed a significantly better fit when leaving the drift rate free (model 2). Accordingly, we chose this model for all subjects.

As expected, the drift rate decreased with decreasing DIFF ($F_{(2,11)} = 11.78$, $p < 0.001$) (fig.20C). Average values of the diffusion model parameters are presented together with the statistics in table 2.

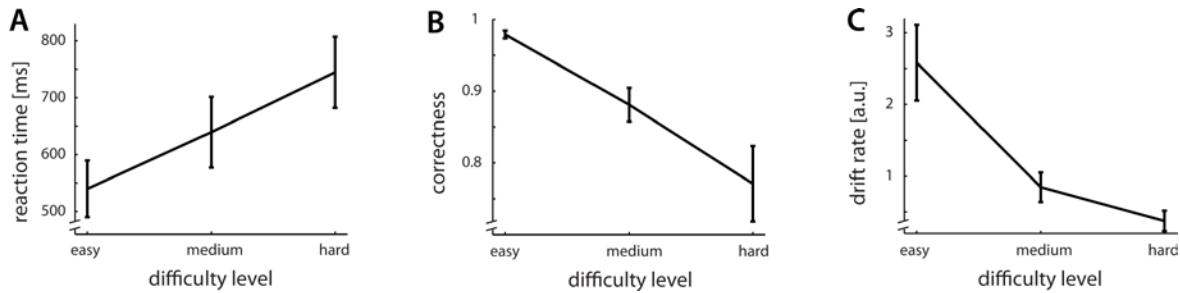


Fig.20 (1000 ms study): Behavioral and modeling results. With increasing difficulty, subjects showed (A) slower RTs ($F_{(2,11)} = 26.85$, $p < 0.001$), (B) higher error rates ($F_{(2,11)} = 12.62$, $p < 0.001$), and, as expected, (C) lower drift rates ($F_{(2,11)} = 11.78$, $p < 0.001$). Error bars present ± 1 SEM.

	Experimental conditions (difficulty levels, DIFF)			Main effect DIFF	
	easy	medium	hard	$F_{(2,18)}$	p
Reaction time	529.75	639.38	744.67	26.85	< 0.001
% correct	97.91	88.10	77.09	12.62	< 0.001
Drift rate	2.58	0.85	0.37	11.78	< 0.001

Table 2 (1000 ms study): Average values and statistics (one-way repeated-measures ANOVAs) for reaction times, percentage of correct responses, and drift rate.

100 ms study

With increasing DIFF, subjects had slower RTs ($F_{(2,10)} = 21.11$, $p < 0.001$) (fig.21A) and lower % correct ($F_{(2,10)} = 12.07$, $p < 0.001$) (fig.21B). Average values per condition (easy versus medium versus hard) as well as statistics of RT and % correct are presented in table 3.

Like in the 1000 ms study, we nested two models as follows: (1) all parameters were restricted to be equal across conditions, (2) the drift rate was free to vary across conditions. For all subjects, BIC values revealed a significantly better fit when leaving the drift rate free (model 2) so that we chose this model for all subjects.

As expected, the drift rate decreased with decreasing DIFF ($F_{(2,10)} = 33.35$, $p < 0.001$) (fig.21C). Average values of the diffusion model parameters are presented together with the statistics in table 3.

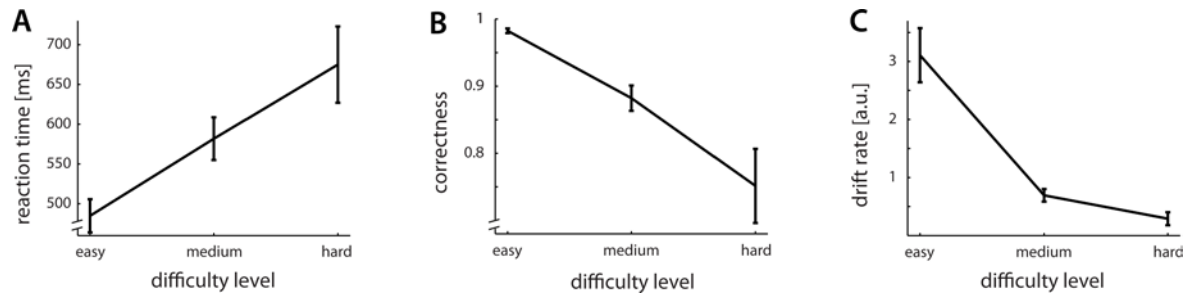


Fig.21 (100 ms study): Behavioral and modeling results. With increasing difficulty, subjects showed (A) slower RTs ($F_{(2,10)} = 21.11$, $p < 0.001$), (B) higher error rates ($F_{(2,10)} = 12.07$, $p < 0.001$), and, as expected, (C) lower drift rates ($F_{(2,10)} = 33.35$, $p < 0.001$). Error bars present ± 1 SEM.

	Experimental conditions (DIFF)			Main effect DIFF	
	easy	medium	hard	$F_{(2,18)}$	p
Reaction time	484.82	581.77	675.00	21.11	< 0.001
% correct	98.25	88.22	75.14	12.07	< 0.001
Drift rate	3.11	0.69	0.29	33.35	< 0.001

Table 3 (100 ms study): Average values and statistics (one-way repeated-measures ANOVAs) for reaction times, percentage of correct responses, and drift rate.

3.4.2. Effects of tactile stimulation in the time domain

EEG time-domain data on the sensor level were baseline-corrected to the period before stimulus onset (-100 to 0 ms), and EEG amplitudes were averaged using a sliding time window of 50 ms. To test for statistically significant effects between DIFF conditions, we calculated one-way repeated-measures ANOVAs with the factor DIFF and a significance threshold of 0.001.

EEG time-domain data on the beamformer source level were computed for the following regions of interest (ROIs): S1 area 3b, S1 area 1, S2 contralateral, S2 ipsilateral. ERP calculations were otherwise identical to the one on the sensor level. To test for statistically significant effects between DIFF conditions, we calculated one-way repeated-measures ANOVAs analysis with the factor DIFF and a significance threshold of 0.005.

We correlated the differential (easy-hard) DIFF effects with the differential (easy-hard) drift rate parameter of the diffusion model to investigate whether neural activity could predict the drift rate calculated from behavioral data. Also, we correlated the sensor space EEG components with the RT to investigate whether neural activity could predict the behavioral outcome.

3.4.2.1. *Stimulus-locked ERP components across difficulty levels*

1000 ms study

Consistent with previous human electrophysiological studies using mechanical tactile stimulation, the first brain response peaked around 50 ms after stimulus onset (P50, P stands for positive deflection when using EEG) in the left hemisphere, contralateral to the stimulated finger (fig.22A,B) (Bauer et al., 2006; Desmedt et al., 1983; Hämäläinen et al., 1990). Both, topography and peak activity at the same time in the S1 area 3b beamformer (fig.23A) suggest this component to originate from contralateral S1 area 3b. It is well established that the P50 originates from Brodmann area 3b (Elbert et al., 1995; Simões et al., 2001).

Approximately 30 ms later, a second component emerged in the left hemisphere (fig.22A,B), and peak activity at the same time in the S1 area 1 beamformer (fig.23B) as well as the results from Bauer et al. (2006) suggest this component to originate from contralateral S1 area 1.

From around 120 ms after stimulus onset on, activity became increasingly bilateral (fig.22A,D). In accordance with the literature (e.g., Bauer et al., 2006; Tanaka et al., 2008), activity might originate from bilateral S2. Also the S2 contralateral beamformer (fig.23C right) shows marked activity from around 120 ms. Please note that ipsilateral S2 displays no peak around 150 ms (fig.23D right) but the time course is different from the time course in S2 ipsilateral in the 100 ms study (fig.25C right).

Around 300 to 500 ms after stimulus onset, activity in the occipital to temporo-parietal cortex emerged (fig.22A,E). Bauer et al. (2006) also found time-locked activation of the medial occipital, presumably visual, cortex without any visual stimulation. Timing and topography suggest this component to be the P3b, a subcomponent of the P300 (Polich, 2007; Verleger, 2008; Verleger et al., 2005).

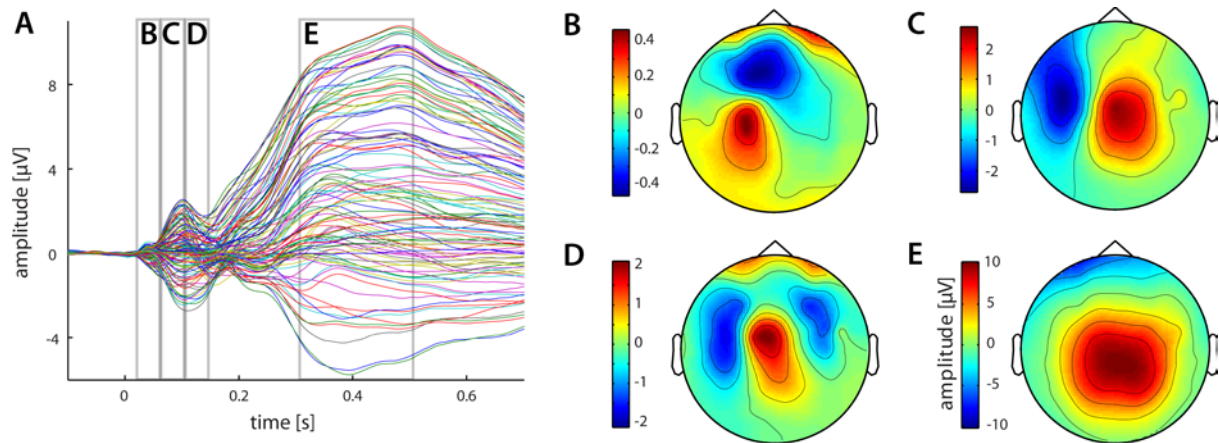


Fig.22 (1000 ms study): Stimulus-locked ERP components occurring across the difficulty levels. (A) Time course of the grand averaged, stimulus-locked ERP depicts four components (B-E, highlighted by gray boxes). Timings are given relative to stimulus onset. (B) The scalp topography of the stimulus-locked ERP across conditions around 35 to 85 ms. (C) Around 75 to 125 ms, a second component emerged. (D) From around 120 ms until 175 ms this component became increasingly bilateral. (E) Topography and timing between 300 and 550 ms.

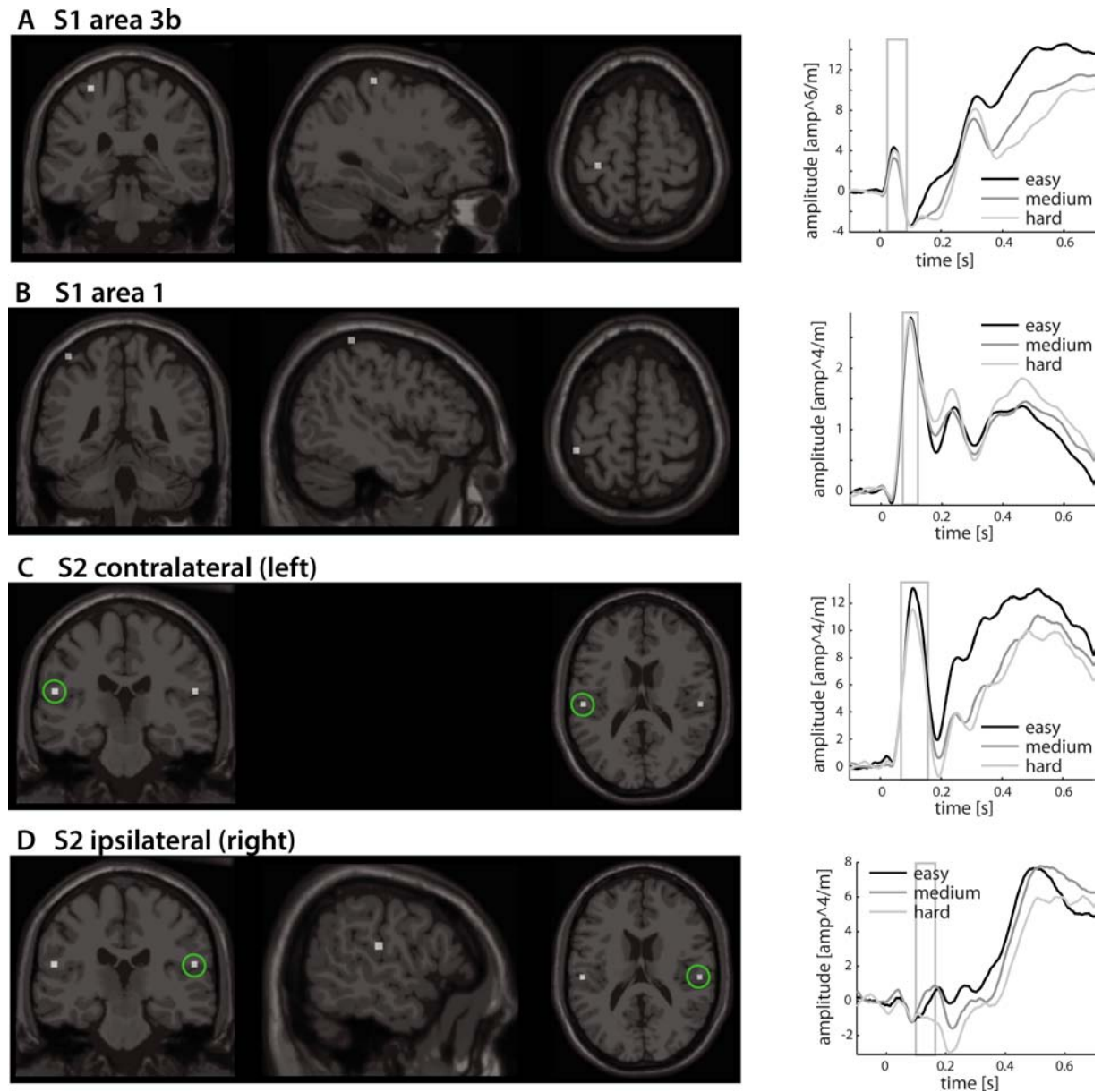


Fig.23 (1000 ms study): Grand average beamformer source estimates in the time domain in (A) S1 area 3b, (B) S1 area 1, (C) S2 contralateral, (D) S2 ipsilateral. (left) Location overlaid on a structural image of the brain. (right) For the four different locations, the time courses of activity per difficulty level (easy, medium, hard) are displayed. Time windows of interest are highlighted by gray boxes.

100 ms study

Matching the results of the 1000 ms study, the first brain response peaked around 50 ms after stimulus onset (P50) in the left hemisphere (fig.24A,B), as well as in the contralateral S1 area 3b beamformer (fig.25A).

Approximately 10 ms later, a second component emerged in the left hemisphere (fig.24A,C), as well as in the S1 area 1 beamformer (fig.25B).

From around 125 ms until 175 ms after stimulus onset on, activity spread out to both hemispheres (fig.24A,D), corresponding to the bilateral S2 beamformer (fig.25C,D).

Around 350 to 500 ms after stimulus onset, activity in medial parietal to temporal areas was measured (fig.24E).

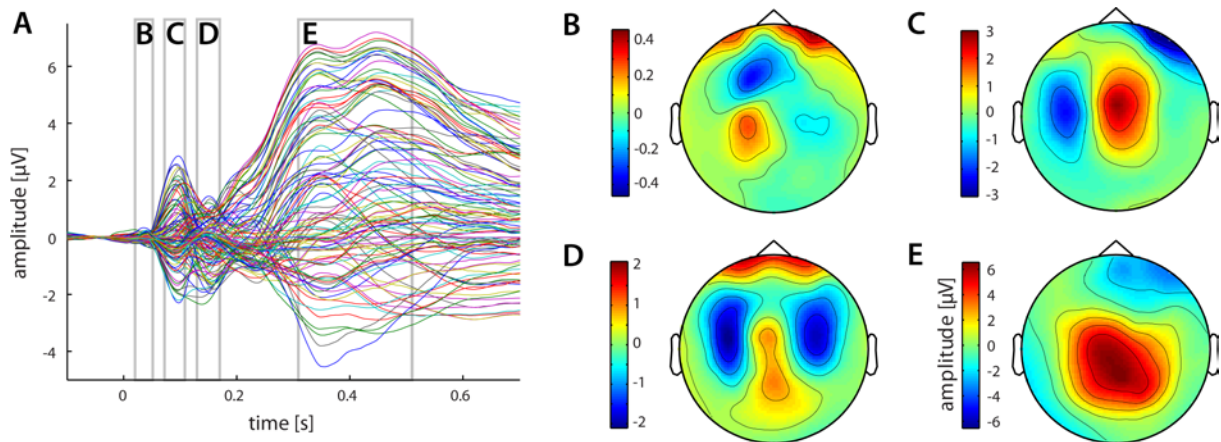


Fig.24 (100 ms study): Stimulus-locked ERP components occurring across the difficulty levels. (A) Time course of the stimulus-locked ERP depicts four components (B-E, highlighted by gray boxes). Timings are given relative to stimulus onset. (B) The scalp topography of the stimulus-locked ERP across conditions around 25 to 75 ms. (C) Around 85 to 135 ms a component emerged. (D) Topography and timing between 125 and 175 ms. (E) Topography and timing between 350 and 500 ms.

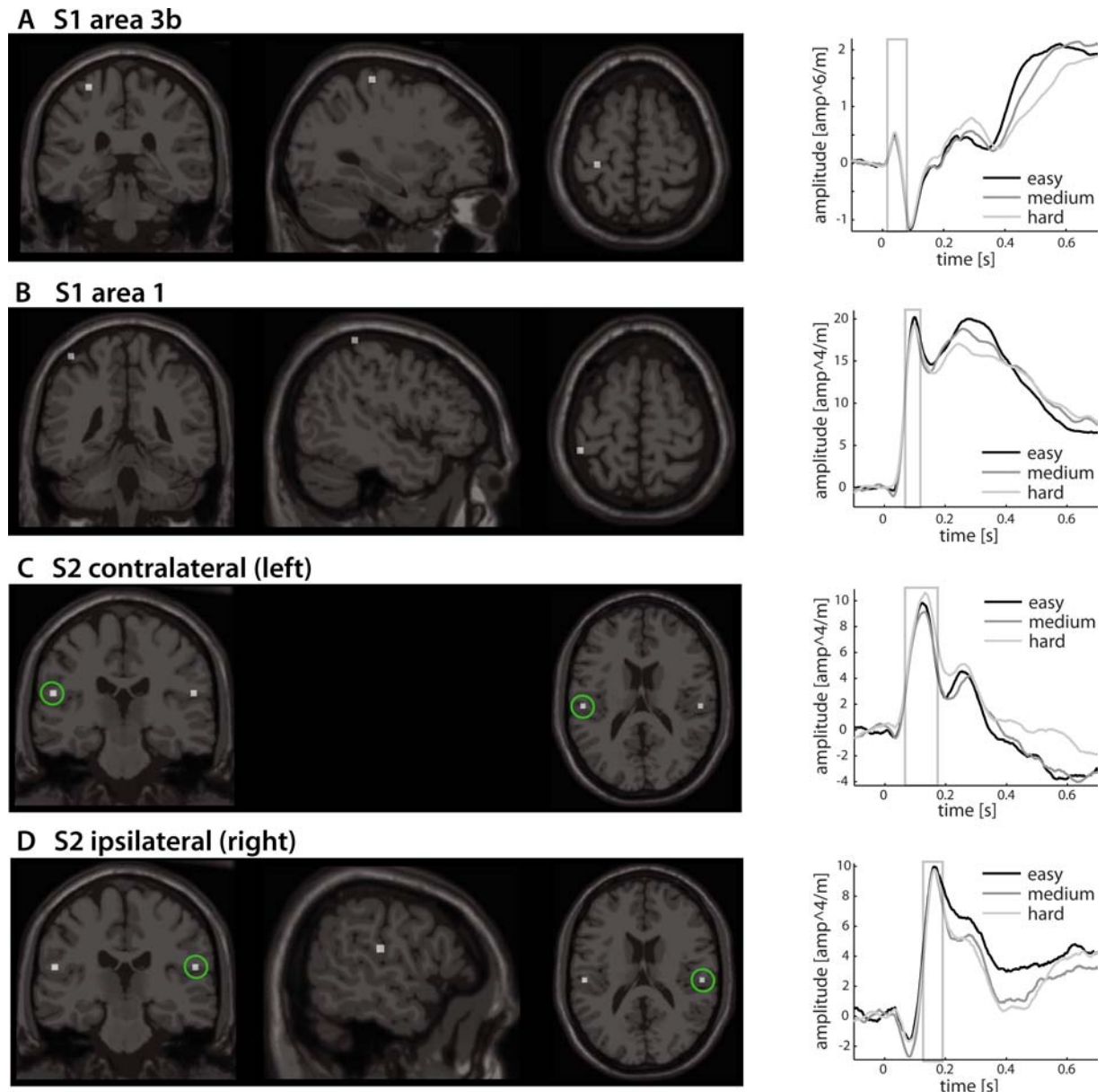


Fig.25 (100 ms study): Grand average beamformer source estimates in the time domain in (A) S1 area 3b, (B) S1 area 1, (C) S2 contralateral, (D) S2 ipsilateral. (left) Location overlaid on a structural image of the brain. (right) For the four different locations, the times course of activity per difficulty level (easy, medium, hard) are displayed.

3.4.2.2. *DIFF component in left medio-frontal channels*

1000 ms study

Time courses of evoked fields differed between the three DIFF conditions. Multiple left medio-frontal channels showed a significant DIFF effect on the EEG amplitude between 320 and 370 ms after stimulus onset ($F_{(2,11)} = 16.06$, $p < 0.001$) (fig.26A). These sensors also showed great differential activity (easy-hard DIFF) (fig.26B). The time courses for the DIFF

levels reveal that in this time interval the amplitude increased with increasing DIFF (fig.26C). The differential (easy-hard) EEG amplitude was not significantly correlated with either the drift rate ($r = 0.27$, $p = 0.40$) or RT ($r = -0.51$, $p = 0.094$).

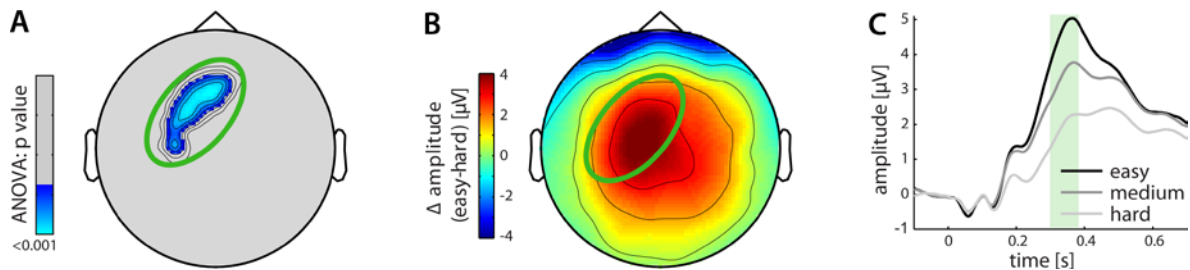


Fig.26 (1000 ms study): Significant DIFF effect between 320 and 370 ms after the stimulus onset in left medio-frontal channels not significantly correlated with either the drift rate or RT. (A) Significant DIFF effect on the EEG amplitude during the epoch of interest in left medio-frontal channels ($F_{(2,11)} = 16.06$, $p < 0.001$). (B) Group average of difference topography (easy-hard DIFF) during the epoch of interest. (C) Time course of these channels of interest in response to easy, medium, and hard DIFF stimuli showing that with decreasing DIFF the amplitude decreased. Stimulus onset at 0 ms. The epoch of interest is highlighted by a green box.

100 ms study

As in the 1000 ms study, left medio-frontal channels showed a significant DIFF effect on the EEG amplitude around 325 to 375 ms after stimulus ($F_{(2,10)} = 15.98$, $p < 0.001$) (fig.27A). These sensors also showed great differential activity (easy-hard DIFF) (fig.27B), and the time courses for the DIFF levels show that in this time interval the amplitude increased with increasing DIFF (fig.27C). The differential (easy-hard) EEG amplitude did not correlate significantly with either DR ($r = 0.32$, $p = 0.31$) or RT ($r = -0.27$, $p = 0.41$).

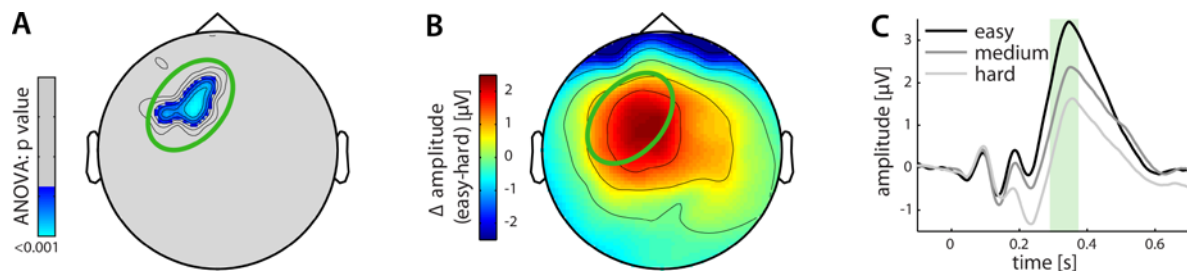


Fig.27 (100 ms study): Significant DIFF effect between 325 and 375 ms after the stimulus onset in left medio-frontal channels not significantly correlated with either the drift rate or RT. (A) Significant DIFF effect on the EEG amplitude during the epoch of interest in left medio-frontal channels ($F_{(2,10)} = 15.98$, $p < 0.001$). (B) Group average of difference topography (easy-hard DIFF) during the epoch of interest. (C) Time course of these channels of interest in response to easy, medium, and hard DIFF stimuli showing that with decreasing DIFF the amplitude decreased. Stimulus onset at 0 ms. The epoch of interest is highlighted by a green box.

3.4.2.3. *DIFF component in left lateral channels*

1000 ms study

Multiple left lateral channels showed a significant DIFF effect on the EEG amplitude between 340 and 490 ms after stimulus onset ($F_{(2,11)} = 19.80$, $p < 0.001$) (fig.28A). These sensors also showed great differential activity (easy-hard DIFF) (fig.28B). The time courses for the DIFF levels reveal that in this time interval the amplitude increased with increasing DIFF (fig.28C). The differential (easy-hard) EEG amplitude was positively correlated with the drift rate ($r = 0.58$, $p = 0.049$) (fig.28D), and negatively correlated with RT ($r = -0.67$, $p = 0.018$) (fig.28E). DR and RT have an inverse relationship, i.e., the more difficult the task, the longer the RT but the lower the drift rate.

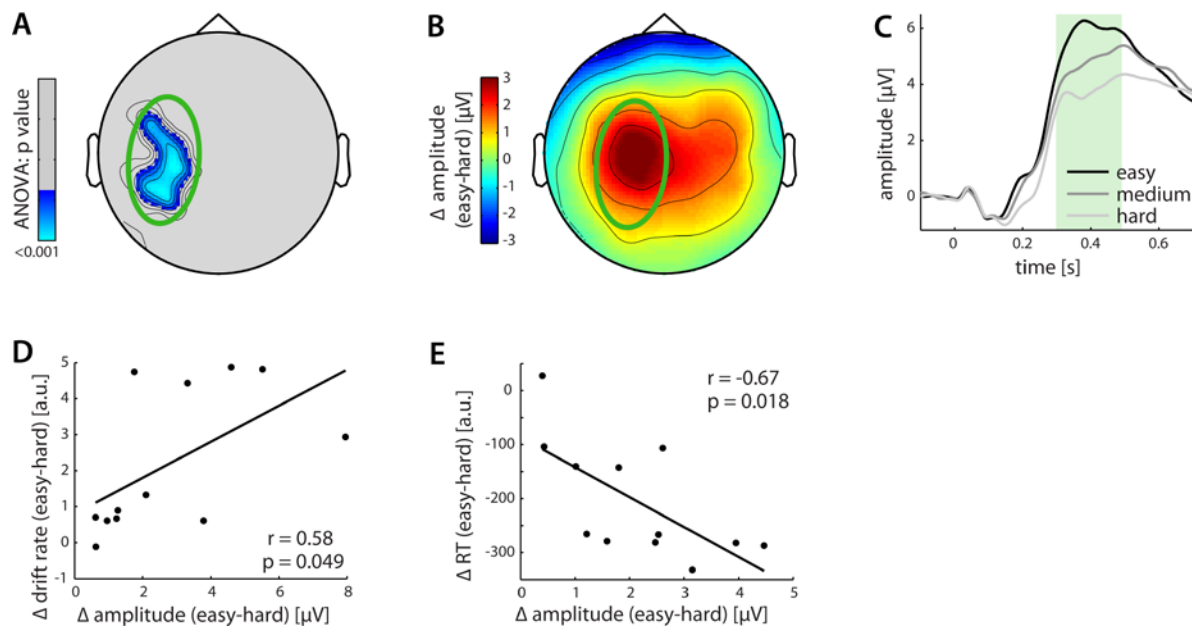


Fig.28 (1000 ms study): Significant DIFF effect between 340 and 490 ms after the stimulus onset in left lateral channels positively correlated with the drift rate and negatively correlated with the RT. (A) Significant DIFF effect on the EEG amplitude during the epoch of interest in left lateral channels ($F_{(2,11)} = 19.80$, $p < 0.001$). (B) Group average of difference topography (easy-hard DIFF) during the epoch of interest. (C) Time course of these channels of interest in response to easy, medium, and hard DIFF stimuli showing that with decreasing DIFF the amplitude decreased. Stimulus onset at 0 ms. The epoch of interest is highlighted by a green box. (E) Positive correlation between differential (easy-hard DIFF) EEG activity and the drift rate ($r = 0.58$, $p = 0.049$), and (F) negative correlation between differential (easy-hard DIFF) EEG activity and RT ($r = -0.67$, $p = 0.018$).

100 ms study

Multiple left frontal channels showed a significant DIFF effect on the EEG amplitude between 425 and 475 ms after stimulus onset ($F_{(2,10)} = 15.21$, $p < 0.001$) (fig.29A). These sensors also showed the greatest activity in the difference topography (easy-hard DIFF) (fig.29B). The amplitude decreased with increasing DIFF in this time interval as can be seen from the time courses for the DIFF levels (fig.29C). The differential (easy-hard) EEG amplitude correlated significantly positively with DR ($r = 0.69$, $p = 0.020$) (fig.29D), but not significantly with RT ($r = -0.48$, $p = 0.13$).

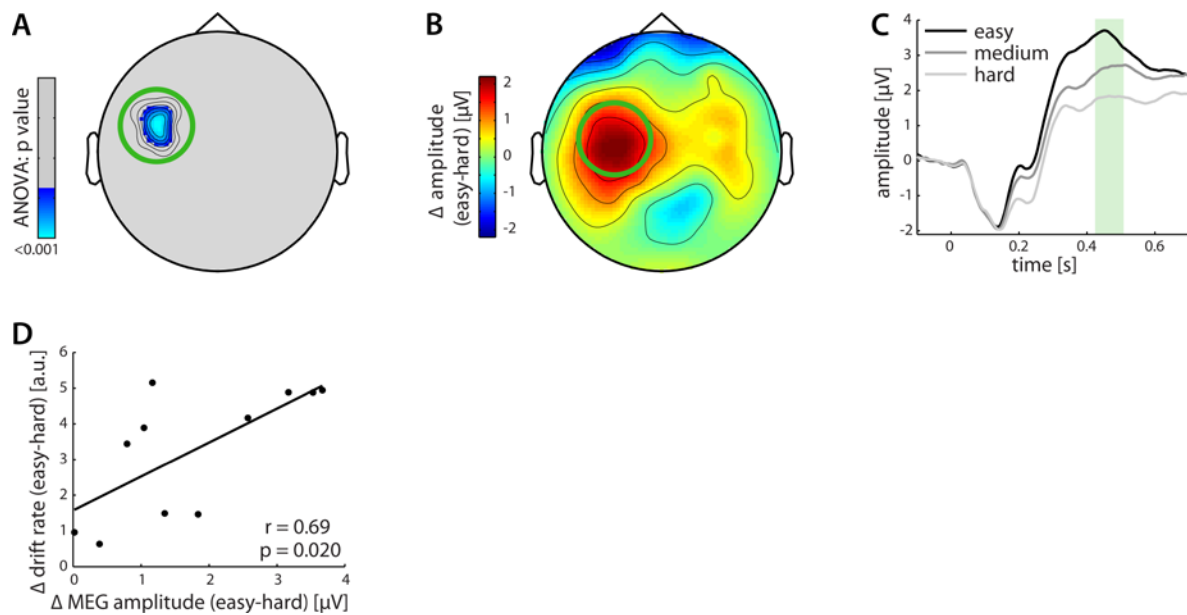


Fig.29 (100 ms study): Significant DIFF effect between 425 and 475 ms after the stimulus onset in left lateral channels positively correlated with the drift rate but not significantly correlated with the RT. (A) Significant DIFF effect on the EEG amplitude during the epoch of interest in left lateral channels ($F_{(2,10)} = 15.21$, $p < 0.001$). (B) Group average of difference topography (easy-hard DIFF) during the epoch of interest. (C) Time course of these channels of interest in response to easy, medium, and hard DIFF stimuli showing that with decreasing DIFF the amplitude decreased. Stimulus onset at 0 ms. The epoch of interest is highlighted by a green box. (E) Positive correlation between differential (easy-hard DIFF) EEG activity and the drift rate ($r = 0.69$, $p = 0.020$).

3.4.2.4. DIFF component in left S1 area 3b

1000 ms study

S1 area 3b showed a significant DIFF effect on the EEG amplitude between 370 and 590 ms after stimulus onset ($F_{(2,11)} = 17.23$, $p < 0.001$) (fig.30A). The amplitude decreased with increasing DIFF in this time interval as can be seen from the time courses for the DIFF levels (fig.30B). Interestingly, the significant effect started before the amplitude reached its maximum in the three conditions (around 500 ms) suggesting that the slope might differ between the conditions (for information on how we calculated it, please see section 3.3.8.). We found a significant DIFF effect on the EEG slope between 380 and 480 ms ($F_{(2,11)} = 8.54$, $p = 0.0018$), and the differential (easy-hard) EEG slope showed a positive trend in correlation with DR ($r = 0.56$, $p = 0.060$) (fig.30C) but there was no significant correlation between the EEG slope and RT ($r = -0.50$, $p = 0.10$). The differential (easy-hard) EEG amplitude was positively correlated with DR ($r = 0.62$, $p = 0.032$) (fig.30D), and the amplitude showed a negative trend in correlation with RT ($r = -0.55$, $p = 0.065$) (fig.30E).

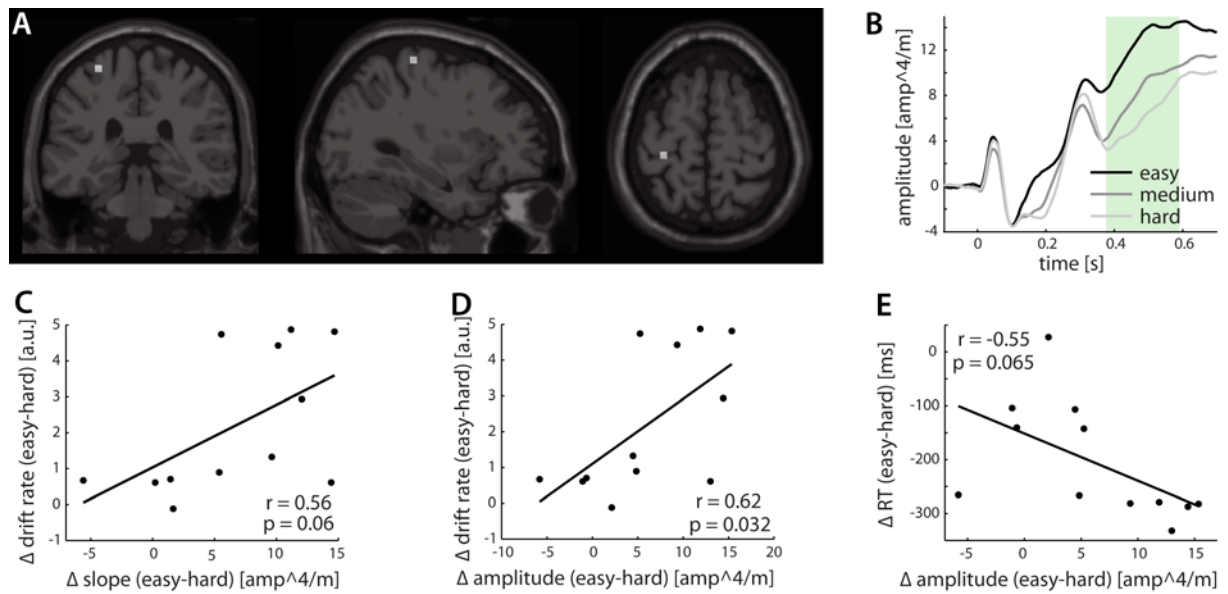


Fig.30 (1000 ms study): Significant DIFF effect between 370 and 590 ms after the stimulus onset in left S1 area 3b positively correlated with the drift rate and negatively correlated with RT. (A) Beamformer location overlaid on a structural image of the brain. (B) Time course of activity in response to easy, medium, and hard DIFF stimuli showing that with decreasing DIFF the amplitude decreased. Stimulus onset at 0 ms. The epoch of interest is highlighted by a green box. (C) Positive trend in correlation between differential (easy-hard DIFF) EEG slope activity and the drift rate ($r = 0.56$, $p = 0.060$). (D) Positive correlation between differential EEG amplitude and the drift rate ($r = 0.62$, $p = 0.032$). (E) Negative trend in correlation between differential EEG activity and RT ($r = -0.55$, $p = 0.065$).

100 ms study

S1 area 3b showed a significant DIFF effect on the EEG amplitude between 450 and 515 ms after stimulus onset ($F_{(2,10)} = 7.78$, $p = 0.0028$) (fig.31A). The amplitude decreased with increasing DIFF in this time interval as can be seen from the time courses for the DIFF levels (fig.31B). As in the 1000 ms study, the significant effect started before the amplitude reached its maximum in the three conditions (around 500 ms) suggesting that the slope might differ between the conditions. We found, however, no significant DIFF effect on the EEG slope between 370 and 470 ms ($F_{(2,10)} = 1.27$, $p = 0.30$). The differential (easy-hard) EEG slope was neither significantly correlated with DR ($r = 0.10$, $p = 0.77$) nor RT ($r = 0.56$, $p = 0.071$). Contradicting the results from the 1000 ms study, the differential (easy-hard) EEG amplitude was not significantly correlated with either DR ($r = -0.02$, $p = 0.96$) or RT ($r = 0.09$, $p = 0.79$). One possible reason might be that we conducted only one session in the 100 ms study. Though this yielded a sufficient number of trials for the EEG analysis, diffusion model

parameter estimations might have been suboptimal due to the relatively low number of error trials, at least in the easy DIFF condition.

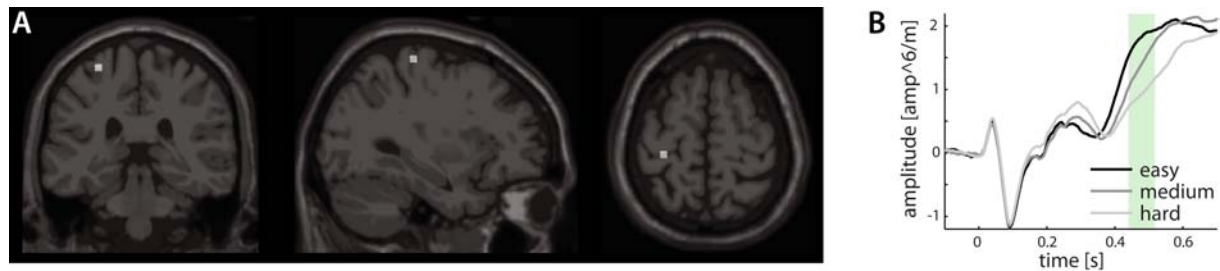


Fig.31 (100 ms study): Significant DIFF effect between 450 and 515 ms after the stimulus onset in left S1 area 3b not significantly correlated with either the drift rate or RT. (A) Beamformer location overlaid on a structural image of the brain. (B) Time course of activity in response to easy, medium, and hard DIFF stimuli showing that with decreasing DIFF the amplitude decreased. Stimulus onset at 0 ms. The epoch of interest is highlighted by a green box.

3.4.3. Effects of tactile stimulation in the frequency domain

We conducted time-frequency analyses because modulations in task-related cortical activity are often induced by, but not phase-locked to, external events, e.g., stimulus onset (Donner and Siegel, 2011; Pfurtscheller and Lopes da Silva, 1999). The following figures display z -scores resulting from intraindividual statistical comparisons between stimulation and baseline, computed for each time-frequency bin and pooled across subjects. To test for statistical significance between the difficulty levels on the sensor level, we calculated one-way repeated-measures ANOVAs with the factor DIFF and a significance threshold of 0.001.

For EEG low frequency-domain data on the sensor level, 2 to 40 Hz in 2 Hz steps were chosen as frequencies of interest and 0 to 1000 ms in 25 ms steps as time windows of interest. Amplitudes were averaged using a sliding frequency window of 7.5 Hz, and a sliding time window of 125 ms. We did not further analyze theta activity because it is dominated by the evoked field which cannot be subtracted entirely.

For EEG high frequency-domain data on the sensor level, 40 to 150 Hz in 5 Hz steps were chosen as frequencies of interest and 0 to 1000 ms in 50 ms steps as time windows of interest. Amplitudes were averaged using a sliding frequency window of 25 Hz and a sliding time window of 250 ms. The designation of the high frequencies should not be taken literally because multitapers (cf. materials and methods, section 3.3.9) smooth over frequencies, i.e., when looking at activity around 40 Hz, it is in reality activity between 30 and 50 Hz.

Additionally, low frequencies dominate all frequencies due to the $1/f$ drop off of the power spectrum (Mitra and Pesaran, 1999).

EEG frequency-domain data on the beamformer source level were calculated for the following regions of interest (ROIs): S1 area 3b, S1 area 1, S2 contralateral, S2 ipsilateral. Here, we tested for significant DIFF effects by calculating one-way repeated-measures ANOVAs for the stimulus-locked analysis with the factor DIFF and a significance threshold of 0.005. No region of interest showed a significant DIFF effect.

We correlated the frequency-domain, sensor space DIFF components with the drift rate parameter of the diffusion model to investigate if neural activity could predict the drift rate calculated from behavioral data. Also, we correlated the frequency-domain, sensor space EEG components with the RT to investigate if neural activity could predict the behavioral outcome.

3.4.3.1. Stimulus-induced components across difficulty levels

Multiple sensorimotor studies report gamma activations in combination with alpha/beta suppressions and subsequent beta rebound (for review, see Donner and Siegel, 2011). We focused on these effects when examining activation patterns across difficulty levels (DIFF). The 1000 and the 100 ms studies are described together because the results are comparable. We divided the data into high and low frequencies.

Suppression of low-frequency oscillations

In the 1000 ms and the 100 ms studies, the most salient effect of tactile stimulation was a widespread suppression of low-frequency oscillatory activity ranging from around 7 to 35 Hz, in the time range of around 200 to 750 ms peaking around 400 to 600 ms, in left and right lateral channels (more confined in the 100 ms study) (fig.32A,B 1000 ms study; fig34A,B 100 ms study). Please note the shift towards lower frequencies over time. Such an effect was also found by Bauer et al. (2006) who localized this effect into primary sensorimotor areas, consistent with other studies (Crone et al., 1998; Nikouline et al., 2000).

Correspondingly, we measured an alpha/beta suppression in S1 area 3b contralateral, S1 area 1 contralateral, and S2 bilateral (localized using the beamformer technique) in both studies from around 250 to 500 ms (fig.33A-D3 1000 ms study; fig.35A-D3 100 ms study). In contrast to the very broad distribution on the sensor level, the activity here showed two

distinct peaks from 8 to 14 Hz and 16 to 24 Hz, matching the standard mu (8-15 Hz) and beta (15-25 Hz) bands. It is not surprising to find more concise activation on the beamformer level because, unlike time series from individual electrodes which contain a mixture of signals from multiple generators with different spectral profiles, time courses extracted from beamformer spatial filters derive from a restricted region of interest (cf. materials and methods section 3.3.10.).

Interestingly, we also measured an alpha-/beta suppression in the same left medio-frontal channels (fig.32C1 1000 ms study; fig.34C1 100 ms study) where we measured a DIFF effect in the time-locked analysis (cf. 3.4.2.2).

Rebound of low-frequency oscillations

In both studies, suppression of low-frequency oscillations was followed by a beta rebound, ranging from around 15 to 22 Hz. The time window started at around 1000 ms in left and right lateral channels (fig.32A1,B1 1000 ms study, fig.34A1,B1 100 ms study). In the study of Bauer et al (2006), the beta rebound lasted until the next stimulus, and was localized into bilateral somatosensory/sensorimotor regions. Correspondingly, we measured a beta rebound in contralateral S1 area 3b, contralateral S1 area 1, contralateral S2 (fig.33A-C2,3 1000 ms; fig.35A-C2,3 100 ms study) but, in contrast to the measured activity on the sensor level, the rebound started at around average response time. Please note that in ipsilateral S2 the beta rebound started later in the 100 ms study (fig.35D2-3), and was absent in the 1000 ms study (fig.33D2-3) (note that S2 ipsilateral showed weak activity in the 1000 ms study in the time domain data, section 3.4.2.).

In left fronto-medial channels, we also measured a beta rebound after the alpha-/beta suppression (cf. preceding section) at around average response time (fig.32C1 1000 ms study, fig.34C1 100 ms study).

Enhancement of high-frequency oscillations

In both studies, we found an increase of gamma power in left and right lateral regions ranging from 40 to 100 Hz, at an early time window between 100 and 250 ms (fig.32D,E 1000 ms study, fig.34D,E 100 ms study). The distribution was more focal than in the low frequencies, which might be at least partly due to the relatively low signal-to-noise ratio. Similar activity was localized into primary somatosensory cortex by Bauer et al (2006) who also showed that

the enhancement in gamma frequencies was largely non-phase locked to the stimulus. Correspondingly, we measured gamma activation between 100 and 250 ms in contralateral S1 area 3b and S1 area 1 with a stronger enhancement at a broader frequency range in S1 area 3b (fig.33A-B4,5 1000 ms study; fig.35A-B4,5 100 ms study). Please note that the frequency range was narrower on the beamformer source level than on the sensor level, as was already the case for the low frequencies.

Gamma-band enhancement was also measured in fronto-medial channels from around 200 ms on (more concise in 100 ms study) (fig.32F 1000 ms study, fig.34F 100 ms study). Here, the frequency range became broader over time. Interestingly, especially in the 1000 ms study, fronto-medial activation seemed to be part of a broader network that also involved more parietal to occipital central regions (fig.32F2). Gamma activations are often involved in encoding functions such as motor planning (Donner and Siegel, 2011) but source localization would be necessary to investigate if the observed activity originated from motor-related or other areas, such as the anterior cingulate cortex (ACC). Beamformer analysis was not applied here because onset time windows varied considerably between subjects and the specification of MNI coordinates was unclear (motor-related areas or ACC).

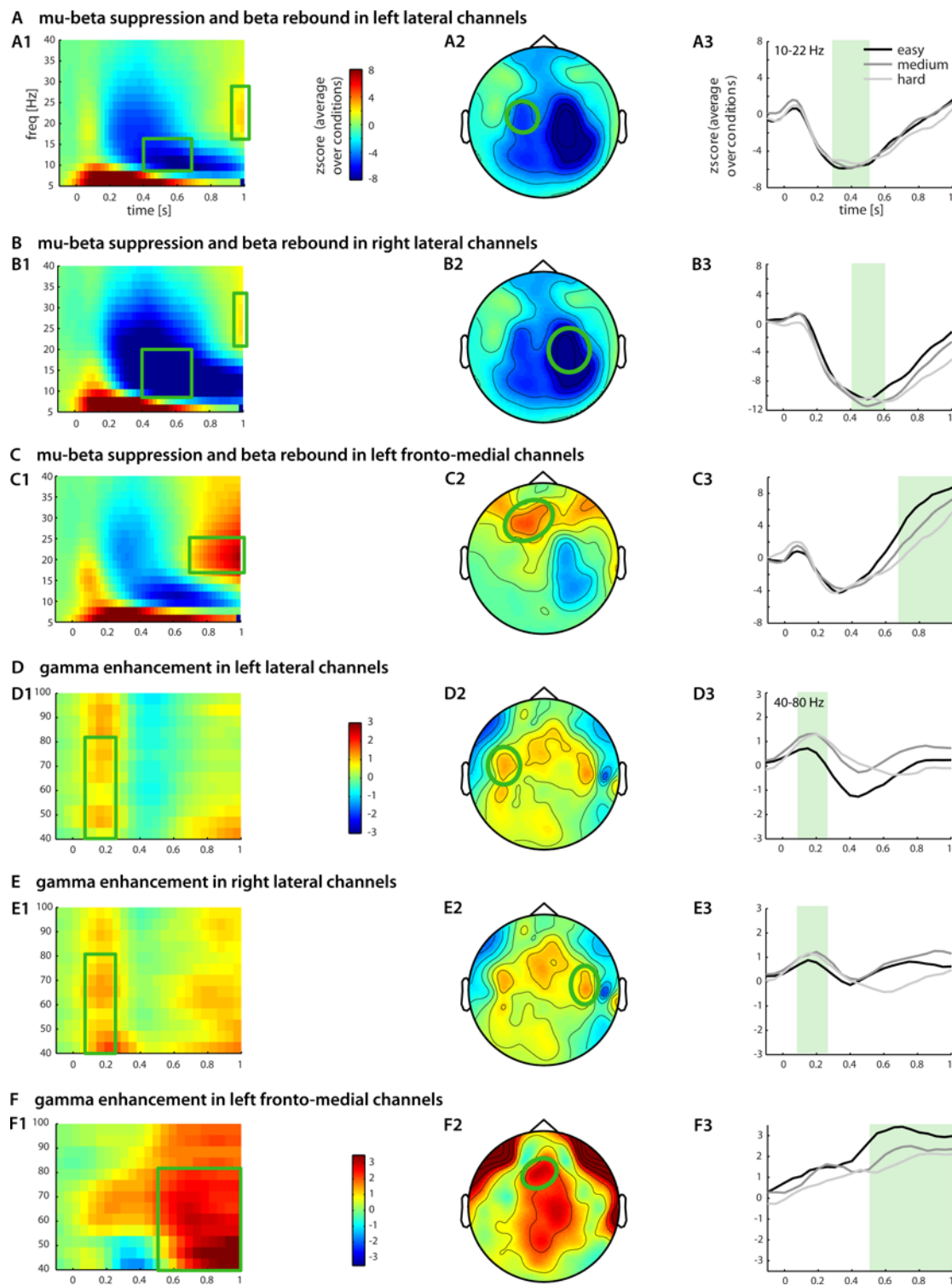


Fig.32 (1000 ms study): Components in the frequency domain across the difficulty levels revealed six components: (A) mu-beta suppression (10 to 22 Hz) between 400 and 650 ms in left lateral channels, (B) mu-beta suppression between 400 and 650 ms in right lateral channels, (C) enhanced beta activity (15 to 25 Hz) between 700 and 1000 ms in left fronto-medial channels, (D) enhanced gamma activity (40 to 80 Hz) between 100 and 250 ms in left lateral channels, (E) enhanced gamma activity between 100 and 250 ms in right lateral channels, and (F) enhanced gamma activity between 500 and 1000 ms in fronto-medial channels. (A-F 1) Time-frequency resolved power change after stimulation, time-frequency windows of interest bordered by a green box. (A-F 2) Topography of activation patterns in time-frequency windows of interest, channels of interest bordered by a green circle. (A-F 3) Time course of activation in channels of interest in selected frequency windows of interest. The time window of interest is highlighted by a green box.

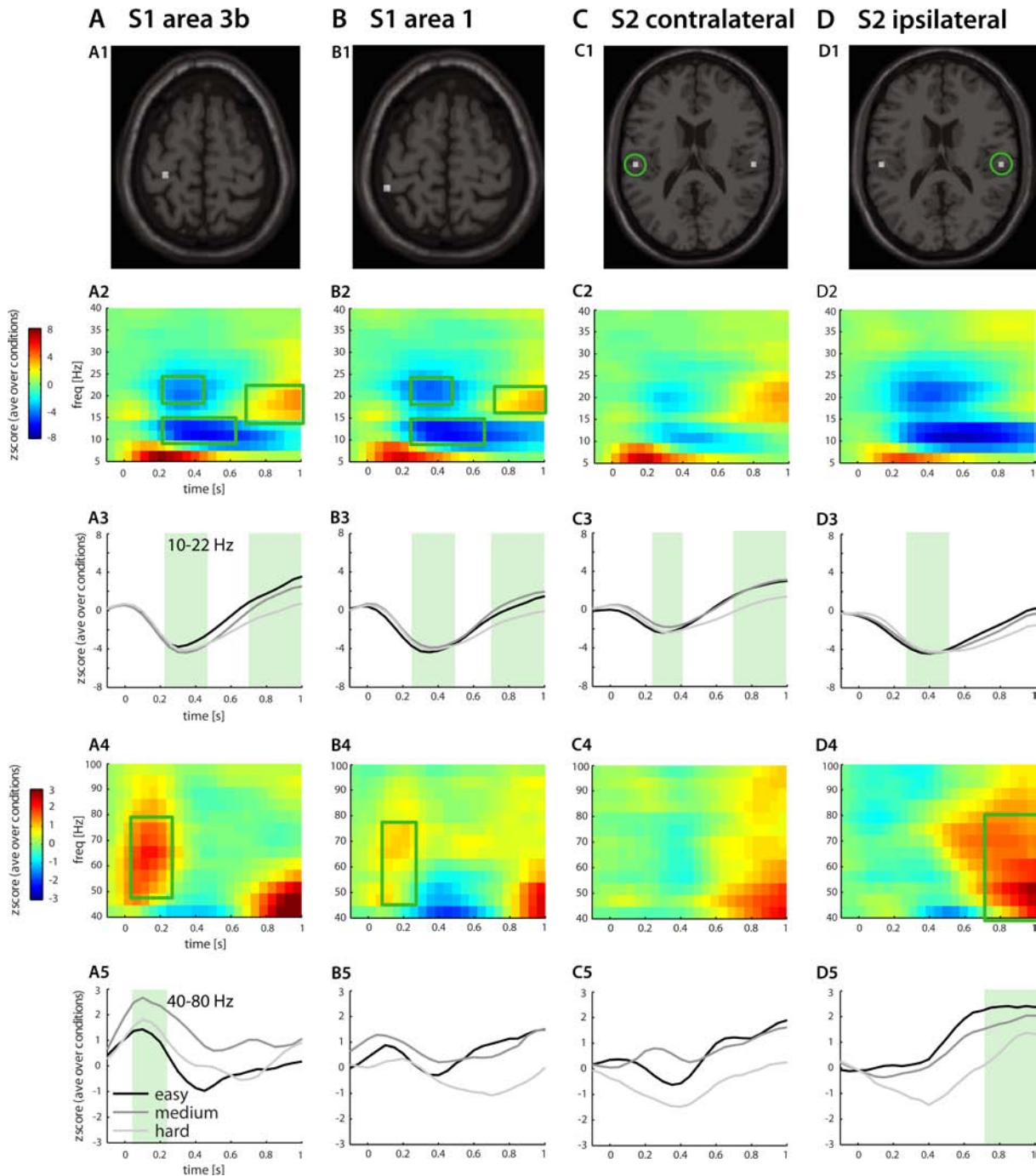


Fig.33 (1000 ms study): Grand average beamformer source estimates in the frequency domain in (A) S1 area 3b, (B) S1 area 1, (C) S2 contralateral, (D) S2 ipsilateral. (A-D 1) Beamformer location overlaid on a structural image of the brain. (A-D 2) Time-frequency resolved power change after stimulation for low frequencies, time-frequency windows of interest bordered by a green box. (A-D 3) Time course of activity in frequency band of interest (10 to 22 Hz) in response to easy, medium, and hard DIFF stimuli. Stimulus onset at 0 ms. The epoch of interest is highlighted by a green box. (A-D 4) Time-frequency resolved power change after stimulation for high frequencies, time-frequency windows of interest bordered by a green box. (A-D 5) Time course of activity in high frequency band of interest (40 to 80 Hz) in response to easy, medium, and hard DIFF stimuli. Stimulus onset at 0 ms. The epoch of interest is highlighted by a green box.

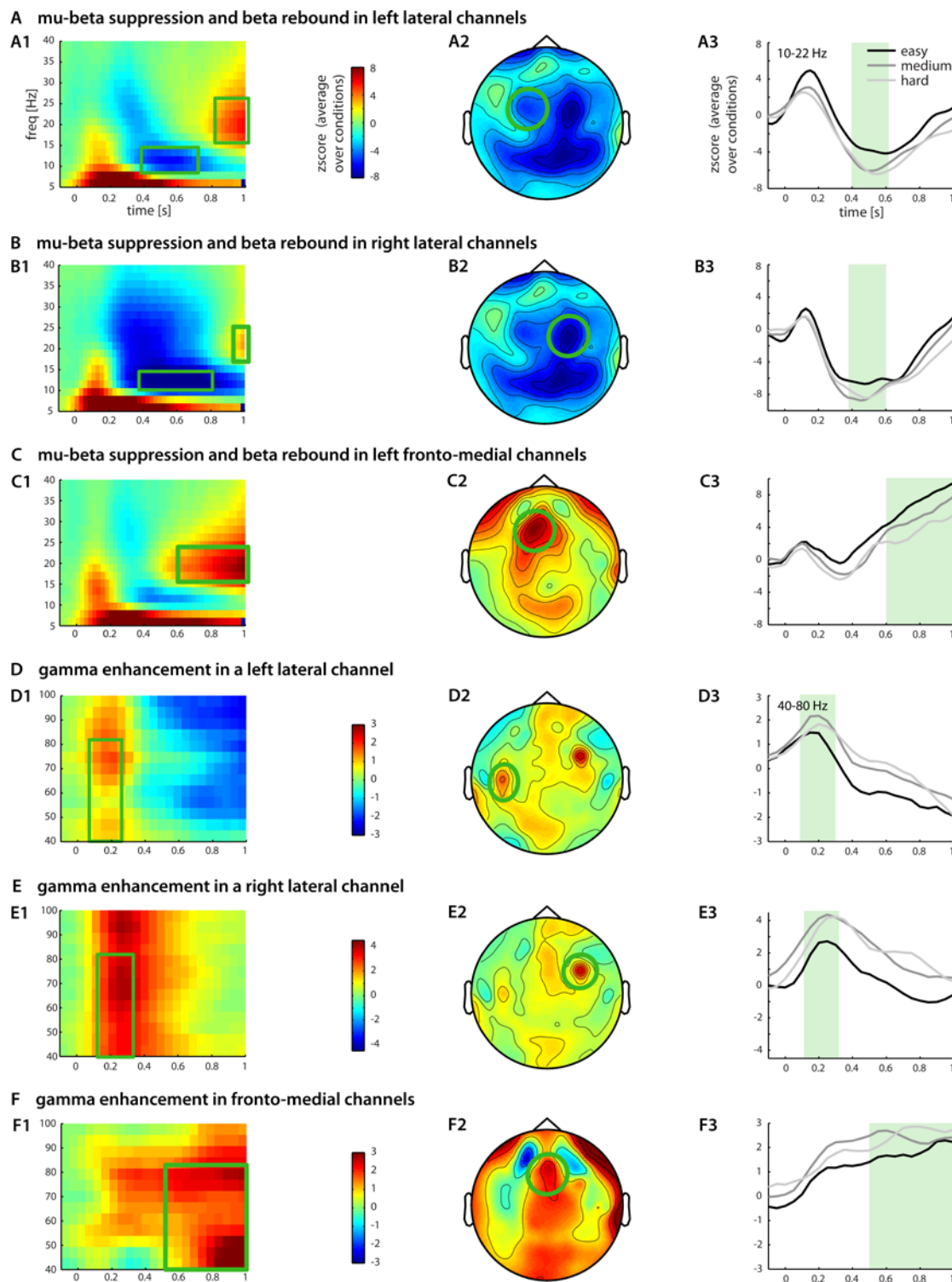


Fig.34 (100 ms study): Components in the frequency domain across the difficulty levels revealed six components: (A) mu-beta suppression (10 to 22 Hz) between 400 and 600 ms in left lateral channels, (B) mu-beta suppression between 400 and 600 ms in right lateral channels, (C) enhanced beta activity (15 to 25 Hz) between 600 and 1000 ms in left fronto-medial channels, (D) enhanced gamma activity (40 to 80 Hz) between 100 and 250 ms in a left lateral channel, (E) enhanced gamma activity between 100 and 300 ms in a right lateral channel, and (F) enhanced gamma activity between 500 and 1000 ms in fronto-medial channels. (A-F 1) Time-frequency resolved power change after stimulation, time-frequency windows of interest bordered by a green box. (A-F 2) Topography of activation patterns in time-frequency windows of interest, channels of interest bordered by a green circle. (A-F 3) Time course of activation in channels of interest in selected frequency windows of interest. The time window of interest is highlighted by a green box.

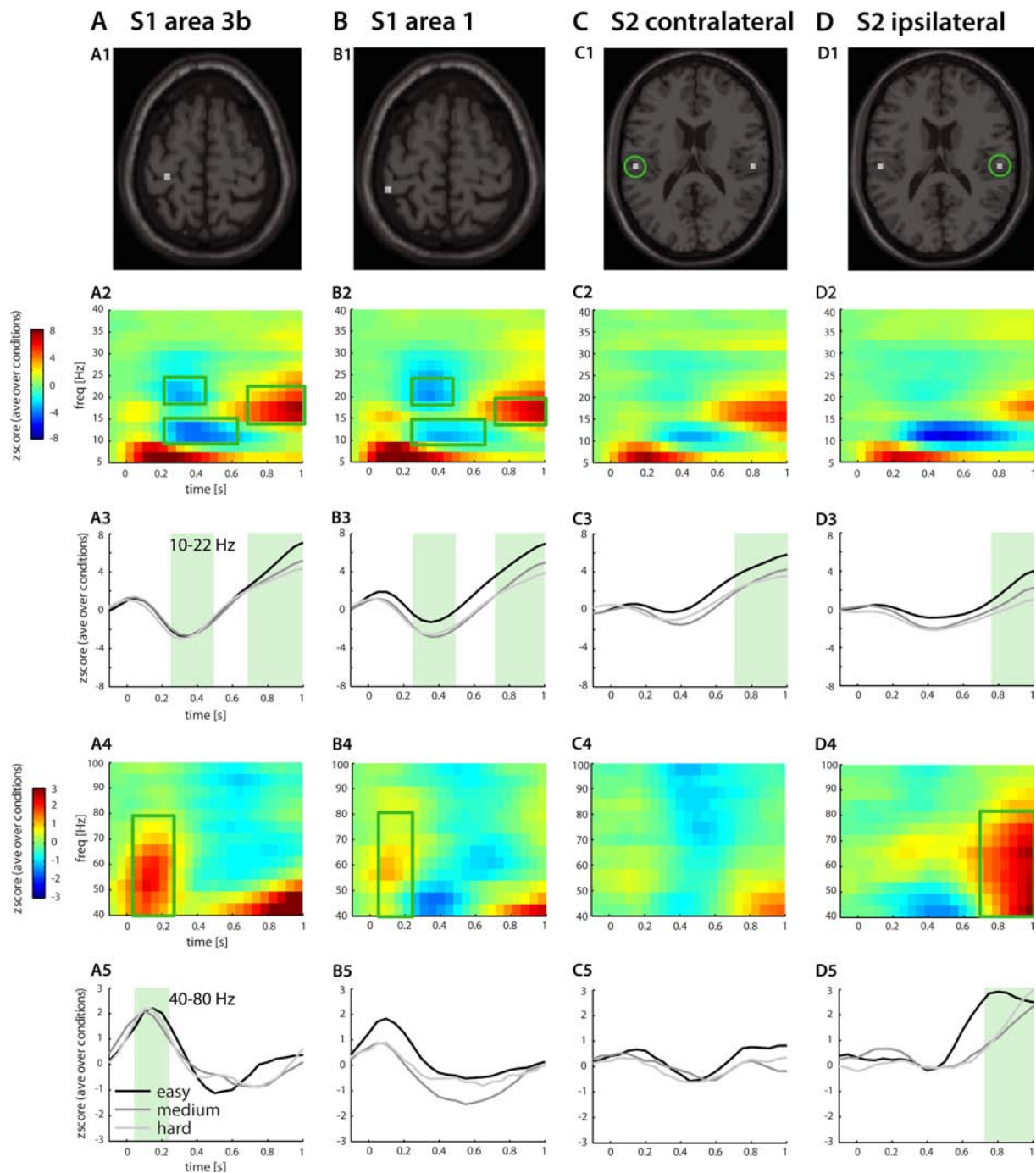


Fig.35 (100 ms study): Grand average beamformer source estimates in the frequency domain in (A) S1 area 3b, (B) S1 area 1, (C) S2 contralateral, (D) S2 ipsilateral. (A-D 1) Beamformer location overlaid on a structural image of the brain. (A-D 2) Time-frequency resolved power change after stimulation for low frequencies, time-frequency windows of interest bordered by a green box. (A-D 3) Time course of activity in frequency band of interest (10 to 22 Hz) in response to easy, medium, and hard DIFF stimuli. Stimulus onset at 0 ms. The epoch of interest is highlighted by a green box. (A-D 4) Time-frequency resolved power change after stimulation for high frequencies, time-frequency windows of interest bordered by a green box. (A-D 5) Time course of activity in high frequency band of interest (40 to 80 Hz) in response to easy, medium, and hard DIFF stimuli. Stimulus onset at 0 ms. The epoch of interest is highlighted by a green box.

DIFF component in central occipital channels

Besides an overall suppression in parieto-occipital channels, especially in the 100 ms study (fig.34A2, occipital channels), multiple central occipital channels also showed a significant DIFF effect in both studies in the alpha-beta range (12-20 Hz). The harder the task, the deeper and longer lasting the alpha-beta band suppression (fig.36C 1000 ms study; fig.37C 100 ms study).

1000 ms study

Multiple central occipital channels showed a significant DIFF effect on the EEG low frequencies (12-22 Hz) between 500 and 650 ms after stimulus onset ($F_{(2,11)} = 16.89$, $p < 0.001$) (fig.36A). These sensors also showed great differential activity (easy-hard DIFF) (fig.36B). The amplitude increased with increasing DIFF in this time interval as can be seen from the time courses for the DIFF levels (fig.36C). The time-frequency resolved power change after stimulation (differential z score) showed enhanced activity between 12-22 Hz (fig.36D). The differential (easy-hard) EEG amplitude correlated positively with DR ($r = 0.59$, $p = 0.043$) (fig.36E) but not significantly with RT ($r = -0.43$, $p = 0.16$).

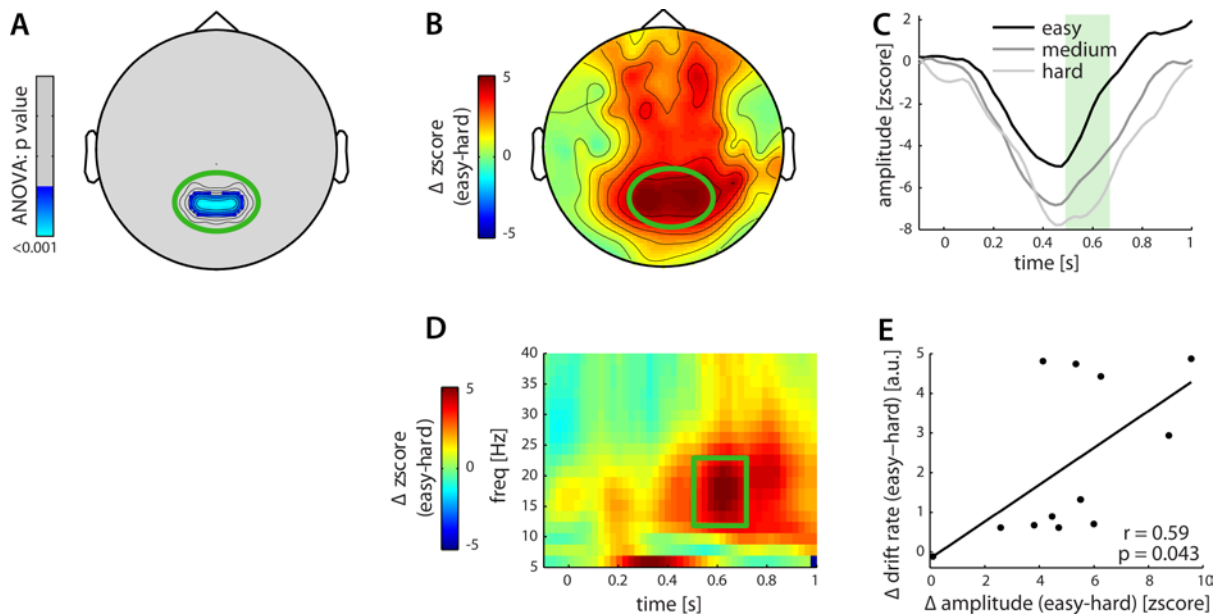


Fig.36 (1000 ms study): Significant DIFF effect between 500 and 650 ms after the stimulus onset in central occipital channels positively correlated with the drift rate. (A) Significant DIFF effect on the EEG amplitude during the epoch of interest in central occipital channels ($F_{(2,11)} = 16.89$, $p < 0.001$). (B) Group average of difference topography (easy-hard DIFF) of the power change during the epoch of interest. (C) Time course of these channels of interest in response to easy, medium, and hard DIFF stimuli showing that with decreasing DIFF the amplitude decreased. Stimulus onset at 0 ms. The epoch of interest is highlighted by a green box. (D) Time-frequency resolved power change after stimulation, time-frequency windows of interest bordered by a green box. (E) Positive correlation between differential (easy-hard DIFF) EEG activity in the time-frequency window of interest and the drift rate ($r = 0.59$, $p = 0.043$).

100 ms study

Multiple left occipital channels showed a significant DIFF effect on the EEG low frequencies (12-17 Hz) between 500 and 600 ms after stimulus onset ($F_{(2,10)} = 13.86$, $p < 0.001$) (fig.37A). These sensors also showed great differential activity in the difference topography (easy-hard DIFF) (fig.37B). The amplitude decreased with increasing DIFF in this time interval as can be seen from the time courses for the DIFF levels (fig.37C). The time-frequency resolved power change after stimulation (differential z score) showed enhanced activity between 12-17 Hz (fig.37D). The differential (easy-hard) EEG amplitude did not correlate significantly with either DR ($r = -0.05$, $p = 0.89$) or RT ($r = 0.12$, $p = 0.72$).

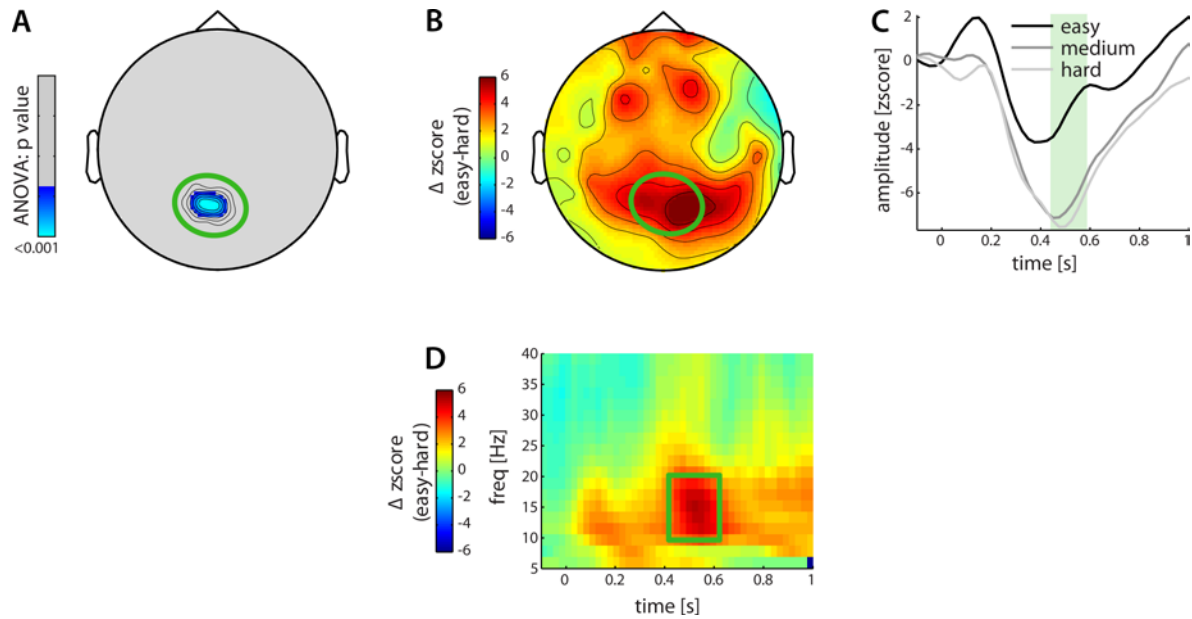


Fig.37 (100 ms study): Significant DIFF effect between 500 and 600 ms after the stimulus onset in left occipital channels not significantly correlated with either the drift rate or RT. (A) Significant DIFF effect on the EEG amplitude during the epoch of interest in central occipital channels ($F_{(2,11)} = 13.86$, $p < 0.001$). (B) Group average of difference topography (easy-hard DIFF) of the power change during the epoch of interest. (C) Time course of these channels of interest in response to easy, medium, and hard DIFF stimuli showing that with decreasing DIFF the amplitude decreased. Stimulus onset at 0 ms. The epoch of interest is highlighted by a green box. (D) Time-frequency resolved power change after stimulation, time-frequency windows of interest bordered by a green box.

3.4.4. Short versus long stimulus presentation

On the behavioral as well as on the neurophysiological level, significant differences between the two studies were tested but did not reach significance (table 4).

	Mauchly's test of sphericity		Within-subjects effects: DIFF * study number			Between-subjects effects: study number		
	p	epsilon (Greenhouse-Geisser)	df	F	p	df	F	p
reaction time	0.51	0.94	2	0.76	0.47	1	0.19	0.67
% correct	0.001	0.650	1.30	0.06	0.87	1	0.06	0.62
ERP: left medio-frontal channels	0.052	0.80	2	1.60	0.21	1	0.75	0.40
ERP: left lateral channels	0.00	0.63	1.97	1.40	0.26	1	2.60	0.12
ERP: S1 area 3b	0.12	0.84	2	0.76	0.47	1	1.71	0.21
Beta activity: occipital chan.s	0.04	0.79	1.58	0.58	0.53	1	0.02	0.89

Table 4 (1000 ms study): Statistics for comparison between the two studies presenting Braille patterns for 1000 ms or 100 ms, respectively. Firstly, Mauchly's sphericity test tested if the variances in the two studies were equal. Secondly, ANOVAs for within- and between-subjects effects were calculated. If sphericity was violated, degrees of freedom were adjusted using the Greenhouse-Geisser correction to produce a more accurate p value.

Also, all electrophysiological components identified in the 100 ms study were also found in the 1000 ms study. Still, three differences were detected. Firstly, in the 1000 ms study, some subjects showed a bimodal RT distribution (fig.18). Secondly, we found a greater number of significant correlations between electrophysiological activity and the drift rate parameter in the 1000 ms than in the 100 ms study.

3.5. *Discussion and interim conclusions*

We investigated the effects of tactile stimulation at varying levels of task difficulty on electrophysiological activity in humans.

3.5.1. Behavioral and diffusion model data

Our hypotheses were confirmed in both studies as with increasing task difficulty (DIFF) RTs were slower and error rates higher. Also, meeting the expectations, the drift rate decreased with increasing difficulty (e.g., Ratcliff and McKoon, 2008).

3.5.2. Effects of tactile stimulation on S1 area 3b

3.5.2.1. *Time domain, decision-related DIFF effect in S1 area 3b*

We measured a significant effect of task difficulty (DIFF) in left central parietal regions between 370 to 590 ms after stimulus onset in the 1000 ms study (fig.28A), and between 450 to 515 ms in the 100 ms study (fig.29A), with highest activity in the easy DIFF condition. This effect was found (1) in individual electrodes in locations corresponding to the topography of the P50, known to originate from Brodmann area 3b (Elbert et al., 1995; Simões et al., 2001), and (2) on the level of the extracted beamformer time courses associated with area 3b (identified by location and orientation). The differential (easy-hard DIFF) EEG activity was positively correlated with the differential drift rate in the 1000 ms study, i.e., subjects with a large difference in drift rate also showed a large difference in electrophysiological activity. Additionally, there was a negative trend in correlation of the differential EEG activity with differential RT in the 1000 ms study. A negative relation with RT as opposed to a positive correlation with the DR was expected because DR and RT have an inverse relationship: the more difficult the task, the longer the RT but the lower the drift rate. Interestingly, the significant DIFF effect started before the amplitude reached its maximum in the three conditions, suggesting that also the slopes differed between the conditions. The drift rate parameter expresses the average rate of an evidence accumulation process towards a boundary (i.e., a slope). It is the model-derived analogue to the slope of the ERP if we assume that it captures the scalp effect of a neuronal integrator process (Gold and Shadlen, 2007; Lo and Wang, 2006; Philiastides et al., 2006). It is thus not surprising that the

differential slope in EEG activity and the differential drift rate showed a positive trend in correlation. Altogether, this implies that contralateral S1 area 3b, at least in the 1000 ms study, was involved in the representation of the sensory evidence necessary to generate the decision. How might this be implemented neurally?

S1 area 3b occupies the rostral bank of the postcentral gyrus (Geyer et al., 1999), and neurons are predominantly responsive to stimulation of cutaneous receptors (e.g., van Westen et al., 2004). S1 area 3b is connected to areas 1 and 2 (Shanks et al., 1985), it is strongly connected to S2 (Burton et al., 1995; Krubitzer et al., 1995), and to frontal regions, e.g., the middle frontal gyrus or Brodmann area 46/6 including the DLPFC (Hannula et al., 2010). Hannula et al. (2010), by applying transcranial magnetic stimulation (TMS) to the middle frontal gyrus, showed that increased top-down suppression of interfering sensory processing in S1 facilitates tactile working memory and thereby performance by means of shorter response latencies (the connection between the middle frontal gyrus and S1 is inhibitory). In that sense, backward connections from higher cortical areas might drive and modulate activity in sensory areas (Friston, 2005) such as S1 area 3b. On a local scale, stability of working memory processes might be achieved by synaptic reverberations mediated by N-Methyl-D-aspartic acid (NMDA) receptors (Wang, 2001). In future studies, top-down influences versus local circuit dynamics could be tested using dynamic causal modeling, transcranial magnetic stimulation, and/or neuropharmacological interventions.

In the 100 ms study no significant correlation was found between the differential activity in S1 area 3b and the differential drift rate. This might be due to suboptimal diffusion model parameter estimation because one session yielded only few error trials in the easy DIFF condition.

3.5.2.2. *Early gamma enhancement in S1 area 3b*

We found enhanced gamma oscillations between 50 and 250 ms in S1 area 3b in both studies (fig.33A4-5 1000 ms study; fig.35A4-5 100 ms study). Gamma oscillations in the sensorimotor cortex were also found by others (e.g., Bauer et al., 2006; Roelfsema et al., 1997). We did not use ‘blind’ source localization by projecting sensor-level gamma-band activity onto the whole brain using beamformer algorithms (Gross et al., 2001). Instead, we used beamformer filters fitted in location and orientation to evoked field components known to originate from the anatomically described sources S1 area 1 and S1 area 3b. The oriented beamformers are likely to give spatially more sharp results (Adjamian et al., 2009; Robinson,

2004). Gamma oscillations in presumably the primary somatosensory area were also found by Bauer et al. (2006) using MEG. Bauer and colleagues (2006) furthermore found enhanced and prolonged gamma oscillations when the stimulus was attended as compared to when it was unattended. They speculated that gamma-band synchronization in primary somatosensory cortex might be instrumental in communicating with higher somatosensory areas in order to process behaviorally relevant stimuli. Surprisingly, we found neither sustained gamma oscillations in the estimated S1 time courses, nor an impact of stimulus difficulty on the power or duration of these oscillations. We can only speculate on the reasons for this. Firstly, the beamformer used in Bauer et al. (2006) might show higher spatial selectivity as time-frequency spectra were derived from planar gradient sensors overlying somatosensory and sensorimotor cortex. However, it cannot be excluded that particularly the later sustained gamma oscillations in Bauer et al. (2006) derived from (pre-)motor regions though they performed another beamformer analysis on this ROI without orientation and with less spatial selection that revealed qualitatively the same results with a poorer signal-to-noise ratio. Secondly, in contrast to the task applied in this study, the task from Bauer et al. (2006) engaged high working-memory load. The sample stimulus could change randomly on each trial and subjects had to memorize the currently relevant pattern for up to eight seconds. In future studies, the nature of these gamma oscillations and whether they play a specific role in working-memory operations should be investigated more explicitly.

3.5.2.3. *Alpha-beta suppression and subsequent beta rebound in S1 area 3b*

We found mu and beta suppression in S1 area 3b contralateral in both studies from around 250 to 500 ms (fig.33A2-3 1000 ms study; fig.35A2-3 100 ms study). Mu-beta suppression was followed by a beta (15-22 Hz) rebound, starting after the average RT (fig.33A2-3 1000 ms study; fig.35A2-3 100 ms study). Other studies also measured alpha-beta suppression and beta rebound in primary sensorimotor areas (Bauer et al., 2006; Crone et al., 1998; Nikouline et al., 2000). Like in the gamma range, we measured no modulatory impact of task difficulty. Possibly beta suppression and rebound were not directly linked to encoding or decision making but to more general, e.g., attention-related, processes.

Different spectral profiles within one region might result from different network interactions: local interactions in the gamma-band range are primarily involved in encoding functions, e.g., encoding sensory features or motor plans, whereas long-range interactions often involve oscillations in the beta range and are primarily involved in integrative functions,

e.g., decision making or perceptual inference (Donner and Siegel, 2011). In accordance with this, gamma enhancement started shortly after stimulus presentation and was transient whereas alpha-beta band oscillations started around 250 ms after stimulus onset and lasted until about 100 ms before mean RT (the remaining 100 ms might be necessary for response execution).

3.5.3. Effects of tactile stimulation on lateral channels similar to effects on S1 area 3b

Lateral channels on the sensor level showed activity patterns comparable to the ones found in S1 area 3b. In the *time domain*, we measured a significant DIFF effect in left lateral channels in similar time windows (between 340 and 490 ms in the 1000 ms study, cf. fig.28A, and between 425 and 475 ms after stimulus onset in the 100 ms study, cf. fig.29A), with highest activity in the easy DIFF condition. Also the time courses of activity in left lateral channels and S1 area 3b show similarities (compare fig.28C and fig.30B from the 1000 ms study, and fig.29C and fig.31C from the 100 ms study). Furthermore, differential activity (easy-hard DIFF) was positively correlated with the differential drift rate in both studies, and negatively correlated with the differential RT in the 1000 ms study. In the *frequency domain*, the alpha-beta suppression showed a more wide-spread spectral (7 to 35 Hz) and temporal (200 to 750 ms) distribution than in S1 area 3b (fig.32A,B 1000 ms study; fig.34A,B 100 ms study) but, similar to S1 area 3b, no differential activity due to task difficulty was measured. Also comparable, alpha-beta suppression was followed by a beta rebound (15-22 Hz) (fig.32A,B 1000 ms study; fig.34A,B 100 ms study). Again in accordance with S1 area 3b activity patterns, gamma oscillations were enhanced between 100 and 250 ms in both studies (figs.32D,E 1000 ms study; fig.34D,E 100 ms study).

Though effect time windows, time courses, and spectral distributions are similar in left lateral channels and S1 area 3b, activity in left lateral channels might have also originated from anterior insulae or premotor cortex (PMC), including the SMA or the cingulate motor cortex (cf., e.g., Thees et al., 2003). Activity in anterior insulae is seen to represent somatosensory processing (Coghill et al., 1994), and PMC is part of the motor system. Future studies, e.g., using simultaneous EEG-fMRI, should determine the origins of beta suppression and rebound.

3.5.4. Effects of tactile stimulation on parieto-occipital channels, possibly visual areas

We found alpha and beta suppression across all conditions also in occipital sensors. Additionally, it showed an effect of difficulty whereby suppression became stronger with increasing task difficulty (fig.36 1000 ms study; fig.37 100 ms study). This effect was measured shortly before the response, i.e., 500 to 600 ms in the 100 ms study and 500 to 650 ms in the 1000 ms study. Moreover, differential (easy-hard) oscillatory activity and differential drift rate, calculated from behavioral data, were positively correlated (fig.36 1000 ms study). Previous studies using fMRI showed that tactile stimulation can activate various parts of visual cortex in blind (Sadato et al., 1996) and normally sighted human subjects (Amedi et al., 2002; Zangaladze et al., 1999). This might be related to input from heteromodal areas (Falchier et al., 2002; Schroeder and Foxe, 2002), or mechanisms underlying visual imagery that are not yet fully understood (Zhang et al., 2004). After the mean response time, we measured a mu-beta rebound (data not shown) similarly to S1 area 3b (cf. section 3.5.2.2).

Interestingly, tactile stimulation did not only alter non-phase locked oscillatory activity but also stimulus-evoked potentials in occipital cortex (P300, cf. section 3.4.2.1 and fig.22E 1000 ms study; fig.43E 100 ms study). Here, activity was earlier (around 300 to 500 ms), and showed no DIFF modulation. Time point and topography suggest this component to be the P3b (cf. section 3.4.2.1) which was shown to be engaged in transforming a stimulus into an internal or external action (Verleger et al., 2005). To determine if both, event-related and oscillatory modulations, mark identical processes, response requirements could be removed. Koivisto and Revonsuo (2003) showed that the P3b was abolished when response requirements were removed. If, on the contrary, oscillatory activity still persisted, this would be strong evidence that stimulus- and frequency-related activations derive from different mechanisms.

3.5.5. Effects of tactile stimulation on medio-frontal channels, possibly motor-related areas

We measured a significant DIFF effect in left medio-frontal channels between 320 and 370 ms in the 1000 ms study and between 325 and 375 ms in the 100 ms study (fig.26 1000 ms study; fig.27 100 ms study). In both studies, differential (easy-hard DIFF) EEG activity was neither significantly correlated with the differential drift rate nor with the differential RT indicating that this activity was at least not directly involved in decision processing. Thees and colleagues (2003) also used a tactile discrimination task and reported activity in medio-frontal areas. Their dipole source localization and fMRI coregistration

revealed activations in SMA (BA6), and the cingulate motor area of the anterior cingulate cortex (BA 24, 32). The SMA seems to be involved in motor preparation and motor output (for review, see Nachev et al., 2008; Wenzlaff et al., 2011, or cf. discussion in study 1, section 2.5.2 of this dissertation), just like the cingulate motor area (Cole et al., 2009). Motor preparation and output are theoretically not considered to be part of the decision process which is in line with the lack of correlation between the EEG activity and the drift rate as well as RT. Nevertheless, activity is influenced by decision processes and might mirror its outcome as indicated by the measured DIFF effect. Please note that a slightly more dorsal part of BA 32 has been associated with conflict monitoring (Carter et al., 1998) and selective attention (Cabeza and Nyberg, 1997; Posner and Dehaene, 1994). Because the ACC anatomy is extremely variable between individuals, simultaneous EEG-fMRI experiments are better suited to disentangle the impact of dorsal and caudal ACC activity on tactile decision making.

Interestingly, we measured alpha-/beta suppression, followed by a beta rebound from around response time onwards (fig.32C 1000 ms study and fig.34C 100 ms study) in the same channels. It was also not significantly correlated with either drift rate or RT.

Additionally, we measured gamma-band enhancement in medio-frontal channels from around 200 ms on (fig.32F 1000 ms study; fig.34F 100 ms study). Gamma activations are often involved in encoding functions such as motor planning, e.g., neuronal groups involved in generating a motor response might interact via oscillatory synchronization (Rieder et al., 2011). Spectral, temporal, and spatial distributions support the idea that the measured medio-frontal gamma oscillations indicated motor activity but source localization of EEG-fMRI experiments are necessary to further substantiate this.

3.5.6. Differences between the short and long stimulus presentation

The results did not differ substantially between the two studies presenting the Braille stimuli for either 1000 ms or 100 ms; all electrophysiological components identified in one study were also found in the other. This might, on the one hand, serve as further evidence that a stimulus must not necessarily be accessible until the response is given, but a short stimulus presentation might be sufficient because the sensory information is internally represented. In the experiment of Philiastides et al. (2006), the ‘late’ ERP component was predictive of the drift rate parameter after a short stimulus exposure of 30 ms. Thereby, a ‘perceptual persistence’ of the visual stimulus after stimulus removal might have been implemented via feedback pathways in LOC (Coltheart, 1980; Di Lollo, 1977; Ferber et al., 2003; Large et al.,

2005; Philiastides and Sajda, 2007). In accordance with this, it has been shown in the visual and olfactory domains that discrete sensory *snapshots* might facilitate the integration of information, and give rise to encoding strategies that take advantage of these short time frames (for review, see Uchida et al., 2006). VanRullen and colleagues showed in several studies (e.g., VanRullen and Koch, 2003) that after visual stimulus presentation for 26 ms, very fast responses carried information about the stimulus because subjects' performance was above chance. Here, response times even suggested that feedback pathways might not be mandatory for visual processing. In contrast, Lamme and Roelfsema (2000) using a figure-ground segregation task showed that only later spiking activity of neurons in the primary visual cortex (V1) distinguished between figure and ground, and this activity was attributed to feedback-related signals. This suggests that in some situations sufficient information is encoded in the first spikes, whereas in other, possibly more complex, situations crucial information is encoded not until the late phases of spiking activity. The later does not only take longer but might also rely on recurrent processing (Wang, 2002), and span across different levels of the processing 'hierarchy' (Friston, 2005; Romo et al., 2002). Interestingly, for neurons in area MT, direction information saturates within ~200 ms if dots move coherently but it does not saturate over long periods (~2 s) if dots move randomly (Buracas et al., 1998; Osborne et al., 2004; Uka and DeAngelis, 2003).

On the other hand, Braille stimuli are incorporated by Meissner's corpuscles. Meissner's corpuscles are rapidly adapting: they send action potentials only 50 to 500 ms (Schmidt et al., 2005), i.e., they react on *changes* in pressure, but do not convey sensory information continuously. Thus, continuous stimulus presentation did not necessarily result in a continuous stimulus perception, which could also explain similar electrophysiological results.

Still, two differences were detected. Firstly, in the 1000 ms study, some subjects showed a bimodal RT distribution (fig.18). As both, elevation of the pins of the Braille stimulator at 0 ms and lowering at 1000 ms gave qualitative information about the stimulus identity, subjects might have waited for the lowering of the pins to gain additional information. They were excluded from the analysis for comparability to the 100 ms study. However, this could also explain longer average RTs of the 1000 ms study. Secondly, we found more significant correlations between electrophysiological activity and the drift rate parameter in the 1000 ms than in the 100 ms study. This might be due to better diffusion model parameter estimations in the 1000 ms study because we conducted two sessions instead of one in the 100 ms study resulting in twice the number of trials.

In conclusion, we show differential ERP activity in S1 area 3b as a function of task difficulty later in the decision process that might be driven or modulated by recurrent processes from frontal areas, such as the DLPFC. Surprisingly, no task difficulty effect was found in the oscillatory activity of S1 as was expected for the gamma range (cf. Bauer et al., 2006). However, an alpha-beta suppression in parieto-occipital channels showed a task difficulty effect and was related to decision processing (as it correlated positively with the drift rate), possibly via input from heteromodal areas. This suggests either a graded recruitment of visual cortex for more complex tactile patterns in the absence of visual stimuli or an attention-related effect (cf. Bauer et al., 2006). Short versus long stimulus presentation did not alter neurophysiological processing suggesting that ‘perceptual persistence’ after stimulus removal could be implemented via feedback pathways.

4. Summary

In the three studies included in this dissertation I investigated the neurophysiology of perceptual decision making in the human brain, and the relation of neural activity to perceptual choices. The aim was to reveal more general perceptual decision making mechanisms by examining evoked phase-locked and induced oscillatory activity in the visual and somatosensory domain. Thereby, the focus was on effects caused by changes in sensory evidence of the stimuli, or emphasis on speed or accuracy, respectively. To link neurophysiological activity with perceptual choices, behavioral data were modeled using sequential sampling models. These assume that the rate of evidence accumulation over time (drift rate) depends on the sensory evidence given, and the amount of accumulated evidence required to commit a response (boundary), depending on the requirement to commit either fast or accurate decisions.

In study 1, we examined whether the speed-accuracy tradeoff (SAT) predominantly influenced later phases of motor preparation or earlier stages of sensory processing in the decision process and whether this depended on the task difficulty. Using magnetoencephalography and a face-house categorization task, I show that decision- and motor-related systems at later stages of processing rather than the early sensory system are modulated by the SAT. Source analysis revealed that the bilateral supplementary motor areas (SMAs) and the medial precuneus were more activated under the speed instruction and correlated negatively (right SMA) with the boundary parameter, whereas the left dorsolateral prefrontal cortex (DLPFC) was more activated under the accuracy instruction and showed a positive correlation with the boundary. We interpreted these findings such that SMA activity dynamically facilitates fast responses during stimulus processing, potentially by disinhibiting thalamo-striatal loops, whereas DLPFC may reflect higher levels of accumulated evidence under emphasis of accuracy as compared to speed. In future experiments it would be of particular interest to study the connectivity of sensorimotor networks, and whether that might be enhanced under speed conditions to gain faster evidence accumulation to the decision threshold.

In studies 2 and 3, we investigated which components of neural activity were related to decision processing in sensory areas, indexed by their covariation with difficulty as well as their behavioral decision outcomes. Specifically, we asked whether more difficult decisions with longer reaction times were associated with longer latencies of sensory ERP components, if neural activity revealed a temporal integration of sensory information similar to Roitman

and Shadlen (2002), and whether more difficult stimuli implied more sustained oscillatory activity, potentially mediating neuronal interactions for recursive stimulus processing (cf. Friston, 2005; Hopfield, 1982; Romo et al., 2002). Using electroencephalography (EEG), tactile Braille patterns that differed in pattern discriminability, thereby modulating task difficulty (DIFF), were presented transiently for 100 ms in the one study, in the other study for 1000 ms. Presentation time did not alter neurophysiological processing significantly which could suggest that ‘perceptual persistence’ after stimulus removal might be implemented via feedback pathways. However, stimulus presentation might not necessarily have resulted in a continuous stimulus perception since Meissner’s corpuscles respond to the transient onset and offset of tactile stimuli, i.e., *changes* in pressure, but do not convey sensory information continuously. In both studies, neurophysiological activity in the primary somatosensory cortex (S1) underwent ramp-like changes modulated by task difficulty in the same direction as in monkey studies (Roitman and Shadlen, 2002). We found differential ERP activity in S1 area 3b as a function of task difficulty later in the decision process that might be driven or modulated by recurrent processes from frontal areas, such as the DLPFC. Contrary to the late ERP components, early components were unaffected by task difficulty. When looking at the oscillatory activity of S1, surprisingly no task difficulty effect was found in the gamma range (cf. Bauer et al., 2006) suggesting that these reflect feedforward processing by tactile stimulation. However, an alpha-beta suppression in parieto-occipital channels showed a pronounced task difficulty effect and was related to decision processing as it correlated positively with the drift rate, possibly via input from heteromodal areas. This suggests either a graded recruitment of visual cortex for more complex tactile patterns in the absence of visual stimuli or an attention-related effect (cf. Bauer et al., 2006). Taken together, the results show that drift-diffusion processes are a more general principle that applies also in situations where stimulus information is either presented briefly or with no continuous afferent input, and it involves areas as low in the cortical hierarchy as S1. In future experiments, the role of oscillations in perceptual decision processing should be addressed in a more detailed fashion, e.g., in tasks involving working memory.

In conclusion, the three studies comprising this dissertation reveal that experimental manipulation of sensory evidence in decision making tasks impact predominantly on sensory cortex whereas experimentally induced changes in the boundary predominantly affect activity in higher level areas such as DLPFC and SMA. Furthermore, we show that even briefly presented stimuli can lead to a graded and persistent built-up of activity as has been described in sustained stimulation paradigms in the monkey. This can be observed in brain areas as

early as primary somatosensory cortex. Sensory driven gamma-band oscillations seem unaffected by parameters like stimulus discriminability and do not co-vary with task difficulty. These results may be of interest for clinical research to better understand the neuronal processes underlying impaired decision making in clinical populations with neurological and psychiatric disorders such as Parkinson's disease.

5. References

- Adjamian P., Worthen S.F., Hillebrand A., Furlong P.L., Chizh B.A., Hobson A.R., Aziz Q., Barnes G.R. (2009) Effective electromagnetic noise cancellation with beamformers and synthetic gradiometry in shielded and partly shielded environments. *Journal of Neuroscience Methods* 178:120-7.
- Amedi A., Jacobson G., Hendler T., Malach R., Zohary E. (2002) Convergence of visual and tactile shape processing in the human lateral occipital complex. *Cerebral Cortex* 12:1202-12.
- Andersen R.A., Brotchie P.R., Mazzoni P. (1992) Evidence for the lateral intraparietal area as the parietal eye field. *Current Opinion in Neurobiology* 2:840-6.
- Asanuma C., Andersen R.A., Cowan W.M. (1985) The thalamic relations of the caudal inferior parietal lobule and the lateral prefrontal cortex in monkeys: divergent cortical projections from cell clusters in the medial pulvinar nucleus. *The Journal of Comparative Neurology* 241:357-81.
- Azouz R., Gray C.M. (2003) Adaptive coincidence detection and dynamic gain control in visual cortical neurons in vivo. *Neuron* 37:513-523.
- Bastiaansen M.C., Knösche T.R. (2000) Tangential derivative mapping of axial MEG applied to event-related desynchronization research. *Clinical Neurophysiology* 111:1300-5.
- Bauer M., Oostenveld R., Fries P. (2009) Tactile stimulation accelerates behavioral responses to visual stimuli through enhancement of occipital gamma-band activity. *Vision Research* 49:931-42.
- Bauer M., Oostenveld R., Peeters M., Fries P. (2006) Tactile spatial attention enhances gamma-band activity in somatosensory cortex and reduces low-frequency activity in parieto-occipital areas. *Journal of Neuroscience* 26:490-501.
- Blatt G.J., Andersen R.A., Stoner G.R. (1990) Visual receptive field organization and cortico-cortical connections of the lateral intraparietal area (area LIP) in the macaque. *The Journal of Comparative Neurology* 299:421-45.
- Bogacz R., Wagenmakers E.-J., Forstmann B.U., Nieuwenhuis S. (2010) The neural basis of the speed-accuracy tradeoff. *Trends in Neurosciences* 33:10-6.
- Brainard D.H. (1997) The Psychophysics Toolbox. *Spatial Vision* 10:433-6.
- Brinkman C., Porter R. (1979) Supplementary motor area in the monkey: activity of neurons during performance of a learned motor task. *Journal of Neurophysiology* 42:681-709.
- Brodmann K. (1909) *Vergleichende Lokalisationslehre der Grosshirnrinde in ihren Prinzipien dargestellt auf Grund des Zellenbaues* Johann Ambrosius Barth Verlag, Leipzig.
- Buracas G.T., Zador A.M., DeWeese M.R., Albright T.D. (1998) Efficient discrimination of temporal patterns by motion-sensitive neurons in primate visual cortex. *Neuron* 20:959-69.

- Burton H., Fabri M., Alloway K. (1995) Cortical areas within the lateral sulcus connected to cutaneous representations in areas 3b and 1: a revised interpretation of the second somatosensory area in macaque monkeys. *The Journal of Comparative Neurology* 355:539-62.
- Cabeza R., Nyberg L. (1997) Imaging cognition: An empirical review of PET studies with normal subjects. *Journal of Cognitive Neuroscience* 9:1-26.
- Carpenter R.H., Williams M.L. (1995) Neural computation of log likelihood in control of saccadic eye movements. *Nature* 377:59-62.
- Carter C.S., Braver T.S., Barch D.M., Botvinick M.M., Noll D., Cohen J.D. (1998) Anterior cingulate cortex, error detection, and the online monitoring of performance. *Science* 280:747-9.
- Cheyne D., Gaetz W., Garnero L., Lachaux J.P., Ducorps A., Schwartz D., Varela F.J. (2003) Neuromagnetic imaging of cortical oscillations accompanying tactile stimulation. *Brain Research. Cognitive Brain Research* 17:599-611.
- Churchland A.K., Kiani R., Shadlen M.N. (2008) Corrigendum: Decision-making with multiple alternatives. *Nature Neuroscience* 11:851.
- Cisek P., Puskas G.A., El-Murr S. (2009) Decisions in changing conditions: the urgency-gating model. *Journal of Neuroscience* 29:11560-71.
- Coghill R.C., Talbot J.D., Evans A.C., Meyer E., Gjedde A., Bushnell M.C., Duncan G.H. (1994) Distributed processing of pain and vibration by the human brain. *Journal of Neuroscience* 14:4095-108.
- Cole M.W., Yeung N., Freiwald W.A., Botvinick M. (2009) Cingulate cortex: diverging data from humans and monkeys. *Trends in Neurosciences* 32:566-74.
- Coltheart M. (1980) The persistences of vision. *Philosophical Transactions of the Royal Society of London. Series B, Biological Sciences* 290:57 - 69.
- Crone N.E., Miglioretti D.L., Gordon B., Sieracki J.M., Wilson M.T., Uematsu S., Lesser R.P. (1998) Functional mapping of human sensorimotor cortex with electrocorticographic spectral analysis. I. Alpha and beta event-related desynchronization. *Brain* 121:2271-99.
- Dale A.M., Fischl B., Sereno M.I. (1999) Cortical surface-based analysis. I. Segmentation and surface reconstruction. *NeuroImage* 9:179-94.
- Desmedt J.E., Huy N.T., Bourguet M. (1983) The cognitive P40, N60 and P100 components of somatosensory evoked potentials and the earliest electrical signs of sensory processing in man. *Electroencephalography and Clinical Neurophysiology* 56:272-82.
- Desmurget M. (2000) Forward modeling allows feedback control for fast reaching movements. *Trends in Cognitive Sciences* 4:423-431.
- Di Lollo V. (1977) Temporal characteristics of iconic memory. *Nature* 267:241-3.

- Ditterich J. (2006) Stochastic models of decisions about motion direction: behavior and physiology. *Neural Networks* 19:981-1012.
- Ditterich J., Mazurek M.E., Shadlen M.N. (2003) Microstimulation of visual cortex affects the speed of perceptual decisions. *Nature Neuroscience* 6:891.
- Donner T.H., Siegel M. (2011) A framework for local cortical oscillation patterns. *Trends in Cognitive Sciences* 15:191-9.
- Donner T.H., Siegel M., Fries P., Engel A.K. (2009) Buildup of choice-predictive activity in human motor cortex during perceptual decision making. *Current Biology* 19:1581-5.
- Donner T.H., Siegel M., Oostenveld R., Fries P., Bauer M., Engel A.K. (2007) Population activity in the human dorsal pathway predicts the accuracy of visual motion detection. *Journal of Neurophysiology* 98:345-59.
- Eckhorn R., Bauer R., Jordan W., Brosch M., Kruse W., Munk M., Reitboeck H.J. (1988) Coherent oscillations: a mechanism of feature linking in the visual cortex? Multiple electrode and correlation analyses in the cat. *Biological Cybernetics* 60:121-30.
- Elbert T., Junghöfer M., Scholz B., Schneider S. (1995) The separation of overlapping neuromagnetic sources in first and second somatosensory cortices. *Brain Topography* 7:275-82.
- Falchier A., Clavagnier S., Barone P., Kennedy H. (2002) Anatomical evidence of multimodal integration in primate striate cortex. *Journal of Neuroscience* 22:5749-59.
- Ferber S., Humphrey G.K., Vilis T. (2003) The lateral occipital complex subserves the perceptual persistence of motion-defined groupings. *Cerebral Cortex* 13:716-21.
- Fischl B., Sereno M.I., Dale A.M. (1999a) Cortical surface-based analysis. II: Inflation, flattening, and a surface-based coordinate system. *NeuroImage* 9:195-207.
- Fischl B., Sereno M.I., Tootell R.B., Dale A.M. (1999b) High-resolution intersubject averaging and a coordinate system for the cortical surface. *Human Brain Mapping* 8:272-284.
- Fischl B., Salat D.H., Busa E., Albert M., Dieterich M., Haselgrove C., van der Kouwe A., Killiany R., Kennedy D., Klaveness S., Montillo A., Makris N., Rosen B., Dale A.M. (2002) Whole brain segmentation: automated labeling of neuroanatomical structures in the human brain. *Neuron* 33:341-55.
- Forstmann B.U., Dutilh G., Brown S., Neumann J., von Cramon D.Y., Ridderinkhof K.R., Wagenmakers E.-J. (2008) Striatum and pre-SMA facilitate decision-making under time pressure. *Proceedings of the National Academy of Sciences of the United States of America* 105:17538-42.
- Fries P. (2005) A mechanism for cognitive dynamics: neuronal communication through neuronal coherence. *Trends in Cognitive Sciences* 9:474-480.
- Friston K. (2005) A theory of cortical responses. *Philosophical transactions of the Royal Society of London. Series B, Biological sciences* 360:815-36.

- Geyer S., Schleicher A., Zilles K. (1999) Areas 3a, 3b, and 1 of human primary somatosensory cortex. *NeuroImage* 10:63-83.
- Gold J.I., Shadlen M.N. (2007) The neural basis of decision making. *Annual Review of Neuroscience* 30:535-74.
- Gonzalez Andino S.L., Michel C.M., Thut G., Landis T., Grave De Peralta R. (2005) Prediction of response speed by anticipatory high-frequency (gamma band) oscillations in the human brain. *Human Brain Mapping* 24:50-58.
- Gray C.M., Singer W. (1989) Stimulus-specific neuronal oscillations in orientation columns of cat visual cortex. *Proceedings of the National Academy of Sciences of the United States of America* 86:1698-1702.
- Gray C.M., Konig P., Engel A.K., Singer W. (1989) Oscillatory responses in cat visual cortex exhibit inter-columnar synchronization which reflects global stimulus properties. *Nature* 338:334-7.
- Grill-Spector K., Kourtzi Z., Kanwisher N. (2001) The lateral occipital complex and its role in object recognition. *Vision Research* 41:1409-22.
- Grosbras M.H., Lobel E., Van De Moortele P.F., LeBihan D., Berthoz A. (1999) An anatomical landmark for the supplementary eye fields in human revealed with functional magnetic resonance imaging. *Cerebral Cortex* 9:705-11.
- Gross J., Kujala J., Hamalainen M., Timmermann L., Schnitzler A., Salmelin R. (2001) Dynamic imaging of coherent sources: Studying neural interactions in the human brain. *Proceedings of the National Academy of Sciences of the United States of America* 98:694-699.
- Hämäläinen H., Kekoni J., Sams M., Reinikainen K., Näätänen R. (1990) Human somatosensory evoked potentials to mechanical pulses and vibration: contributions of SI and SII somatosensory cortices to P50 and P100 components. *Electroencephalography and Clinical Neurophysiology* 75:13-21.
- Hämäläinen M.S., Sarvas J. (1989) Realistic conductivity geometry model of the human head for interpretation of neuromagnetic data. *IEEE Transactions on Bio-Medical Engineering* 36:165-71.
- Hannula H., Neuvonen T., Savolainen P., Hiltunen J., Ma Y.-Y., Antila H., Salonen O., Carlson S., Pertovaara A. (2010) Increasing top-down suppression from prefrontal cortex facilitates tactile working memory. *NeuroImage* 49:1091-8.
- Hari R., Salmelin R. (1997) Human cortical oscillations: a neuromagnetic view through the skull. *Trends in Neurosciences* 20:44-49.
- Haxby J., Hoffman E., Gobbini M. (2000) The distributed human neural system for face perception. *Trends in Cognitive Sciences* 4:223-233.
- Heekeren H.R., Marrett S., Ungerleider L.G. (2008) The neural systems that mediate human perceptual decision making. *Nature Reviews. Neuroscience* 9:467-479.

- Heekeren H.R., Marrett S., Bandettini P.A., Ungerleider L.G. (2004) A general mechanism for perceptual decision-making in the human brain. *Nature* 431:859-862.
- Heekeren H.R., Marrett S., Ruff D.A., Bandettini P.A., Ungerleider L.G. (2006) Involvement of human left dorsolateral prefrontal cortex in perceptual decision making is independent of response modality. *Proceedings of the National Academy of Sciences of the United States of America* 103:10023-10028.
- Hernández A., Zainos A., Romo R. (2000) Neuronal correlates of sensory discrimination in the somatosensory cortex. *Proceedings of the National Academy of Sciences of the United States of America* 97:6191-6.
- Hirata M., Kato A., Taniguchi M., Ninomiya H., Cheyne D., Robinson S.E., Maruno M., Kumura E., Ishii R., Hirabuki N., Nakamura H., Yoshimine T. (2002) Frequency-dependent spatial distribution of human somatosensory evoked neuromagnetic fields. *Neuroscience Letters* 318:73-6.
- Ho T.C., Brown S., Serences J.T. (2009) Domain general mechanisms of perceptual decision making in human cortex. *Journal of Neuroscience* 29:8675-87.
- Hopfield J.J. (1982) Neural networks and physical systems with emergent collective computational abilities. *Proceedings of the National Academy of Sciences of the United States of America* 79:2554-8.
- Hotelling H. (1933) Analysis of a complex of statistical variables into principal components. *Journal of Educational Psychology* 24:417-41.
- Ihara A., Hirata M., Yanagihara K., Ninomiya H., Imai K., Ishii R., Osaki Y., Sakihara K., Izumi H., Imaoka H., Kato A., Yoshimine T., Yorifuji S. (2003) Neuromagnetic gamma-band activity in the primary and secondary somatosensory areas. *Neuroreport* 14:273-7.
- Ikeda A., Lüders H.O., Burgess R.C., Shibasaki H. (1992) Movement-related potentials recorded from supplementary motor area and primary motor area. Role of supplementary motor area in voluntary movements. *Brain* 115:1017-43.
- Ivanoff J., Branning P., Marois R. (2008) fMRI evidence for a dual process account of the speed-accuracy tradeoff in decision-making. *PloS one* 3:e2635.
- Jensen O., Goel P., Kopell N., Pohja M., Hari R., Ermentrout B. (2005) On the human sensorimotor-cortex beta rhythm: sources and modeling. *NeuroImage* 26:347-55.
- Johansen-Berg H., Behrens T.E.J., Robson M.D., Drobnyak I., Rushworth M.F.S., Brady J.M., Smith S.M., Higham D.J., Matthews P.M. (2004) Changes in connectivity profiles define functionally distinct regions in human medial frontal cortex. *Proceedings of the National Academy of Sciences of the United States of America* 101:13335-40.
- Kanwisher N., McDermott J., Chun M.M. (1997) The fusiform face area: a module in human extrastriate cortex specialized for face perception. *Journal of Neuroscience* 17:4302.
- Kayser C., Montemurro M.A., Logothetis N.K., Panzeri S. (2009) Spike-phase coding boosts and stabilizes information carried by spatial and temporal spike patterns. *Neuron* 61:597-608.

- Kim J.N., Shadlen M.N. (1999) Neural correlates of a decision in the dorsolateral prefrontal cortex of the macaque. *Nature Neuroscience* 2:176-185.
- Kim S.G., Ashe J., Hendrich K., Ellermann J.M., Merkle H., Ugurbil K., Georgopoulos A.P. (1993) Functional magnetic resonance imaging of motor cortex: hemispheric asymmetry and handedness. *Science* 261:615-7.
- Koivisto M., Revonsuo A. (2003) An ERP study of change detection, change blindness, and visual awareness. *Psychophysiology* 40:423-9.
- Krubitzer L., Clarey J., Tweedale R., Elston G., Calford M. (1995) A redefinition of somatosensory areas in the lateral sulcus of macaque monkeys. *Journal of Neuroscience* 15:3821-39.
- Laming D.R.J. (1968) *Information theory of choice-reaction times*. Academic Press, Oxford, England.
- Lamme V.A., Spekreijse H. (1998) Neuronal synchrony does not represent texture segregation. *Nature* 396:362-6.
- Lamme V.A., Roelfsema P.R. (2000) The distinct modes of vision offered by feedforward and recurrent processing. *Trends in Neurosciences* 23:571-579.
- Large M.-E., Aldcroft A., Vilis T. (2005) Perceptual continuity and the emergence of perceptual persistence in the ventral visual pathway. *Journal of Neurophysiology* 93:3453-62.
- Lewis J.W., Van Essen D.C. (2000) Corticocortical connections of visual, sensorimotor, and multimodal processing areas in the parietal lobe of the macaque monkey. *The Journal of Comparative Neurology* 428:112-37.
- Liu J., Higuchi M., Marantz A., Kanwisher N. (2000) The selectivity of the occipitotemporal M170 for faces. *Neuroreport* 11:337-341.
- Lo C.C., Wang X.J. (2006) Cortico-basal ganglia circuit mechanism for a decision threshold in reaction time tasks. *Nature Neuroscience* 9:956-963.
- Luck S.J. (2005) *An Introduction to the Event-related potential technique (Cognitive Neuroscience)* MIT Press.
- Margulies D.S., Vincent J.L., Kelly C., Lohmann G., Uddin L.Q., Biswal B.B., Villringer A., Castellanos F.X., Milham M.P., Petrides M. (2009) Precuneus shares intrinsic functional architecture in humans and monkeys. *Proceedings of the National Academy of Sciences of the United States of America* 106:20069-74.
- Mazurek M.E., Roitman J.D., Ditterich J., Shadlen M.N. (2003) A role for neural integrators in perceptual decision making. *Cerebral Cortex* 13:1257-1269.
- McLachlan G., Peel D. (2000) *Finite Mixture Models*. John Wiley & Sons, New York.
- Miller E.K., Cohen J.D. (2001) An integrative theory of prefrontal cortex function. *Annual Reviews Neuroscience* 24:167.

- Mitra P.P., Pesaran B. (1999) Analysis of dynamic brain imaging data. *Biophysical Journal* 76:691-708.
- Nachev P., Kennard C., Husain M. (2008) Functional role of the supplementary and pre-supplementary motor areas. *Nature reviews. Neuroscience* 9:856-69.
- Nambu A., Takada M., Inase M., Tokuno H. (1996) Dual somatotopical representations in the primate subthalamic nucleus: evidence for ordered but reversed body-map transformations from the primary motor cortex and the supplementary motor area. *Journal of Neuroscience* 16:2671-83.
- Nikouline V.V., Linkenkaer-Hansen K., Wikstrom H., Kesaniemi M., Antonova E.V., Ilmoniemi R.J., Huttunen J. (2000) Dynamics of mu-rhythm suppression caused by median nerve stimulation: a magnetoencephalographic study in human subjects. *Neuroscience Letters* 294:163-6.
- Oldfield R.C. (1971) The assessment and analysis of handedness: the Edinburgh inventory. *Neuropsychologia* 9:97-113.
- Osborne L.C., Bialek W., Lisberger S.G. (2004) Time course of information about motion direction in visual area MT of macaque monkeys. *Journal of Neuroscience* 24:3210-22.
- Osman A., Lou L., Muller-Gethmann H., Rinkenauer G., Mattes S., Ulrich R. (2000) Mechanisms of speed-accuracy tradeoff: evidence from covert motor processes. *Biological Psychology* 51:173-199.
- Pascual-Marqui R.D. (2002) Standardized low-resolution brain electromagnetic tomography (sLORETA): technical details. *Methods and Findings in Experimental and Clinical Pharmacology* 24 Suppl D:5-12.
- Pascual-Marqui R.D., Esslen M., Kochi K., Lehmann D. (2002) Functional imaging with low-resolution brain electromagnetic tomography (LORETA): a review. *Methods and Findings in Experimental and Clinical Pharmacology* 24 Suppl C:91-5.
- Pearson K. (1901) On lines and planes of closest fit to systems of points in space. *Philosophical Magazine* 2:559-72.
- Pfurtscheller G., Lopes da Silva F.H. (1999) Event-related EEG/MEG synchronization and desynchronization: basic principles. *Clinical Neurophysiology* 110:1842-57.
- Pfurtscheller G., Woertz M., Muller G., Wriessnegger S., Pfurtscheller K. (2002) Contrasting behavior of beta event-related synchronization and somatosensory evoked potential after median nerve stimulation during finger manipulation in man. *Neuroscience Letters* 323:113-6.
- Philiastides M.G., Sajda P. (2006) Temporal characterization of the neural correlates of perceptual decision making in the human brain. *Cerebral Cortex* 16:509-18.
- Philiastides M.G., Sajda P. (2007) EEG-informed fMRI reveals spatiotemporal characteristics of perceptual decision making. *Journal of Neuroscience* 27:13082-13091.

- Philiastides M.G., Ratcliff R., Sajda P. (2006) Neural Representation of Task Difficulty and Decision Making during Perceptual Categorization: A Timing Diagram. *Journal of Neuroscience* 26:8965-8975.
- Polich J. (2007) Updating P300: an integrative theory of P3a and P3b. *Clinical Neurophysiology* 118:2128-48.
- Posner M.I., Dehaene S. (1994) Attentional networks. *Trends in Neurosciences* 17:75-9.
- Preuschhof C., Heekeren H.R., Taskin B., Schubert T., Villringer A. (2006) Neural correlates of vibrotactile working memory in the human brain. *Journal of Neuroscience* 26:13231-9.
- Ratcliff R. (1978) A theory of memory retrieval. *Psychological Review* 85:59-108.
- Ratcliff R. (2006) Modeling response signal and response time data. *Cognitive psychology* 53:195-237.
- Ratcliff R., McKoon G. (2008) The diffusion decision model: theory and data for two-choice decision tasks. *Neural computation* 20:873-922.
- Ratcliff R., Van Zandt T., McKoon G. (1999) Connectionist and diffusion models of reaction time. *Psychological Review* 106:261-300.
- Rieder M.K., Rahm B., Williams J.D., Kaiser J. (2011) Human gamma-band activity and behavior. *International Journal of Psychophysiology* 79:39-48.
- Rinkenauer G., Osman A., Ulrich R., Muller-Gethmann H., Mattes S. (2004) On the locus of speed-accuracy trade-off in reaction time: inferences from the lateralized readiness potential. *Journal of experimental psychology. General* 133:261-82.
- Robinson S.E. (2004) Localization of event-related activity by SAM(erp). *Neurology and Clinical Neurophysiology* 2004:109.
- Roelfsema P.R., Engel A.K., Konig P., Singer W. (1997) Visuomotor integration is associated with zero time-lag synchronization among cortical areas. *Nature* 385:157-161.
- Roitman J.D., Shadlen M.N. (2002) Response of neurons in the lateral intraparietal area during a combined visual discrimination reaction time task. *Journal of Neuroscience* 22:9475-89.
- Romo R., Salinas E. (2003) Flutter discrimination: neural codes, perception, memory and decision making. *Nature reviews. Neuroscience* 4:203-218.
- Romo R., Brody C.D., Hernández A., Lemus L. (1999) Neuronal correlates of parametric working memory in the prefrontal cortex. *Nature* 399:470-3.
- Romo R., Hernandez A., Zainos A., Salinas E. (2003) Correlated neuronal discharges that increase coding efficiency during perceptual discrimination. *Neuron* 38:649-57.
- Romo R., Hernandez A., Zainos A., Brody C., Salinas E. (2002) Exploring the cortical evidence of a sensory-discrimination process. *Philosophical Transactions of the Royal Society of London. Series B, Biological Sciences* 357:1039-1051.

- Rose M., Buchel C. (2005) Neural coupling binds visual tokens to moving stimuli. *Journal of Neuroscience* 25:10101-4.
- Rugg M.D., Coles M.G.H. (1996) *Electrophysiology of Mind: Event-related brain potentials and cognition* Oxford Psychology Press, Oxford.
- Rushworth M.F., Johansen-Berg H., Young S.A. (1998) Parietal cortex and spatial-postural transformation during arm movements. *Journal of neurophysiology* 79:478-82.
- Sadato N., Pascual-Leone A., Grafman J., Ibañez V., Deiber M.P., Dold G., Hallett M. (1996) Activation of the primary visual cortex by Braille reading in blind subjects. *Nature* 380:526-8.
- Salinas E., Sejnowski T.J. (2001) Correlated neuronal activity and the flow of neural information. *Nature Reviews. Neuroscience* 2:539-550.
- Salinas E., Hernandez A., Zainos A., Romo R. (2000) Periodicity and firing rate as candidate neural codes for the frequency of vibrotactile stimuli. *Journal of Neuroscience* 20:5503-15.
- Sangals J., Sommer W., Leuthold H. (2002) Influences of presentation mode and time pressure on the utilisation of advance information in response preparation. *Acta Psychologica* 109:1-24.
- Schmidt R.F., Lang F., Thews G. (2005) *Physiologie des Menschen*. 29 ed. Springer, Heidelberg.
- Schroeder C.E., Foxe J.J. (2002) The timing and laminar profile of converging inputs to multisensory areas of the macaque neocortex. *Brain Research. Cognitive Brain Research* 14:187-98.
- Ségonne F., Dale A.M., Busa E., Glessner M., Salat D., Hahn H.K., Fischl B. (2004) A hybrid approach to the skull stripping problem in MRI. *NeuroImage* 22:1060-75.
- Shadlen M.N., Newsome W.T. (2001) Neural basis of a perceptual decision in the parietal cortex (area LIP) of the rhesus monkey. *Journal of neurophysiology* 86:1916-1936.
- Shadlen M.N., Kiani R., Hanks T.D., Churchland A.K. (2008) *Neurobiology of Decision Making: an intentional framework*, in: C. Engel and W. Singer (Eds.), *Better Than Conscious?: Decision Making, the Human Mind, and Implications For Institutions*, MIT Press. pp. 71-102.
- Shanks M.F., Pearson R.C., Powell T.P. (1985) The ipsilateral cortico-cortical connexions between the cytoarchitectonic subdivisions of the primary somatic sensory cortex in the monkey. *Brain Research* 356:67-88.
- Siegel M., Konig P. (2003) A functional gamma-band defined by stimulus-dependent synchronization in area 18 of awake behaving cats. *Journal of Neuroscience* 23:4251-4260.
- Siegel M., Donner T.H., Oostenveld R., Fries P., Engel A.K. (2007) High-Frequency Activity in Human Visual Cortex Is Modulated by Visual Motion Strength. *Cerebral Cortex* 17:732-41.

- Simões C., Mertens M., Forss N., Jousmäki V., Lütkenhöner B., Hari R. (2001) Functional overlap of finger representations in human SI and SII cortices. *Journal of Neurophysiology* 86:1661-5.
- Smith P.L., Ratcliff R. (2004) Psychology and neurobiology of simple decisions. *Trends in Neurosciences* 27:161-168.
- Spitzer B., Blankenburg F. (2011) Stimulus-dependent EEG activity reflects internal updating of tactile working memory in humans. *Proceedings of the National Academy of Sciences of the United States of America* 108:8444-9.
- Stone M. (1960) Models for choice-reaction time. *Psychometrika* 25:251-260.
- Switkenby S.J., Bailey A.J., Bräutigam S., Josephs O.E., Jousmäki V., Tesche C.D. (1998) Neural processing of human faces: a magnetoencephalographic study. *Experimental brain research. Experimentelle Hirnforschung. Expérimentation cérébrale* 118:501-10.
- Takada M., Tokuno H., Nambu A., Inase M. (1998) Corticostriatal projections from the somatic motor areas of the frontal cortex in the macaque monkey: segregation versus overlap of input zones from the primary motor cortex, the supplementary motor area, and the premotor cortex. *Experimental brain research. Experimentelle Hirnforschung. Expérimentation cérébrale* 120:114-28.
- Talairach J., Tournoux P. (1988) *Co-planar stereotaxic atlas of the human brain* Thieme, New York.
- Tallon-Baudry C., Bertrand O. (1999) Oscillatory gamma activity in humans and its role in object representation. *Trends in Cognitive Sciences* 3:151-162.
- Tallon-Baudry C., Bertrand O., Delpuech C., Permier J. (1997) Oscillatory gamma-band (30-70 Hz) activity induced by a visual search task in humans. *Journal of Neuroscience* 17:722-734.
- Tanaka E., Inui K., Kida T., Miyazaki T., Takeshima Y., Kakigi R. (2008) A transition from unimodal to multimodal activations in four sensory modalities in humans: an electrophysiological study. *BMC Neuroscience* 9:116.
- Tanji J., Kurata K. (1982) Comparison of movement-related activity in two cortical motor areas of primates. *Journal of Neurophysiology* 48:633-53.
- Taulu S., Kajola M., Simola J. (2004) Suppression of interference and artifacts by the Signal Space Separation Method. *Brain topography* 16:269-75.
- Taulu S., Simola J., Kajola M. (2005) Applications of the signal space separation method. *IEEE Transactions on Signal Processing* 53:3359-3372.
- Thees S., Blankenburg F., Taskin B., Curio G., Villringer A. (2003) Dipole source localization and fMRI of simultaneously recorded data applied to somatosensory categorization. *NeuroImage* 18:707-19.
- Thiele A., Stoner G. (2003) Neuronal synchrony does not correlate with motion coherence in cortical area MT. *Nature* 421:366-70.

- Townsend J.T., Ashby F.G. (1983) *The Stochastic Modeling of Elementary Psychological Processes*. Cambridge University Press, Cambridge.
- Uchida N., Kepecs A., Mainen Z.F. (2006) Seeing at a glance, smelling in a whiff: rapid forms of perceptual decision making. *Nature reviews. Neuroscience* 7:485-491.
- Uka T., DeAngelis G.C. (2003) Contribution of middle temporal area to coarse depth discrimination: comparison of neuronal and psychophysical sensitivity. *Journal of Neuroscience* 23:3515-30.
- Van Veen B.D., van Drongelen W., Yuchtman M., Suzuki A. (1997) Localization of brain electrical activity via linearly constrained minimum variance spatial filtering. *IEEE Transactions on Bio-Medical Engineering* 44:867-880.
- van Veen V., Krug M.K., Carter C.S. (2008) The neural and computational basis of controlled speed-accuracy tradeoff during task performance. *Journal of cognitive neuroscience* 20:1952-65.
- van Westen D., Fransson P., Olsrud J., Rosén B., Lundborg G., Larsson E.-M. (2004) Fingersomatotopy in area 3b: an fMRI-study. *BMC Neuroscience* 5:28.
- Vandekerckhove J., Tuerlinckx F. (2007) Fitting the Ratcliff diffusion model to experimental data. *Psychonomic Bulletin and Review* 14:1011-26.
- Vandekerckhove J., Tuerlinckx F. (2008) Diffusion model analysis with MATLAB: a DMAT primer. *Behavior research methods* 40:61-72.
- VanRullen R., Koch C. (2003) Visual selective behavior can be triggered by a feed-forward process. *Journal of Cognitive Neuroscience* 15:209-217.
- Verleger R. (2008) P3b: towards some decision about memory. *Clinical neurophysiology : official journal of the International Federation of Clinical Neurophysiology* 119:968-70.
- Verleger R., Jaskowski P., Wascher E. (2005) Evidence for an Integrative Role of P3b in Linking Reaction to Perception. *Journal of Psychophysiology* 19:165-181.
- Wang X.-J. (2002) Probabilistic decision making by slow reverberation in cortical circuits. *Neuron* 36:955-68.
- Wang X.J. (2001) Synaptic reverberation underlying mnemonic persistent activity. *Trends in Neurosciences* 24:455-63.
- Wenzlaff H., Bauer M., Maess B., Heekeren H.R. (2011) Neural characterization of the speed-accuracy tradeoff in a perceptual decision-making task. *Journal of Neuroscience* 31:1254-66.
- Womelsdorf T., Fries P., Mitra P.P., Desimone R. (2006) Gamma-band synchronization in visual cortex predicts speed of change detection. *Nature* 439:733-736.
- Zangaladze A., Epstein C.M., Grafton S.T., Sathian K. (1999) Involvement of visual cortex in tactile discrimination of orientation. *Nature* 401:587-90.

-
- Zhang M., Weisser V.D., Stilla R., Prather S.C., Sathian K. (2004) Multisensory cortical processing of object shape and its relation to mental imagery. *Cognitive, Affective and Behavioral Neuroscience* 4:251-9.

6. List of Figures

Fig.1: Diffusion model (modified from Ratcliff, 1978).....	2
Fig.2: Visual stimuli presented in study 1.....	13
Fig.3: Experimental design of study 1.....	16
Fig.4: MEG setup of study 1.....	17
Fig.5: Behavioral and modeling results of study 1.....	24
Fig.6: SAT effect between 275 and 325 ms after stimulus onset in the right SMA negatively correlated with the boundary in study 1.....	26
Fig.7: SAT effect between 300 and 350 ms after stimulus onset in the left SMA not correlated with the boundary in study 1.....	28
Fig.8: SAT effect between 200 and 150 ms before the response in the medial precuneus not correlated with the boundary in study 1.....	29
Fig.9: SAT effects between 300 and 250 ms and 150 and 100 ms before the response in the left dorsolateral prefrontal cortex (DLPFC), middle frontal gyrus, BA9. Early differential (accuracy-speed) activity positively correlated with the boundary in study 1.....	30
Fig.10: COH effect between 150 and 200 ms (M170) after stimulus onset in the right fusiform gyrus not correlated with the drift rate in study 1.....	31
Fig.11: Significant COH effect between 185 and 235 ms (M170) after the stimulus onset in the left fusiform gyrus not correlated with the drift rate in study 1.....	33
Fig.12: Significant COH effect between 285 and 335 ms after the stimulus onset in the right DLPFC highly positively correlated with the drift rate in study 1.....	34
Fig.13: Significant COH effect between 350 and 400 ms after the stimulus onset in the right calcarine gyrus not significantly correlated with the drift rate in study 1.....	35
Fig.14: Significant COH effect between 315 and 265 ms before the response in left BA6 not correlated with the drift rate in study 1.....	36
Fig.15: Tactile stimuli presented in studies 2 and 3.....	46
Fig.16: Fig. Fig.16: Trial course for training, test and experimental sessions in studies 2 and 3.....	48
Fig.17: Experimental setup of studies 2 and 3.....	49
Fig.18 (1000 ms study): RT distribution per subject.....	56
Fig.19 (100 ms study): RT distribution per subject.....	57
Fig.20 (1000 ms study): Behavioral and modeling results of study 2.....	58

Fig.21 (100 ms study): Behavioral and modeling results of study 3.....	59
Fig.22 (1000 ms study): Stimulus-locked ERP components occurring across the difficulty levels in study 2.....	61
Fig.23 (1000 ms study): Grand average beamformer source estimates in the time domain in (A) S1 area 3b, (B) S1 area 1, (C) S2 contralateral, (D) S2 ipsilateral of study 2.	62
Fig.24 (100 ms study): Stimulus-locked ERP components occurring across the difficulty levels in study 3.....	63
Fig.25 (100 ms study): Grand average beamformer source estimates in the time domain in (A) S1 area 3b, (B) S1 area 1, (C) S2 contralateral, (D) S2 ipsilateral of study 3.....	64
Fig.26 (1000 ms study): Significant DIFF effect between 320 and 370 ms after the stimulus onset in left medio-frontal channels not significantly correlated with either the drift rate or RT in study 2.	65
Fig.27 (100 ms study): Significant DIFF effect between 325 and 375 ms after the stimulus onset in left medio-frontal channels not significantly correlated with either the drift rate or RT in study 3	66
Fig.28 (1000 ms study): Significant DIFF effect between 340 and 490 ms after the stimulus onset in left lateral channels positively correlated with the drift rate and negatively correlated with RT in study 2.....	67
Fig.29 (100 ms study): Significant DIFF effect between 425 and 475 ms after the stimulus onset in left lateral channels positively correlated with the drift rate but not significantly correlated with RT in study 3.....	68
Fig.30 (1000 ms study): Significant DIFF effect between 370 and 590 ms after the stimulus onset in left S1 area 3b positively correlated with the drift rate and negatively correlated with RT in study 2.	69
Fig.31 (100 ms study): S Significant DIFF effect between 450 and 515 ms after the stimulus onset in left S1 area 3b not significantly correlated with either the drift rate or RT in study 3.	70
Fig.32 (1000 ms study): Components in the frequency domain across the difficulty levels revealed six components in study 2.....	74
Fig.33 (1000 ms study): Grand average beamformer source estimates in the frequency domain in (A) S1 area 3b, (B) S1 area 1, (C) S2 contralateral, (D) S2 ipsilateral in study 2	75
Fig.34 (100 ms study): Components in the frequency domain across the difficulty levels revealed six components in study 3.....	76
Fig.35 (100 ms study): Grand average beamformer source estimates in the frequency domain in (A) S1 area 3b, (B) S1 area 1, (C) S2 contralateral, (D) S2 ipsilateral in study 3	77
Fig.36 (1000 ms study): Significant DIFF effect between 500 and 600 ms after the stimulus onset in left occipital channels not significantly correlated with either the drift rate or RT in study 2	79

Fig.37 (100 ms study): Significant DIFF effect between 500 and 650 ms after the stimulus onset in central occipital channels positively correlated with the drift rate in study 2. 80

7. List of Tables

Table 1: Average values and statistics (two-way repeated-measures analysis of variance) for behavioral data (reaction times and percentage of correct responses), and diffusion model parameters (boundary, drift rate and nondecision time).	24
Table 2 (1000 ms study): Average values and statistics (one-way repeated-measures ANOVAs) for reaction times, percentage of correct responses, and drift rate.	58
Table 3 (100 ms study): Average values and statistics (one-way repeated-measures ANOVAs) for reaction times, percentage of correct responses, and drift rate.....	59
Table 4 (1000 ms study): Statistics for comparison between the two studies presenting Braille patterns for 1000 ms or 100 ms, respectively.....	81

8. List of Abbreviations

ACC	anterior cingulate cortex
ANOVA	analysis of variance
Area LIP	lateral intraparietal area
Area MT	middle temporal area
Area MST	medial superior temporal area
BA	Brodmann area
BIC	Bayesian Information Criterion
BO	boundary
cHPI	continuous head position indicator
COH	coherence level or level of visual sensory evidence, applied in study 2 using visual stimuli
DIFF	task difficulty, applied in the studies 2 and 3 using tactile stimuli
DLPFC	dorsolateral prefrontal cortex
DMAT	diffusion model analysis toolbox
DR	drift rate
EEG	electroencephalography
EMG	electromyogram
EOG	electrooculogram
ERD	event-related desynchronization
ERP	event-related potentials
FEF	frontal eye field
FFA	fusiform face area
fMRI	functional magnetic resonance imaging
LATER	Linear Approach to Threshold with Ergodic Rate
LOC	lateral occipital complex
μV	microvolt
M	magnetic field activation when using MEG
MEG	magnetoencephalography
MNI	Montreal Neurological Institute
ms	milliseconds
N	negative deflection when using EEG
NMDA	N-Methyl-D-aspartic acid

pT	picotesla
P	positive deflection when using EEG
PFC	prefrontal cortex
PMC	premotor cortex
ROI	regions of interest
RT	reaction time
s	seconds
S1	primary somatosensory cortex
S2	secondary somatosensory cortex
SAT	speed-accuracy tradeoff
SC	superior colliculus
sd	standard deviation
SE	standard error of the mean
sLORETA	standardized Low Resolution Electromagnetic Tomography
SMA	supplementary motor area
TMS	transcranial magnetic stimulation
V1	primary visual cortex
V2	visual area V2
V3	visual area V3

9. Acknowledgements

This dissertation is the result of research I have carried out in the Neurocognition of decision making group of the Max Planck Institute for Human Development. Many colleagues, friends and my family helped me to conclude this work and I like to thank them in manifold ways.

I dearly thank Hauke Heekeren who has been my main advisor in all those years. Thank you for your patience and intellectual support. You always helped me to see the big picture when I was lost in the details. I also thank you that I was able to join numerous conferences and workshops which had an enormous impact on this dissertation. And last but not least, thank you for working with me on this thesis. For this, I also thank Arno Villringer.

I especially thank Markus Bauer who has accompanied this dissertation at all stages although he has left the group years ago. We had many inspiring discussions, you taught me various data analysis methods and how to program with MatLab. Thanks for all the time taken for skype sessions, optimizing analysis routines together, and for reading this dissertation multiple times.

For the MEG study I thank Prof. Dr. Angela F. Friederici for enabling this fruitful collaboration. Burkhard Maess, you have helped me tremendously with the data analysis, especially the distributed source localization. And your special sense of humour helped me to keep going at frustrating times. Many thanks to Yvonne Wolff who recorded the data with me. I would have loved to work with you for longer! Thanks also to Björn Herrmann who helped me to convert MNI to Talairach space and was a humorous companion.

For the EEG studies, I thank Sonali Beckmann for recording the data with me and being unique in finding practical solutions to seemingly unsolvable problems.

Thank you, Niki Vavatzenidis and Helen Blank, for good discussions and motivation when needed. Thanks to Marios Philiastides for answering questions patiently and helping me with some MatLab scripts, to Flavia Filimon for great discussions late at night, and to Dorit Kliemann for ensuring a personal and lively atmosphere in the group.

I thank you, Aga Burzynska, for lively discussions about science, future perspectives, and how much life is what you make it. And thank you, Lars and Karolina Tykwinska, for remembering me that there is a life outside science, namely climbing. Also thank you, Jean Berlescu, for helping me to develop my personality through the world of music.

My biggest thanks belong to Lars and my parents. Your love and firmly held belief that I can do it encouraged me to move on and accomplish this work and chapter in my life.

10. Eidesstattliche Versicherung

Ich, Hermine Wenzlaff, versichere an Eides statt durch meine eigenhändige Unterschrift, dass ich die vorgelegte Dissertation mit dem Thema:

„Human perceptual decision making in the visual and tactile domain“

selbstständig und ohne nicht offengelegte Hilfe Dritter verfasst und keine anderen als die angegebenen Quellen und Hilfsmittel genutzt habe.

Alle Stellen, die wörtlich oder dem Sinne nach auf Publikationen oder Vorträgen anderer Autoren beruhen, sind als solche in korrekter Zitierung (siehe „Uniform Requirements for Manuscripts (URM)“ des ICMJE -www.icmje.org) kenntlich gemacht. Die Abschnitte zu Methodik (insbesondere praktische Arbeiten, Laborbestimmungen, statistische Aufarbeitung) und Resultaten (insbesondere Abbildungen, Graphiken und Tabellen) entsprechen den URM (s.o) und werden von mir verantwortet.

Mein Anteil an der ausgewählten Publikation entspricht dem, der in der untenstehenden gemeinsamen Erklärung mit dem/der Betreuer/in, angegeben ist.

Die Bedeutung dieser eidesstattlichen Versicherung und die strafrechtlichen Folgen einer unwahren eidesstattlichen Versicherung (§156,161 des Strafgesetzbuches) sind mir bekannt und bewusst.

Datum

Unterschrift

Anteilerklärung an etwaigen erfolgten Publikationen

Hermine Wenzlaff hatte folgenden Anteil an den folgenden Publikationen:

Publikation 1: *Autoren:* Wenzlaff H., Bauer M., Maess B., Heekeren H.R., *Titel:* Neural characterization of the Speed-Accuracy Tradeoff in a perceptual decision-making task, *Zeitschrift:* Journal of Neuroscience, *Erscheinungsjahr:* 2011

Beitrag im Einzelnen: Erstellen des Experimentdesigns, Datenerhebung, Datenanalyse, Diskussion der Ergebnisse, Verfassen des Artikels

Unterschrift, Datum und Stempel des betreuenden Hochschullehrers

11. Curriculum Vitae

Mein Lebenslauf wird aus datenschutzrechtlichen Gründen in der elektronischen Version meiner Arbeit nicht veröffentlicht.

